

# Homogenization of exchange couplings in quantum dot arrays

Master thesis  
Carles Esteve Boncompte

# Homogenization of exchange couplings in quantum dot arrays

by

Carles Esteve Boncompte

in partial fulfillment of the requirements to obtain the degree of Master of Science  
at the Delft University of Technology,  
to be defended on Friday April 21, 2023.

Student number: 5387116  
Project duration: September, 2022 – April, 2023  
Direct Supervisor: L. M. K. Vandersypen  
Daily Supervisor: P. Cova Fariña  
Thesis committee: L. M. K. Vandersypen (Supervisor)  
M. Blaauboer  
M. Veldhorst



# Summary

In this work we explore the behavior of a small system of spins governed by the Heisenberg nearest-neighbor interaction with the objective of tuning it into the regime where all exchange couplings in the system are equal. In order to do so, we explore the energy spectrum of the eigenstates of a specific subspace of the Hamiltonian, which allows us to determine an experimentally measurable signature when a pair of exchanges take the same value. In particular, focusing on this method, we propose two different approaches to tune a  $2 \times 4$  array, an eight-spin system of interest. Lastly, we introduce possible alternative methods to achieve this same objective of exchange homogenization.

# Contents

<b>Summary</b>	<b>i</b>
<b>1 Introduction</b>	<b>1</b>
1.1 Objective . . . . .	2
1.2 Motivation . . . . .	2
1.3 Technical remarks . . . . .	2
<b>2 Underlying theory</b>	<b>4</b>
2.1 Heisenberg Hamiltonian . . . . .	4
2.2 Theoretical assumptions . . . . .	5
<b>3 Literature replication</b>	<b>7</b>
3.1 Adaptation of the theory . . . . .	7
3.2 Implementation of the code . . . . .	10
3.2.1 Four-spin Hamiltonian . . . . .	10
3.2.2 Basis transformation . . . . .	10
3.2.3 Code checks . . . . .	11
3.3 Tuning a four-spin chain . . . . .	11
3.4 Tuning a four-spin plaquette . . . . .	15
<b>4 Generalization and testing</b>	<b>18</b>
4.1 Generalization of the code . . . . .	18
4.2 Testing . . . . .	20
4.3 Partial readout . . . . .	22
4.3.1 Theory and implementation . . . . .	22
4.3.2 Results and experimental verification . . . . .	23
4.4 Symmetries . . . . .	25
4.5 Visibility . . . . .	26
<b>5 Tuning a <math>2 \times 4</math> ladder</b>	<b>28</b>
5.1 Protocol A . . . . .	28
5.2 Protocol B . . . . .	32
<b>6 Alternative approaches</b>	<b>36</b>
6.1 Resonating valence bond theory . . . . .	36
6.2 Motivation . . . . .	37
<b>7 Conclusions and outlook</b>	<b>41</b>
<b>Acknowledgements</b>	<b>43</b>
<b>References</b>	<b>44</b>
<b>A Three-spins plaquette</b>	<b>45</b>
<b>B Six-spins chain</b>	<b>48</b>
<b>C Supplementary figures</b>	<b>51</b>

# 1

## Introduction

The theory of quantum mechanics describes how nature behaves in the atomic and subatomic scale, where particles behave completely different to what a classical theory would predict. Interesting new phenomena emerge in these small scale systems such as quantum superposition or quantum entanglement. Moreover, interactions between particles in many-body systems play a fundamental role when studying the physical behavior of the ensemble. These interactions cannot be understood if the system is not treated as a whole. These two features characterize many-body quantum systems. Being able to fully understand how these systems of interacting particles behave is highly important and it is still a current research topic.

One way to understand such systems is by means of using analog quantum simulations. These simulators rely on using a quantum system that evolves according to a specific Hamiltonian from which we can control its parameter values and that shares Hamiltonian with the quantum system we aim to study [1]. Different types of controllable quantum systems can be used as analog quantum simulators. However, quantum dots are a very promising platform in that sense because of their easy manipulation, long coherence times and already-developed readout techniques of both charge and spin states [2][3][4]. Apart from this, spin- $\frac{1}{2}$  particles in quantum dots naturally obey the Hubbard Hamiltonian, and the typical parameter values they exhibit allow us to simulate many-body behavior of very physically interesting regimes [5]. This work centers on better understanding the capabilities of analog quantum simulation using this above-mentioned platform.

The Hubbard model allows us to study the behavior of interacting localized charged spins only by assuming that the origin of their interaction is given by its quantum mechanical nature and the strong Coulomb interaction between them. Despite being too simple for a complete description of a quantum mechanical condensed matter system, it exhibits plenty of interesting phenomena that are worth to be inspected [1]. The Hubbard model Hamiltonian is

$$H_H = - \underbrace{\sum_i \epsilon_i n_i}_A + \underbrace{\sum_i \frac{U_i}{2} n_i (n_i - 1)}_B + \underbrace{\sum_{ij, i \neq j} V_{ij} n_i n_j}_C - \underbrace{\sum_{\langle i,j \rangle} t_{ij} (c_i^\dagger c_j + H.c.)}_D \quad (1.1)$$

and it consists of two terms, one that accounts for the short-range Coulomb interaction between electrons ( $B, C$  in Equation 1.1) and another one which describes quantum mechanical motion, or more specifically, tunnel hopping of electrons from one localized site to another ( $D$  in Equation 1.1). Although only the on-site Coulomb interaction can be exclusively considered ( $B$  in Equation 1.1), inter-site interaction can also be added to the Hamiltonian in the same Coulomb term ( $C$  in Equation 1.1) [6]. We will see that from this model we can obtain the Heisenberg Hamiltonian, which govern the physics of the systems we study in this project [1].

Quantum spin chains and other simple geometries are ideal systems for studying the Hubbard and Heisenberg models. One of the main reasons of this is that they can be fabricated and operated

controlling occupancy of each site, allowing experimental research. Furthermore, small enough sizes can still be classically simulated, as we will see along this project trying to tune the exchange couplings of different systems. Although it is likely that computer automated and machine learning approaches will become a key tool in the future when it comes to exchange operation, it is worth to explore other control techniques [2].

## 1.1. Objective

In this project we intend to broaden understanding about the control of the parameters of a Hamiltonian of a system formed by a collection of spin- $\frac{1}{2}$  particles in a quantum dot array. Specifically, we will study some systems undergoing nearest-neighbor interaction Heisenberg Hamiltonian and we will attempt to find conditions for the homogeneous exchange coupling regime of it, or in other words, the case for which all the parameters that characterize the spin-spin interaction are the same. To achieve this, we will follow a method presented in Ref. [6] based on energy spectroscopy measurements that has been successful for a quadruple spin chain. The authors in Ref [7] also follow a similar approach, from which we will also take some knowledge. We will study the new geometries by means of classical computer simulations. The final objective of this work is not only to be able to explore conditions or signatures of the homogeneous regime studying how the energy of the system behaves but also to do it in such a way that the results we obtain can be replicated experimentally. In particular, we want to focus on tuning a  $2 \times 4$  ladder (see Figure 2.2).

## 1.2. Motivation

Classical numerical simulations of many-body quantum systems cannot manage to keep up with the increasing number of possible quantum states that these systems have [5][8]. This is the root problem from which the idea of creating quantum simulators emerged, which could become a reality provided that we have sufficient control of the quantum system we use to simulate. The fact of being able to simulate large quantum systems in the future opens a lot of doors from the research perspective.

Regarding the type of models we aim to simulate, on the one hand, the Hubbard and Heisenberg models are interesting to study because they are very rich in terms of variety of physical phenomena that can be observed. Emergence of exotic magnetic phases [6] or possible emergence of high- $T_c$  superconductivity [2][8], are some of these phenomena of which complete understanding is not yet achieved. On the other hand and for our specific case of interest, being able to achieve a homogeneous exchange condition in a nearest-neighbour Heisenberg interacting system also has its particular relevance. Many of the systems we find in nature tend to show at least a certain degree of homogeneity and some of our idealized theoretical models also tend to assume these sorts of premises. In fact, some of these natural systems, such as solids, are intrinsically bonded to homogeneity because of their periodic lattice structure. For this reason, when it comes to being able to set the free parameters of our Hamiltonian to a specific value we want, tuning it in a partial or total homogeneous regime is an important step towards the better understanding of nature.

While this work attempts to classically simulate a small quantum system to gain insight about how to achieve a specific regime of the Heisenberg Hamiltonian, we must keep in mind that analog quantum simulators are developed as a tool to use when classical approaches are no longer feasible [5]. Therefore, the homogeneous exchange tuning method shown in this work is not extensible to large systems and precisely it should not be. Thus, this work naturally presents the need of new research involving alternative methods aimed at tuning analog quantum simulators to specific regimes of genuinely classically intractable systems.

## 1.3. Technical remarks

We will finish the introduction with some technical remarks about the units and the mathematical notation present in this report. These specifications will be consistently maintained throughout its whole extent.

- The system of units used both in the numerical simulations and in this report is based on setting the reduced Plank constant  $\hbar = 1$ . Therefore, energies are given in units of angular frequency (multiplied by  $2\pi$ ),  $[\omega] = \frac{2\pi rad}{T}$ , and time in units of  $T$ , where  $T$  is free of choice. Given the usual order of magnitude of the experimental values that can be found in Ref. [6], a reasonable reference value for  $T$  could be chosen to be  $T = 1\mu s$ , setting the time units of the system to  $t_0 = T = 1\mu s$ , the frequency units to  $f_0 = \frac{1}{T} = 1MHz$  and energy units to  $E_0 = \frac{2\pi rad}{\mu s} = 1MHz$  using the conversion  $2\pi \frac{rad}{s} = 1Hz$ . It can also be convenient to have in mind the conversion  $1MHz \approx 4.136 \cdot 10^{-9}eV$ .

- The number of spin objects in all the systems that we will consider is denoted by the letter  $n$  and Hilbert space and subspace dimensions is denoted by the letter  $N$ .

- We call “product basis” to the set of vectors

$$\{|\phi_i\rangle\} = \{|i\rangle\}$$

with  $i = 0, \dots, N - 1$ . For example, a system of two spin- $\frac{1}{2}$  particles is described by  $n = 2$  and a Hilbert space of dimension  $N = 4$  and its product basis is labelled by

$$\{|\phi_i\rangle\} = \{|0\rangle, |1\rangle, |2\rangle, |3\rangle\}$$

- Given that we only work with spin- $\frac{1}{2}$  objects, every product-basis vector with label  $i$  written in binary notation represents a chain of a combination of spin up ( $|\uparrow\rangle$ ) and spin down ( $|\downarrow\rangle$ ) states, making the correspondence  $|\uparrow\rangle = |0\rangle$  and  $|\downarrow\rangle = |1\rangle$ . For example, in a Hilbert space of dimension  $N = 4$

$$|9\rangle = |\downarrow\uparrow\uparrow\downarrow\rangle = |\downarrow\uparrow\downarrow\rangle_{1234} = |\downarrow\rangle_1 \otimes |\uparrow\rangle_2 \otimes |\uparrow\rangle_3 \otimes |\downarrow\rangle_4 \quad \text{with} \quad |\uparrow\rangle_j = \begin{pmatrix} 1 \\ 0 \end{pmatrix} \quad \text{and} \quad |\downarrow\rangle_j = \begin{pmatrix} 0 \\ 1 \end{pmatrix}$$

- Identity matrices with no specified Hilbert dimension subspace in the subscript are of dimension  $N = 2$ , that is,  $2 \times 2$  matrices.

- A short notation for quantum states containing singlet and triplet pairs respects the labelling order presented above unless the opposite is indicated. For example,

$$|ST-\rangle = |S\rangle_{12} \otimes |T-\rangle_{34}$$

with

$$|S\rangle_{ij} = \frac{1}{\sqrt{2}} (|\uparrow\downarrow\rangle_{ij} - |\downarrow\uparrow\rangle_{ij}), \quad |T_0\rangle_{ij} = \frac{1}{\sqrt{2}} (|\uparrow\downarrow\rangle_{ij} + |\downarrow\uparrow\rangle_{ij}), \quad |T_+\rangle_{ij} = |\uparrow\uparrow\rangle_{ij}, \quad \text{and} \quad |T_-\rangle_{ij} = |\downarrow\downarrow\rangle_{ij}$$

# 2

## Underlying theory

In this chapter we will briefly present the theory behind the Heisenberg model and the assumptions we make in order to simplify it. Furthermore, the experimental constraints that are applicable to our simulations are also presented.

### 2.1. Heisenberg Hamiltonian

As we commented in the introduction, considering a collection of localized spins trapped in quantum dots, it is reasonable to assume that their behavior is described by the Hubbard model. Specifically, in this work we will focus our study on the half-filled regime of the Hubbard model, in which the number of electrons  $n$  is the same as the number of sites of the lattice. Furthermore, both for simplicity and computational-cost reasons, the numerical simulations done in this work will only consider the physics occurring in the Mott-insulator regime, in which all the sites of the lattice are occupied [6]. Therefore, only one electron is localized at each quantum dot of the system. Under these considerations, the Hubbard Hamiltonian can be treated perturbatively, considering the hopping term as a perturbation of a short-range Coulomb interaction Hamiltonian (see Equation (1.1)), and eventually the Heisenberg Hamiltonian arises. However, despite the fact of coming from an approximation of a rather simple model, the Heisenberg Hamiltonian is both useful and accurate to describe magnetism in this above-mentioned regime [1][2].

The form of the Heisenberg Hamiltonian for a chain of  $n$  spins is

$$H_1^{(n)} = \sum_{\langle i,j \rangle} J_{ij} \left( \vec{S}_i \cdot \vec{S}_j - \frac{1}{4} \right) = \sum_{i=1}^{n-1} J_{ii+1} \left( \vec{S}_i \cdot \vec{S}_{i+1} - \frac{1}{4} \right) \quad (2.1)$$

where the angle brackets indicate a nearest-neighbors sum and  $J_{ij}$  are the exchange coupling values between spins  $i$  and  $j$ . Since our Hamiltonian purely shows spin terms, it is theoretically sufficient to consider that the objects we are treating are spin- $\frac{1}{2}$  particles. Besides the spin-spin interacting part, a Zeeman splitting induced by an external magnetic field  $\vec{B}_{ext}$  must be included if this field is present in the system. This term is shown in Equation (2.4).

An important part of the tuning protocol is based on analyzing the energy of the eigenstates of a subspace of the Hamiltonian we have. This is achieved by (1) expressing the Hamiltonian in a basis in which the Hamiltonian is explicitly split into these subspaces in a block-diagonal shape and (2) computing the energy of the eigenstates using the subspace of interest in the Hamiltonian matrix. While step (1) is not strictly compulsory, there is one main reason why it is desirable to consider it: it makes our numerical simulations less computationally-expensive. In order to complete step (1), we have to find a set of vectors that are eigenvectors of specific operators that commute with the Hamiltonian [9]. In this case, it is typical to use the set of basis vectors with a defined total spin and total spin projection in the  $z$  direction.

We have seen that in order to simulate the method presented in Ref. [6] we need to have the Hamiltonian of our system in a matrix form. The two general geometries of the systems that will be used in this work will be presented in the following. The Hamiltonian for the simplest one, the spin chain, is directly shown in Equation (2.1) for  $n$  spins. A pictorial representation of a chain of  $n = 4$  spins can be found in Figure 2.1. For the other geometry of interest it is convenient to define

$$\begin{aligned} H_2^{(n)} &= \sum_{\langle i,j \rangle} J_{ij} \left( \vec{S}_i \cdot \vec{S}_j - \frac{1}{4} \right) + \sum_{\langle\langle i,j \rangle\rangle} J_{ij} \left( \vec{S}_i \cdot \vec{S}_j - \frac{1}{4} \right) \\ &= \sum_{i=1}^{n-1} J_{ii+1} \left( \vec{S}_i \cdot \vec{S}_{i+1} - \frac{1}{4} \right) + \sum_{i=1}^{n-2} J_{ii+2} \left( \vec{S}_i \cdot \vec{S}_{i+2} - \frac{1}{4} \right) \end{aligned} \quad (2.2)$$

in order to write the Heisenberg ladder Hamiltonian of  $n$  spins when implementing the numerical simulations. It is also more convenient in terms of giving its closed formula. Once again, the angle brackets in Equation (2.2) indicate nearest-neighbor sum and the double angle brackets indicate next-nearest-neighbor sum. Then, we can define

$$H_{ladder}^{(n)} = H_2^{(n)} \quad \text{with} \quad J_{kk+1} = 0 \quad \forall \quad k = 2m : m \in \mathbb{N} \quad (2.3)$$

A pictorial representation of the ladder geometry can be seen in Figure 2.2

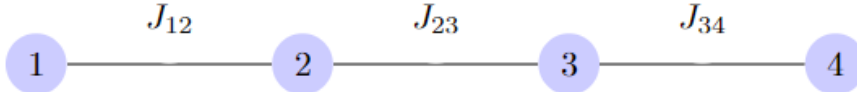


**Figure 2.1:** Geometrical representation and labelling of the spins and exchanges in a quadruple spin chain.

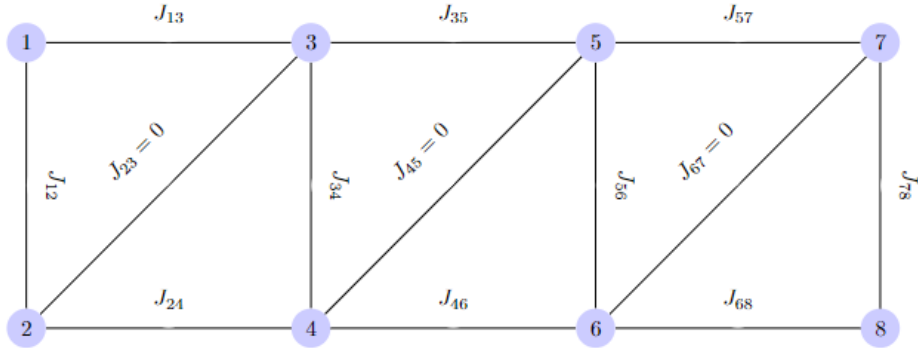


**Figure 2.2:** Geometrical representation and labelling of the spins and exchanges in a  $2 \times 4$  ladder. The couplings  $J_{23}$ ,  $J_{45}$  and  $J_{67}$  are explicitly set to zero for code-development reasons.

For completeness, the Zeeman term that will be present in both Hamiltonians of any of the two main geometries considered is

$$H_{ext} = g\mu_B B_{ext} \sum_{i=1}^n \hat{S}_i^z = \tilde{B} \sum_{i=1}^n \hat{S}_i^z \quad (2.4)$$

with with  $g > 0$  the Landé  $g$  factor,  $\mu_B$  the Bohr magneton. For convenience, we introduce a new quantity  $\tilde{B} = g\mu_B B_{ext}$  which has dimensions of energy.

## 2.2. Theoretical assumptions

In terms of the model, the system we consider is clearly idealized. The main theoretical assumptions we made about our systems include considering identical spins, perfectly spatially localized and steady and with quantization axis perfectly aligned. Furthermore, the surroundings of the system are also assumed

not to interact with our system, except for the external magnetic field in the  $z$  direction  $\vec{B}_{ext} = B_{ext}\hat{z}$ , which is assumed to be uniform and without the presence of fluctuations. The  $g$  factor is also assumed to be homogeneous for all the spins in the system. Inter-system nearest-neighbor spin interaction is thus the only interaction considered and its existence for any two spins  $i$  and  $j$  is therefore given by the geometry of the system.

In terms of capabilities, we assume that we are able to modify at will the  $J_{ij}$  values of the Heisenberg Hamiltonian and that this control is independent for every value  $J_{ij}$  (this is analogous as saying that our system is perfectly virtualized in terms of plunger and barrier gates). Moreover, it will also be assumed that the value of a set of exchanges  $\mathcal{S} = \{J_{ij}\}$  can be controlled simultaneously over a certain range. This control is required to maintain an initial condition of  $\forall J_{ij} \in \mathcal{S}, J_{ij} = J$  throughout the whole process of control. While this has been shown to be possible for a set of two exchanges [7], an extension to a set of at least four exchanges would be needed. The control of the exchange coupling values  $J_{ij}$  can be done varying the detuning between dots or making use of the tunnel couplings.

Lastly, regarding the state initialization-readout constraints, we assume that we are able to initialize and readout only certain specific states, which will be specified along the project for each system. Noticeably, this is due to the initialization and readout methods used experimentally, which only allow us to initialize or distinguish pairs of spins in the singlet or triplet configuration. This pair of spins is bound to have a nearest-neighbors connection. The initialization of the singlet is based on loading two spins in a same quantum dot from a reservoir such that Pauli exclusion principle only allows them to be in the singlet [6][7]. Spin triplet initialization can be done either by loading a thermal mixture of two spins in different quantum dots and post-selecting for triplet loading [6] or by using the singlet initialization and operating it [7].

The readout principle is also based on a process that requires a pair of spins in different quantum dots: The Pauli spin blockade (PSB) readout method. This method detects the spin state of a pair of quantum dots by making one of the spins in a quantum dot to tunnel onto the neighboring one. If the two spins are in the singlet state, a charge sensor can detect the tunneling process, while this current cannot be observed if the two spins are in the triplet state because the tunneling process is blocked by the Pauli exclusion principle [3]. The presence of a magnetic field favours that triplet states are fully polarized.

# 3

## Literature replication

In order to be able to obtain original results in the future, we first need to understand the process used to investigate the homogeneous exchange conditions in our system. Therefore, in this chapter we show the results obtained by our simulation to replicate the ones presented in Ref. [6] and Ref. [7].

### 3.1. Adaptation of the theory

We start the simulation by setting up the Hamiltonian of our system in a matrix form. For the time being, provided that we are just interested in a Hamiltonian describing magnetism in a quadruple spin chain, we only require building up a nearest-neighbour exchange coupling Heisenberg Hamiltonian with a defined number of spins and an extra term describing the Zeeman splitting caused by an external magnetic field (see Equations (2.1) and (2.4)). The mathematical formula of this Hamiltonian is

$$H_{chain}^{(4)} = H_{Heis}^{(4)} + H_{ext}^{(4)} = \sum_{i=1}^3 J_{ii+1} \left( \vec{S}_i \cdot \vec{S}_{i+1} - \frac{1}{4} \right) + \tilde{B} \sum_{i=1}^4 \hat{S}_i^z \quad (3.1)$$

Using the identity and the  $2 \times 2$  Pauli matrices, we can rewrite the spin operators for the first ( $i = 1$ ) terms as

$$\vec{S}_1 \cdot \vec{S}_2 = \frac{1}{4} (\sigma_x \otimes \sigma_x \otimes \mathbb{I} \otimes \mathbb{I} + \sigma_y \otimes \sigma_y \otimes \mathbb{I} \otimes \mathbb{I} + \sigma_z \otimes \sigma_z \otimes \mathbb{I} \otimes \mathbb{I}) \quad (3.2)$$

and

$$\hat{S}_1^z = \frac{1}{2} (\sigma_z \otimes \mathbb{I} \otimes \mathbb{I} \otimes \mathbb{I}) \quad (3.3)$$

Analogously, we can do the same with the rest of the indices taking into account that each ordered position in the tensor product corresponds to the number of each spin.

Building up such a matrix in Python as it is written in Equation (3.1) is a straightforward task when using QuTiP since it only consists of summing up several matrices consisting of tensor products of the  $N_{sub} = 2$  Hilbert subspaces of each spin. The resulting matrix will be written in the product basis  $\{|\phi_i\rangle\}$ , in this case the  $N = 2^4 = 16$  vectors. These are shown in general in Equation (3.4).

$$|0\rangle = \begin{pmatrix} 1 \\ 0 \\ \vdots \\ 0 \end{pmatrix}, |1\rangle = \begin{pmatrix} 0 \\ 1 \\ \vdots \\ 0 \end{pmatrix}, \dots, |N-1\rangle = \begin{pmatrix} 0 \\ 0 \\ \vdots \\ 1 \end{pmatrix} \quad (3.4)$$

If we denote our Hamiltonian in the product basis as  $H_\phi$ , basis-transforming it is also an easy task, we just need to perform two matrix multiplications according to

$$H_\psi = U^\dagger H_\phi U \quad (3.5)$$

The most challenging part in this step is actually finding the matrix  $U$  that allows us to transform our old Hamiltonian and rewrite it in a different desired basis, made out of basis vectors which are simultaneously eigenvectors of the total spin operator  $\vec{S}^2$  and the total spin projection in the  $z$  direction  $\hat{S}_z$  and are all orthonormal within the basis set of vectors. We will call this new basis the total spin basis and we will label its basis vectors with the set  $\{|\psi_i\rangle\}$ .

We can see that the coefficients of  $U$  are equivalent to the dot product between all the possible vectors of both basis:

$$|\psi_j\rangle = \sum_{k=1}^N U_{kj} |\phi_k\rangle \quad \Rightarrow \quad U_{ij} = \langle \phi_i | \psi_j \rangle \quad (3.6)$$

Therefore, we need to know the value of all of these braket overlaps, or as they are more commonly known, the Clebsh-Gordan (C.-G.) coefficients [10][11]. However, since we are coupling more than two spins in this case and C.-G. coefficients are defined for coupling a pair of particles, the coupling has to be done sequentially. Moreover, we need to keep all the possible combinations of intermediate total spin labels (values of  $S_{12}$ ,  $S_{123}$ , etc.) and the total spin projection ( $m_T$ ) to build the product basis states as we can see in Equation (3.10). For example, for our first case of interest, we need to obtain the C.-G. coefficients for a system of four coupled spin- $\frac{1}{2}$  particles. Defining the quantities

$$\vec{S}_{i_1 i_2 \dots i_k} = \sum_{j=1}^k \vec{S}_{i_j} \quad \text{and} \quad \hat{S}_{i_1 i_2 \dots i_k}^z = \sum_{j=1}^k \hat{S}_{i_j}^z \quad (3.7)$$

that satisfy

$$\begin{aligned} \vec{S}_{i_1 i_2 \dots i_k}^2 |S_{i_1 i_2 \dots i_k}\rangle &= S_{i_1 i_2 \dots i_k} (S_{i_1 i_2 \dots i_k} + 1) |S_{i_1 i_2 \dots i_k}\rangle \quad \text{and} \\ \hat{S}_{i_1 i_2 \dots i_k}^z |m_{i_1 i_2 \dots i_k}\rangle &= m_{i_1 i_2 \dots i_k} |m_{i_1 i_2 \dots i_k}\rangle = \sum_{j=1}^k m_{i_j} |m_{i_1 i_2 \dots i_k}\rangle \end{aligned} \quad (3.8)$$

for  $k = 2, 3, 4$ , we can compose the four spins sequentially as we show below [11].

$$\begin{aligned} 1) \left( S_1 = \frac{1}{2} \right) \otimes \left( S_2 = \frac{1}{2} \right) &\rightarrow S_{12} = 0, 1 \\ 2) \left( S_{12} = 0 \right) \otimes \left( S_3 = \frac{1}{2} \right) &\rightarrow S_{123} = \frac{1}{2} \\ 3) \left( S_{123} = \frac{1}{2} \right) \otimes \left( S_4 = \frac{1}{2} \right) &\rightarrow S_{1234} = S_T = 0, 1 \\ 2) \left( S_{12} = 1 \right) \otimes \left( S_3 = \frac{1}{2} \right) &\rightarrow S_{123} = \frac{1}{2}, \frac{3}{2} \\ 3) \left( S_{123} = \frac{1}{2} \right) \otimes \left( S_4 = \frac{1}{2} \right) &\rightarrow S_{1234} = S_T = 0, 1 \\ 3) \left( S_{123} = \frac{3}{2} \right) \otimes \left( S_4 = \frac{1}{2} \right) &\rightarrow S_{1234} = S_T = 1, 2 \end{aligned} \quad (3.9)$$

The reader may note that we will maintain the notation for which for the special case of  $k = n$  in Equation (3.8), eigenvalues are renamed as  $S_{12\dots n} = S_T$  and  $m_{12\dots n} = m_T$ . We can check from Expressions (3.9) that indeed we have two singlets with total spin label  $S_T = 0$ , two triplets with  $S_T = 1$  and one quintuplet with  $S_T = 2$ . The final  $m_T$  label is simply all the possible projections that  $S_T$  can have. However, these labels do not solve the problem of obtaining the coefficients for the  $U$  matrix. Fortunately, there is a closed expression that give us the Clebsh-Gordan coefficients for any

number of coupled spins provided that we input the value of the total spin of each intermediate coupling and the total spin ( $z$ ) projection [10]. We introduce an adapted version for our sequential coupling of four spin- $\frac{1}{2}$  particles in the following expression. Even though Expression 3.10 is not explicitly given in Ref. [10], it can be proven to work for an arbitrary number of spins  $n$ .

$$|S_{12}S_{123}S_T m_T\rangle = \sum_{m_1, m_2, m_3} CG(S_{12}, m_1, m_2, m_{12}) \times CG(S_{12}, S_{123}, m_{12}, m_3, m_{123}) \times \\ CG(S_{123}, S_T, m_{123}, m_4, m_T) |m_1 m_2 m_3 m_4\rangle \quad (3.10)$$

where

$$CG(S_1, S_2, S_{12}, m_1, m_2, m_{12}) = \langle S_1 S_2 m_1 m_2 | S_1 S_2 S_{12} m_{12} \rangle \\ = \delta_{m_{12} m_1 + m_2} [(2S_{12} + 1)AB]^{\frac{1}{2}} \sum_{\nu} \frac{(-1)^{\nu}}{\nu!} C_{\nu}^{-1} \quad (3.11)$$

with

$$A = \frac{(S_1 + S_2 - S_{12})! (S_{12} + S_1 - S_2)! (S_2 + S_{12} - S_1)!}{(S_1 + S_2 + S_{12} + 1)!} \\ B = (S_1 + m_1)! (S_1 - m_1)! (S_2 + m_2)! (S_2 - m_2)! (S_{12} + m_{12})! (S_{12} - m_{12})! \\ C_{\nu} = (S_1 + S_2 - S_{12} - \nu)! (S_1 - m_1 - \nu)! (S_2 + m_2 - \nu)! (S_{12} - S_2 + m_1 + \nu)! (S_{12} - S_1 - m_2 + \nu)! \quad (3.12)$$

and the range of the variable  $\nu$  being every possible integer that makes the argument of the factorials in Expression (3.11) non-negative. It is easy to see that if we extend Equation (3.10) with a sum for the last  $m_4$  label (which will give us 0 coefficient for the cases that do not satisfy  $m_T = m_1 + m_2 + m_3 + m_4$ ), the product of the Clebsh-Gordan coefficients is exactly the same as the  $U_{ij}$  coefficients being  $i$  the index of the product basis states and  $j$  the index of the total spin basis states.

The reader may note that we have dropped the unnecessary labels  $S_i = \frac{1}{2}$  for  $i = 1, 2, 3, 4$  in Expression (3.10). It is also noticeable that the order in which we couple the spins is not important if we are only interested in obtaining a basis made out of vectors which are eigenvectors of  $\vec{S}^2$  and  $\hat{S}_z$ . However, the exact form of the vectors in the new basis may differ depending on the order in which we decide to couple the spins. Given that we intend to automate this process, the last step after knowing how to obtain coefficients  $U_{ij}$  for  $n = 4$  spins is being able to obtain them numerically, which will be discussed in section 3.2. Once we know how to obtain our quadruple spin chain Hamiltonian written in the total spin basis, we are interested in examining the energies of the eigenvectors and the dynamics of a chosen initial state within a specific Hilbert subspace of the Hamiltonian of specific total spin value  $S_T$  and total spin projection in the  $z$  direction  $m_T$ .

As it is done in Ref. [6], we now focus on obtaining the energy plots of the energies of the eigenstates in a chosen subspace of fixed  $S_T$  and  $m_T$ . If  $g$  factor satisfies  $g > 0$ , the Zeeman term tends to lower the energy of the  $|\downarrow\rangle$  states, therefore provided that we want to analyze a triplet subspace ( $S_T = 1$ ), we will choose  $m_T = -1$ . However, since the three three-dimensional triplet subspaces are equal in energy splitting between the eigenstates, any of them could be used in order to study the homogeneous exchange condition of the system. The energy differences between the eigenstates of the chosen block of the Hamiltonian depend on the set of values  $\{J_{ij}\}$ , therefore the homogeneous case where  $J_{ij} = J$  for all couplings between spin  $i$  and spin  $j$  in our system is expected to show a characteristic signature in the energy landscape of the eigenstates of the subspace [6].

We will also be interested in observing how a particular input state  $|\Psi_0\rangle$  evolves over time within this particular subspace of the Hamiltonian that we have chosen. In particular, we are interested in reproducing the oscillations of the probability measurements over time of a certain state in the subspace. Repeating this pattern for different values of the exchange couplings gives us a special characteristic

feature at the points where the exchanges become equal. Specifically, if  $H_s$  is the Hamiltonian for the subspace we are examining, the quantum state as a function of time obeys the Schrödinger equation

$$H_s |\Psi(t)\rangle = i \frac{\partial |\Psi(t)\rangle}{\partial t} \quad \text{with initial condition} \quad |\Psi(t=0)\rangle = |\Psi_0\rangle \quad (3.13)$$

Using the density matrix formalism, we rewrite  $\rho(t) = |\Psi(t)\rangle \langle \Psi(t)|$  and we are left with

$$[H_s, \rho(t)] = i \frac{\partial \rho(t)}{\partial t} \quad (3.14)$$

which is the Von Neumann equation.

In general, the Hamiltonian subspace, as well as the complete Hamiltonian, is allowed to depend on time, in which case Equations (3.13) and (3.14) are still valid. However, in our case, the considered Hamiltonians in this work are time independent. If we are interested in the probability of our final state being our input state  $|\Psi_0\rangle$  during a period of time  $t_f$ , we just need to compute the value

$$P_{|\Psi_0\rangle} = P(\{J_{ij}\}, t_k) = \langle \Psi_0 | \rho(t) | \Psi_0 \rangle = |\langle \Psi_0 | \Psi(t) \rangle|^2 \quad (3.15)$$

for all the chosen  $M$  timesteps  $t_k k \in [1, M]$  we use to discretize our temporal variable  $t \in [0, t_f]$  and some desired sets of  $J_{ij}$  values.

The experimentally possible initializable states put some conditions in what  $|\Psi_0\rangle$  can actually be. Since both the initialization and readout work in the singlet-triplet basis of two spins [6], a natural choice is using an initial state which is a combination of singlets and triplets of pairs of spins. This way, readout of the probability of initial state can also be done experimentally and therefore the results showing these probability oscillations can be compared with experimental data.

## 3.2. Implementation of the code

In the following we will focus on how the procedure depicted in section 3.1 is done numerically. The code that we use to perform the calculations is split into two parts, one for building the Hamiltonian and another one for obtaining the  $U$  matrix and performing the basis transformation. The implementation of these two parts will be discussed in detail in this section. After this is automated, as we previously mentioned, the final step is obtaining the energies of the eigenstates of a chosen subspace with fixed total spin and total spin projection in the  $z$  direction and examining the evolution of  $P_{|\Psi_0\rangle}(t)$  given an initial state belonging to the subspace. This study of  $P_{|\Psi_0\rangle}(t)$  may be repeated for different values of  $J_{ij}$  in order to find the homogeneous exchange condition. This is done by setting a **for-loop** that sweeps through the  $J_{ij}$  values of interest and, for each iteration, computing the time evolution of the initial state under the corresponding subspace of our block-diagonalized Hamiltonian.

### 3.2.1. Four-spin Hamiltonian

Given that a four-spin system is still a small system, we can build its Hamiltonian directly summing up the seven matrices in Equation (3.1) manually, since every summing term can be rewritten as a matrix. These matrices are built from tensor products of four  $N_{sub} = 2$  Hilbert subspaces. Naturally, this cannot be the case when we study larger systems. The way the Hamiltonian is built for the simulations with larger number of spins is automated. However, this will be discussed in the following chapter.

### 3.2.2. Basis transformation

The creation of the matrix  $U$  to basis-transform the Hamiltonian to the total spin basis is obtained from the C.-G. coefficients of a composite system of four  $\frac{1}{2}$ -spins. The first step that we want to automatize is getting all the sets of labels (in this case the values  $S_{12}, S_{123}, S_T$  and  $m_T$ ) for all possible basis states of our system, which is what we did manually in Equation (3.9). The way this is done is by using

$$S_{new} = S_{old} \pm \frac{1}{2} \quad \text{if} \quad S_{new} \geq 0 \quad (3.16)$$

where we use as many  $S_{old}$  as labels we have in a previous step when composing a collection of spins and  $S_{new}$  will be the new labels we obtain. The reader may note that this is only valid for coupling spins in a sequential way, the value “ $\frac{1}{2}$ ” in Equation (3.16) represents the new one being added. Two last considerations may be remarked, the first one is that all the intermediate coupling total spin labels must be stored because we need them for the C.-G. coefficients. The second one is that this method is relatively easy to numerically implement in a general way for any number  $n$  of spins we consider and this is the reason we decided to do it this way.

Once we have all the total spin labels (along with the intermediate ones), the last  $m_T$  label for each state is obtained by simply making  $2S_T + 1$  copies of the labels and assigning an  $m_T$  final label to each of these copies according to

$$m_T = -S_T, -S_T + 1, \dots, S_T - 1, S_T \quad (3.17)$$

We should end up with  $2^n$  sets of labels corresponding to our new basis states.

In the second step we just need to **for-loop** over all possible basis states, as we show in the sums of Equation (3.10) and repeat that for every single set of labels that we have. The reason why the sum is over all  $m_i$  product basis labels except one is because fixing the  $m_T$  value already fixes one of them, which we choose to be the last one  $m_n$ . Therefore, all the missing  $U_{ij}$  elements are zero and we do not need to compute them. Another consideration we may note is that in order to see a properly block-diagonalized Hamiltonian we also need to do some intermediate steps such as sorting our new vectors by same  $S_T$  value or ordering their  $m_T$  value within the same total spin group before using them to create the  $U$  the matrix.

### 3.2.3. Code checks

Apart from checking the code by reproducing Ref. [6] results, we also may comment on some other simple checks that will help us to validate the correctness of our future results. In the first place, we have checked that the Hamiltonian matrices we have, in either of the basis we display it, are Hermitian. Correspondingly, the  $U$  matrix is always checked to be unitary. We have also made sure that the order of the tensor product operation is the same both for the state vectors and the matrices we use throughout the whole simulation, or in other words that the notation remarks given in chapter 1 are consistent with our code.

## 3.3. Tuning a four-spin chain

Now that our tool is ready, we can start getting results. We may start by analyzing the shape of the Hamiltonian. In Figure 3.1a we can see the characteristic shape of the Hamiltonian for a quadruple spin chain with Heisenberg spin-spin interaction and single spin Zeeman splitting in the product basis. Looking at Figure 3.1b we can see the same Hamiltonian in the total spin basis. We can clearly see its block diagonal shape, which splits the Hamiltonian into two singlet, three triplet and one quintuplet subspace, which is consistent with Ref. [6]. It has also been checked that the energy gaps between the three triplets are the same, therefore the eigenstates of each one of the triplets become degenerate in energy with respect to their similar eigenstate in a different triplet when  $\tilde{B} = 0$ , and that all the quintuplet eigenstates are only split in energy when  $\tilde{B} \neq 0$  [6].

Now that we are able to obtain the block-diagonalized Hamiltonian, we are interested in analyzing the eigenenergies of one of the triplet subspaces, specifically the one characterized by  $S_T = 1$  and  $m_T = -1$  (see Figure 3.1b). This subspace is the one chosen because it is energetically favoured by the magnetic field. It must be noted that in Ref. [6], the sign of the  $g$  factor ( $g < 0$ ) makes the  $m_T = 1$  subspace to be the favoured one but the behavior within the subspace is the same in both cases. The eigenenergies of this chosen Hilbert subspace are obtained by exact diagonalization of the matrix, in this case a three by three matrix. The routine that allows us to do that is already built in QuTiP. Likewise, we are also interested in the time evolution of the initial state  $|T\_S\rangle$ , which is obtained using a density matrix solver (DM solver) which was developed in-house by Stephan Philips. Occasionally,

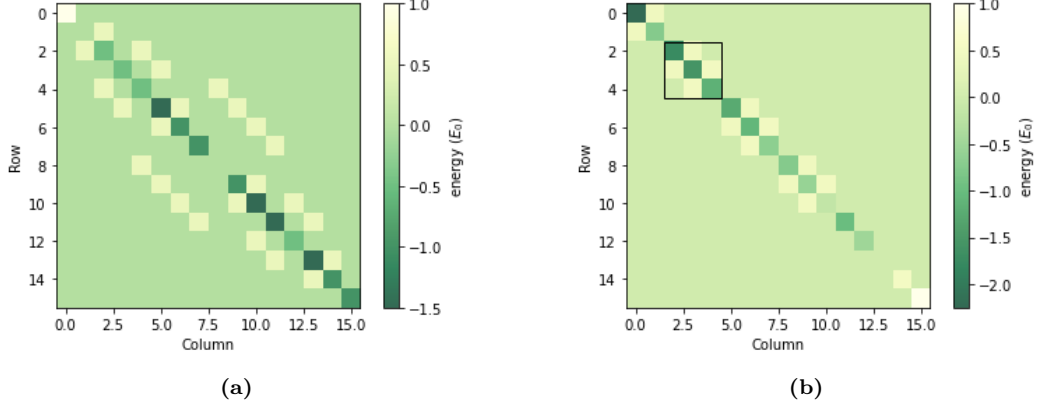


**Figure 3.1:** Representation of the Hamiltonian matrix for the quadruple spin chain (Equation (3.1)) in the homogeneous regime ( $J_{ij} = 1$  for every possible nearest neighbors  $i$  and  $j$  of the system) and for  $\tilde{B} = 0.5$ . (a) The Hamiltonian is represented in the product basis. (b) The Hamiltonian is represented in the total spin basis. The first triplet (enclosed in a black square) is the subspace with  $S_T = 1$  and  $m_T = -1$ .

the time-evolution solver available in QuTiP is also used.

Similarly as the authors propose in Ref. [6], the way we sweep the values  $J_{ij}$  is done as it follows. Having a four-spin chain with no periodic boundary conditions leaves us with three different coupling parameters to play with:  $J_{12}$ ,  $J_{23}$  and  $J_{34}$ . In order to obtain the homogeneous exchange condition throughout the chain, a two step process is proposed [6]. The first step of the process consists of antisymmetrically sweeping exchanges  $J_{12}$  and  $J_{34}$  keeping the mid coupling  $J_{23}$  at a constant value. By “antisymmetric sweeping” we mean that we increase the value of  $J_{34}$  and we decrease the value of  $J_{12}$  keeping  $J_{12} + J_{34}$  constant throughout the whole sweeping process. We will use this concept throughout the development of this project. The evolution of the eigenenergies of the subspace as a function of  $J_{12} - J_{34}$  is presented in Figure 3.2.

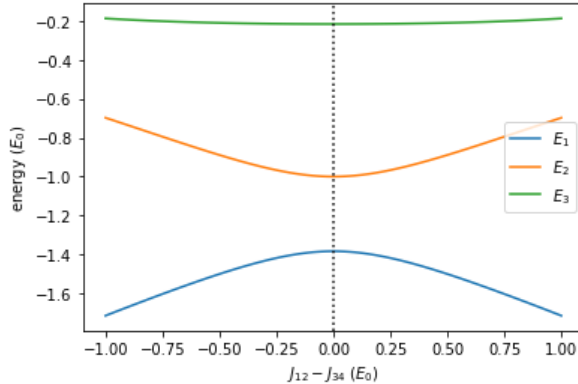


**Figure 3.2:** Energies of the eigenstates of the  $S_T = 1$  and  $m_T = -1$  triplet subspace ordered from lower ( $E_1$ ) to higher ( $E_3$ ) energy as a function of the difference of exchange couplings  $J_{12} - J_{34}$ . Middle exchange coupling is set to  $J_{23} = 0.6$ . The dotted line indicates the point of crossing of the exchanges. In this case, the value of  $J_{34}$  increases from  $J_{34} = 0.5$  to  $J_{34} = 1.5$  keeping  $J_{12} + J_{34}$  therefore  $J_{12}$  decreases from  $J_{34} = 1.5$  to  $J_{34} = 0.5$ .

From Figure 3.2, we can see that when the values of  $J_{12}$  and  $J_{34}$  cross, in this case at  $J_{12} = J_{34} = 1$ , there is a minimum of the energy gap between the first and the second eigenstates. Notably, the actual value of the gap depends on the value of the exchange coupling  $J_{23}$  but the feature we leverage in order to detect this crossing point ( $E_1$  maximizing and  $E_2$  minimizing) does not. Also, the value for which the side exchange couplings are homogeneous between themselves, in this case 1, is arbitrary, so the system would behave the same way if  $J_{12}$  and  $J_{34}$  crossed at a different value.

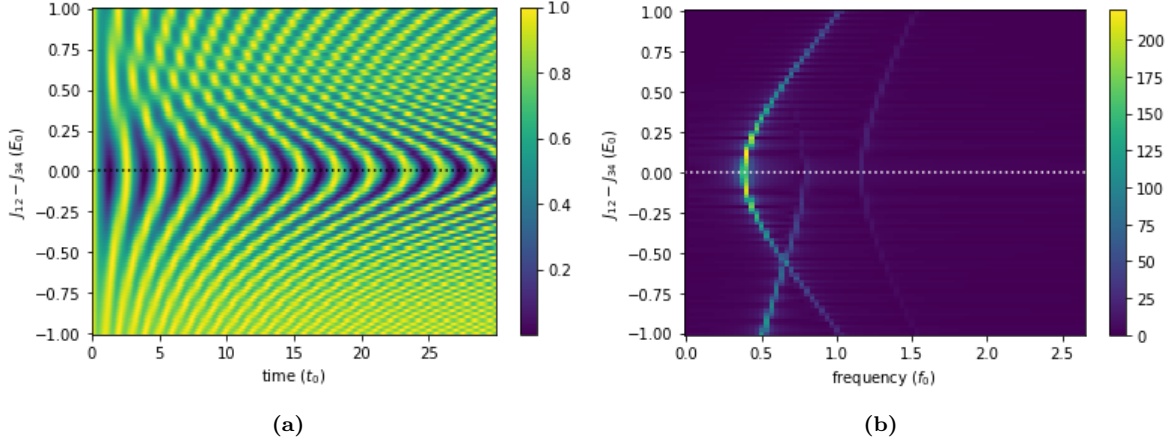


**Figure 3.3:** Time evolution of an initial state of the quadruple spin chain. **(a)** Oscillations of the probability of measuring state  $|T_S\rangle$  as a function of time and the difference of exchange couplings  $J_{12} - J_{34}$ . Middle exchange coupling is set to  $J_{23} = 0.6$ . The colorbar indicates the value of the probability of finding the state in state  $|T_S\rangle$ . **(b)** Fourier transform of the left panel and the colorbar gives a range of the values of the dominating frequency amplitudes and the dotted line indicates the point  $J_{12} = J_{34}$ .

The evolution over time of our initial state  $|T_S\rangle$  can be seen for different values of  $J_{12} - J_{34}$  in Figure 3.3a, which shows that the probability of measuring the initialized state oscillates differently over time as a function of  $J_{12} - J_{34}$ . Since the frequency of oscillation is equal to the energy gap between the eigenstates of the subspace, we can clearly see that there is a minimum in the most visible frequency of these oscillations at  $J_{12} = J_{34}$ , corresponding to the minimum energy gap  $E_2 - E_1$ . The plot showing the Fourier transform of these oscillations (Figure 3.3b) allows us to see this more clearly and shows the three frequencies associated with the three different energy gaps of the subspace we are analyzing. As we mentioned, using  $|T_S\rangle$  as our initial state we can experimentally detect the moment of exchange-crossing using the energy gap between the first and the second eigenstates and therefore get the information of how to tune exchanges  $J_{12}$  and  $J_{34}$  to the same value experimentally. Comparing these results with the ones obtained in Ref. [6] we see perfect qualitative agreement. Quantitative agreement cannot be verified with the approach we have followed regarding the use of exchanges as the independent variables of our results, which on the other hand has notably simplified the study method.

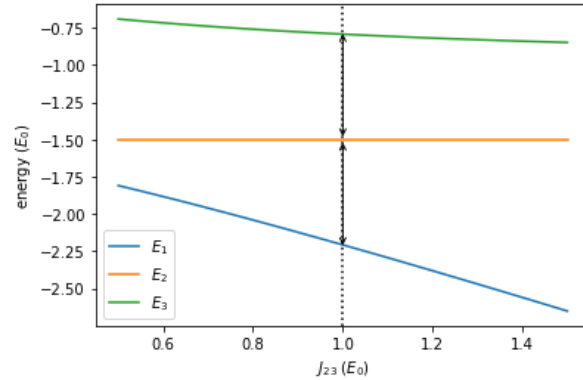


**Figure 3.4:** Energies of the eigenstates of the  $S_T = 1$  and  $m_T = -1$  triplet subspace ordered from lower ( $E_1$ ) to higher ( $E_3$ ) energy as a function of the exchange coupling  $J_{23}$ . The rest of the exchange couplings are set to  $J_{12} = J_{34} = 1$ . The black arrows indicate the point where the energy gaps  $E_2 - E_1$  and  $E_3 - E_2$  have the same value.

The second step of the protocol consists on tuning the exchange  $J_{23}$  to the same value of the other two. To reproduce results obtained in Ref. [6], we follow a similar reasoning as we did for the first step.

Sweeping the middle exchange from  $J_{23} = 0.5$  to  $J_{23} = 1.5$  we are left with the results displayed in Figures 3.4 and 3.5.

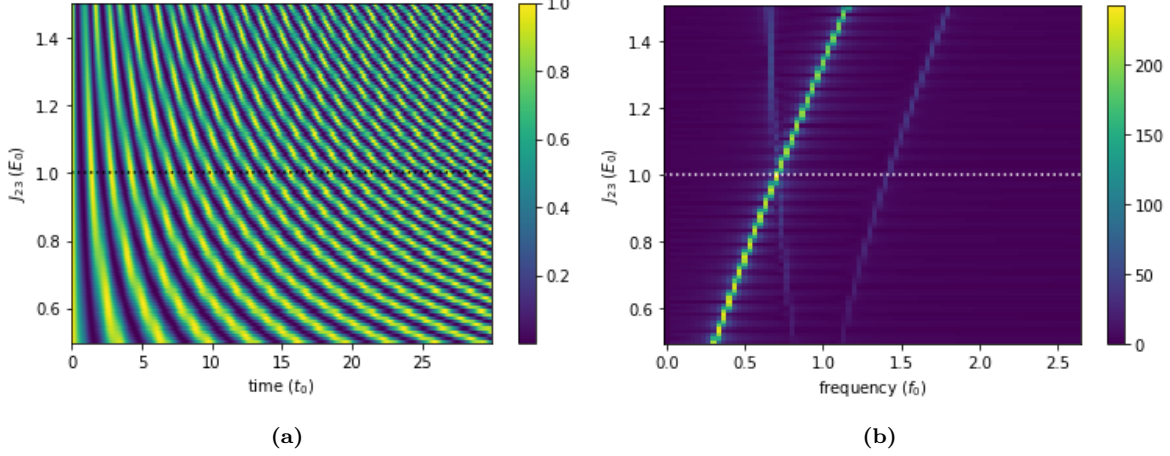


**Figure 3.5:** Time evolution of an initial state of the quadruple spin chain. (a) Oscillations of the probability of measuring state  $|T-S\rangle$  as a function of the exchange coupling  $J_{23}$ . The rest of the exchange couplings are set to  $J_{12} = J_{34} = 1$ . The colorbar indicates the value of the probability of finding the state in  $|T-S\rangle$ . (b) Shows the Fourier transform of (a) and the colorbar gives a range of the values of the dominating frequency amplitudes. The dotted lines indicate the point of crossing of the exchanges.

In Figure 3.4 we see that at the complete homogeneous condition ( $J_{12} = J_{23} = J_{34} = 1$ ), equal energy gaps between adjacent eigenstates is satisfied. The authors propose to use this as a feature to detect the homogeneous condition experimentally. Similarly, using  $|T-S\rangle$  as the initial state, the probability of measuring this same state over time also gives an oscillating pattern, which can be observed in Figure 3.5a. In Figure 3.5b we see that exactly when  $J_{23} = 1$  the two frequencies associated with the energy gaps of these above-mentioned pairs of eigenstates cross, manifesting equal spacing in energies and therefore allowing us to detect our condition of interest. These results also agree with the ones obtained in Ref. [6].

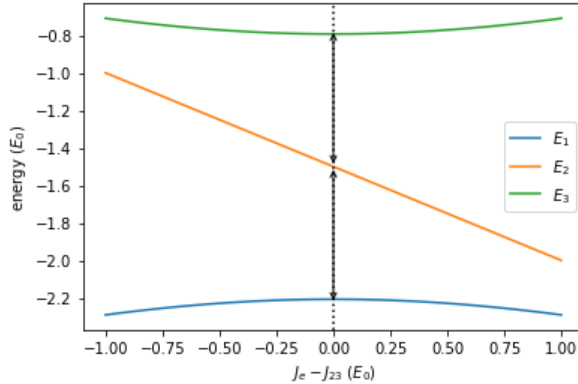


**Figure 3.6:** Energies of the eigenstates of the  $S_T = 1$  and  $m_T = -1$  triplet subspace ordered from lower ( $E_1$ ) to higher ( $E_3$ ) energy as a function of  $J_e - J_{23}$  with  $J_{12} = J_{34} = J_e$ . The black arrows indicate the point where the energy gaps  $E_2 - E_1$  and  $E_3 - E_2$  have the same value and the dotted line indicates the point in which the chain becomes homogeneous in terms of exchanges.

As a side note, it is also interesting to see what happens to the eigenenergies of this second step when we attempt to do what we previously called antisymmetric sweep. This consists on instead of sweeping  $J_{23}$  directly, defining  $J_{12} = J_{34} = J_e$  and using the variable  $J_e - J_{23}$  for the sweeping, keeping  $J_e + J_{23} = 2$ . It is illustrative to see that now the eigenenergy spectrum still gives equal energy gap

between adjacent eigenstates at the crossing point but the single signal corresponding to the energy gap between the first and the third eigenstates would be enough to determine the homogeneous condition because of the special way the energy of these eigenstates depends on the variable  $J_e - J_{23}$ . These observations can be derived from Figure 3.6.

This behavior gives us insight which may be useful when attempting to tune other types of systems in a similar way. On the one hand, when seeking for exchange-crossing conditions, we realize that it is not only important which exchange value we sweep but also the way in which we sweep them. Naturally, depending on how we do these sweepings experimentally, certain sweepings may be more challenging than others. On the other hand, because the energy spacing between states has to be the same for all these cases, once we choose which exchanges to sweep, we can always rely on using frequency crossings (if there are any) to tune no matter the way we do the sweeping.

### 3.4. Tuning a four-spin plaquette

It is also interesting to look at how the authors of Ref. [7] tune a four-spin plaquette into the homogeneous regime, which is analogous to the simplest case of a spin ladder ( $2 \times 2$ ). A scheme of this geometry can be found in Figure (3.7). It should be noted that the labelling of the spins is not the same as the one they use in Ref. [7].

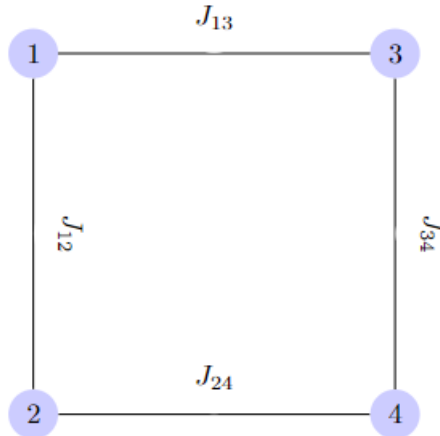


**Figure 3.7:** Geometrical representation and labelling of the spins and exchanges in a four-spin plaquette.

In order to investigate the homogeneous exchange condition, a sensible way to proceed is to antisymmetrically sweep symmetrical pairs of exchange couplings, specifically  $J_{12}$  with  $J_{34}$  and  $J_{13}$  with  $J_{24}$  using the variables  $J_{12} - J_{34}$  and  $J_{13} - J_{24}$  respectively [7]. These are steps one and two respectively. After both horizontal exchanges have the same value and both vertical exchanges are also equalized (in general at a different value with respect to the horizontal ones), a final step consisting on equalizing the value of these two pairs of exchanges is carried out in a similar way as described for the other two.

Similarly to what we observed in section 3.3, getting a feature of exchange crossing in the first and the second steps does not depend on which value the remaining exchanges have. The energies of the eigenstates as a function of the exchanges for these steps can be found in Figure 3.8 and we can indeed see the exchange crossing feature that can be leveraged to perform the tuning. This allows us to tune  $J_{12} = J_{34} = J_{d1}$  and  $J_{13} = J_{24} = J_{d2}$ .

In order to see the crossing features experimentally, it is proposed to initialize the state  $|S\rangle_{13}|T-\rangle_{24}$  and we let it evolve over time. This state will evolve within the first triplet block of the Hamiltonian. Measuring the probability of the final state being in the  $|T-\rangle_{13}|S\rangle_{24}$  state gives us the results displayed in Figure 3.9 for steps one and two. These results qualitatively agree with the ones presented in Ref.

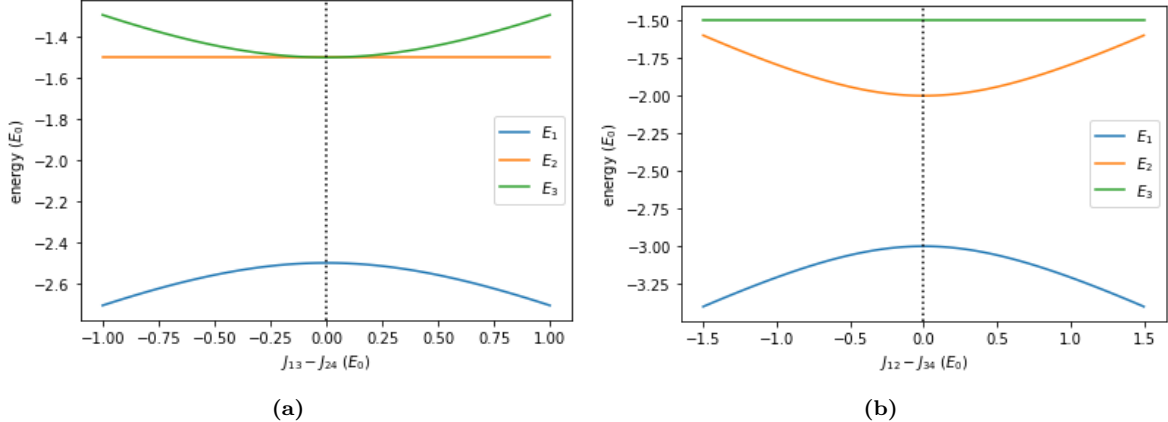


**Figure 3.8:** Energies of the eigenstates of the  $S_T = 1$  and  $m_T = -1$  triplet subspace ordered from lower ( $E_1$ ) to higher ( $E_3$ ) energy for the first (a) and second (b) steps. For the first step the energies are plotted as a function of  $J_{13} - J_{24}$  keeping  $J_{12} = 0.5$  and  $J_{34} = 0.8$ . For the second step the energies are plotted as a function of  $J_{12} - J_{34}$  with a crossing value of  $J_{12} = J_{34} = 1.5$  and  $J_{13} = J_{24} = 1$  kept constant. The dotted lines indicate the point where the swept exchanges become equal.

[7]. It is remarkable to say that this initialize-measure set of states is particularly good to observe the feature given by the second step of the protocol (Figure 3.9b) because it exclusively gives the signal corresponding to the energy difference  $E_2 - E_1$ . In the first step, all three energy gaps between the eigenstates contribute to the oscillations of the probability measurements, making the crossing feature slightly less visible. Using  $|ST-\rangle$  as initial state and measuring  $|T-S\rangle$  for step one allows us to obtain an exclusive signal of frequency  $E_2 - E_1$ .

The third step proposed by Ref. [7] relies on being able to control the values of the horizontal and vertical exchanges maintaining the condition achieved in the previous two steps,  $J_{12} = J_{34}$  and  $J_{13} = J_{24}$ . When a crossing of  $J_{d1}$  with  $J_{d2}$  occurs, a crossing in the energies of the second and third eigenstates can be observed. This can be seen in Figure 3.10, where the sweeping of exchanges is done in two ways. In order to detect the condition of exchange crossing for the third step a sweeping similar to the one shown in Figure 3.10a is done. With a smart choice of an initialize-measure set of states we can obtain an exclusive signal for the energy gaps  $E_2 - E_1$  and  $E_3 - E_1$ , which allows us to distinguish the  $J_{d1} = J_{d2}$  point as the authors utilize in Ref. [7].

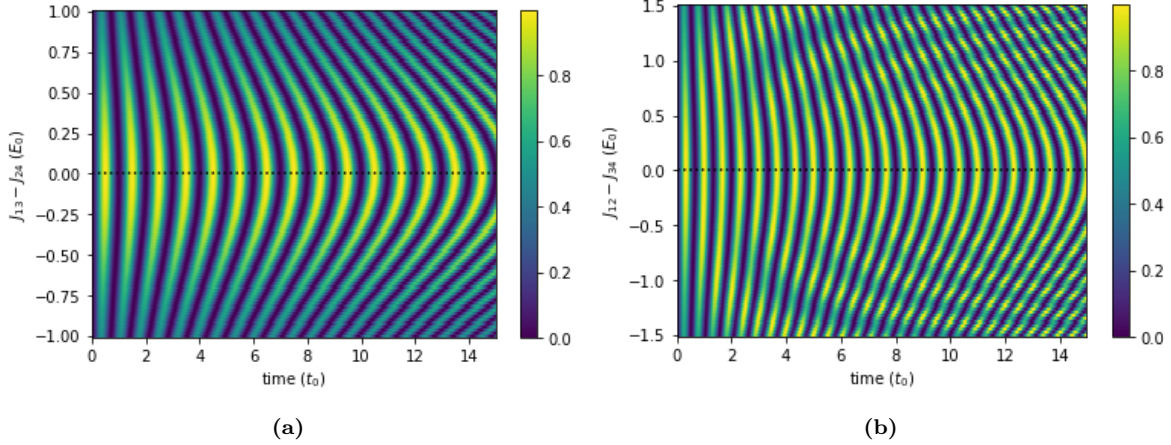


**Figure 3.9:** Time evolution of the initial state of steps one and two of the  $2 \times 2$  spin ladder protocol. The colorbar indicates the probability of measuring the state  $|T_-\rangle_{13}|S\rangle_{24}$ . In both cases the initialized state is  $|S\rangle_{13}|T_-\rangle_{24}$  and the probability of measurement is given as a function of time and the difference of exchange couplings  $J_{13} - J_{24}$  ((a), first step) and  $J_{12} - J_{34}$  ((b), second step). The remaining exchange couplings are set to the same values as we present in Figure 3.8. The dotted lines indicate the point where the swept exchanges become equal.

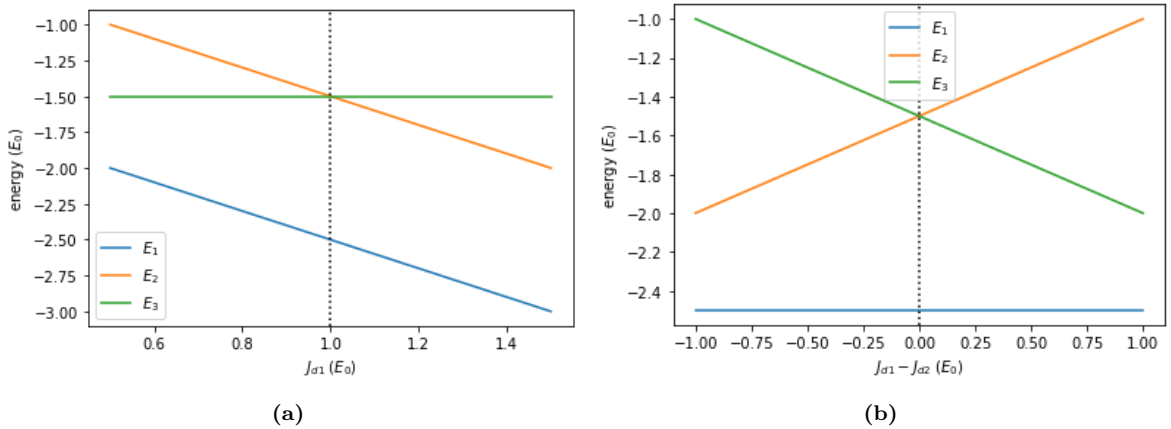


**Figure 3.10:** Energies of the eigenstates of the  $S_T = 1$  and  $m_T = -1$  triplet subspace for the third step as a function  $J_{d1}$  keeping  $J_{d2} = 1$  (a) and as a function of  $J_{d1} - J_{d2}$  (b). The dotted lines indicate the point in which the four-spin plaquette becomes exchange-homogeneous.

# 4

## Generalization and testing

In this chapter, we extend the tool we developed in section 3.2 and prepare it to investigate the steps to follow when attempting to exchange-homogenize small spin systems. After that, we test it with a three spins toy model and we examine some ways that may ease the process of tuning, either experimentally and theoretically.

### 4.1. Generalization of the code

The generalization of the original code for a quadruple spin chain (discussed in subsection 3.3) to an  $n$ -spin chain will also consist of two parts, the creation of the Hamiltonian and the basis transformation procedure. We will first focus on the process of how we can obtain a general Hamiltonian given by Expression (4.1).

$$H_{chain}^{(n)} = H_{Heis,1}^{(n)} + H_{ext}^{(n)} = \sum_{i=1}^{n-1} J_{ii+1} \left( \vec{S}_i \cdot \vec{S}_{i+1} - \frac{1}{4} \right) + \tilde{B} \sum_{i=1}^n \hat{S}_i^z \quad (4.1)$$

Since the way of performing arbitrary number of different tensor products in QuTiP is not trivial, we found that the best way to achieve this is by using a recursive function. We define the objects

$$A_2 = \sigma_x \otimes \sigma_x + \sigma_y \otimes \sigma_y + \sigma_z \otimes \sigma_z - \mathbb{I} \otimes \mathbb{I} \quad (4.2)$$

and

$$B_2 = \sigma_z \otimes \mathbb{I} + \mathbb{I} \otimes \sigma_z \quad (4.3)$$

which are  $4 \times 4$  matrices. Then, it is easy to see that

$$H_{chain}^{(2)} = \frac{J_{12}}{4} A_2 + \frac{\tilde{B}}{2} B_2 \quad (4.4)$$

If our input variable is  $n = 2$  spins, we return the Hamiltonian given in Equation (4.4). We call  $H_{chain}^{(2)}$  the initial chain Hamiltonian and we build it explicitly inside the function. If  $n = 3$ , we call the function for  $n - 1 = 2$  spins and we compute the quantities

$$A_3 = \mathbb{I} \otimes A_2 \quad (4.5)$$

and

$$C_3 = \mathbb{I} \otimes \mathbb{I} \otimes \sigma_z = \mathbb{I}_{(N=4)} \otimes \sigma_z \quad (4.6)$$

Since

$$\begin{aligned}
H_{chain}^{(3)} &= \frac{J_{12}}{4} (A_2 \otimes \mathbb{I}) + \frac{J_{23}}{4} (\mathbb{I} \otimes A_2) + \frac{\tilde{B}}{2} (\sigma_z \otimes \mathbb{I} \otimes \mathbb{I} + \mathbb{I} \otimes \sigma_z \otimes \mathbb{I} + \mathbb{I} \otimes \mathbb{I} \otimes \sigma_z) \\
&= H_{chain}^{(2)} \otimes \mathbb{I} + \frac{J_{23}}{4} (\mathbb{I} \otimes A_2) + \frac{\tilde{B}}{2} (\mathbb{I} \otimes \mathbb{I} \otimes \sigma_z) \\
&= H_{chain}^{(2)} \otimes \mathbb{I} + \frac{J_{23}}{4} A_3 + \frac{\tilde{B}}{2} C_3
\end{aligned} \tag{4.7}$$

and we called the function for  $n = 2$  spins, which is already properly built because it only relies on the initial chain Hamiltonian, we can return our desired Hamiltonian for  $n = 3$ . In general,

$$\begin{aligned}
H_{chain}^{(n)} &= H_{chain}^{(n-1)} \otimes \mathbb{I} + \frac{J_{n-1n}}{4} (\mathbb{I} \otimes A_{n-1}) + \frac{\tilde{B}}{2} (\mathbb{I}_{(N=2^{n-1})} \otimes \sigma_z) \\
&= H_{chain}^{(n-1)} \otimes \mathbb{I} + \frac{J_{n-1n}}{4} A_n + \frac{\tilde{B}}{2} C_n
\end{aligned} \tag{4.8}$$

holds, so our target Hamiltonian only depends on obtaining the quantities  $A_n = \mathbb{I}_{(N=2^{n-2})} \otimes A_2$  and  $C_n$ .

We have just shown that we can build a spin chain Hamiltonian for an arbitrary number of spins, which corresponds to only nearest-neighbor interaction as it can be seen in Equation (4.1). Although a bit more challenging, an arbitrary  $n$  spins ladder Hamiltonian (4.9) can also be obtained in a similar way. As mentioned in chapter 2 and keeping in mind the labelling for the spins presented in Figure 2.2, we can make use of the next-nearest-neighbor Heisenberg Hamiltonian to construct the ladder Hamiltonian.

$$H_{ladder}^{(n)} = H_{chain}^{(n)} + H_{Heis,2}^{(n)} = H_{chain}^{(n)} + \sum_{i=1}^{n-2} J_{ii+2} \left( \vec{S}_i \cdot \vec{S}_{i+2} - \frac{1}{4} \right) \quad \text{with} \quad J_{23} = J_{45} = J_{67} = \dots = 0 \tag{4.9}$$

Certainly, rewriting the ladder Hamiltonian this way invites us to use again a recursive function for the next-nearest-neighbors term. Therefore, using

$$H_{Heis,2}^{(3)} = \frac{J_{13}}{4} A'_3 \tag{4.10}$$

as our initial ladder Hamiltonian, with

$$A'_3 = \sigma_x \otimes \mathbb{I} \otimes \sigma_x + \sigma_y \otimes \mathbb{I} \otimes \sigma_y + \sigma_z \otimes \mathbb{I} \otimes \sigma_z - \mathbb{I} \otimes \mathbb{I} \otimes \mathbb{I} \tag{4.11}$$

and

$$A'_n = \mathbb{I} \otimes A'_{n-1} = \mathbb{I}_{(N=2^{n-3})} \otimes A'_3 \tag{4.12}$$

we can obtain an arbitrarily long Heisenberg Hamiltonian for a spin ladder using the relation

$$H_{Heis,2}^{(n)} = H_{Heis,2}^{(n-1)} \otimes \mathbb{I} + \frac{J_{n-1n}}{4} A'_n \tag{4.13}$$

Note that the Zeeman splitting of the magnetic field is already included in the chain Hamiltonian for all the spins of the ladder, so there is no need to include it in the next-nearest-neighbors term.

If periodic boundary conditions to our spin chain are desired, only an extra matrix is required to be summed up to our matrix Hamiltonian, so this does not entail any difficulty. In particular, if we know the size of the quantum system (the number of spins  $n$ ) we have

$$H_{chain}^{(n)p} = H_{chain}^{(n)} + J_{1n} \left( \vec{S}_1 \cdot \vec{S}_n - \frac{1}{4} \right) \tag{4.14}$$

Regarding the generalization of the basis transformation of the Hamiltonian, the only way it differs from the scheme presented in section 3.2 is that now the number of spins  $n$  is an input parameter instead

of being fixed to  $n = 4$ . Despite being the most challenging task to automatize, we finally managed overcome this problem by appealing to recursiveness, similarly as what we did for constructing the general Hamiltonian, and additional `for-loops` ranging a variable that goes over the number of spins  $n$ . For example, to obtain the labels of the Clebsh-Gordan coefficients for a collection of  $n$  spin objects, we exploit the fact that we need to consider all the possible  $S_{12\dots(n-1)}$  values for  $n - 1$  spins and couple them with an extra  $S_n = \frac{1}{2}$  spin, hence the recursion. Moreover, we have to add an extra `for-loop` to include an arbitrary number of Clebsh-Gordan coefficient products in an expression resulting from generalizing the one provided in Equation (3.10) for  $n = 4$ .

Lastly, the process of choosing a subspace of our block-diagonal Hamiltonian and letting a given initial state evolve in time is the same as depicted in section 3.2. For the time being, we will restrict ourselves exclusively using the most energetically favorable  $(\frac{n}{2} - 1)$ -total spin subspace. We may refer to this subspace with the name of “single-singlet” subspace. The code developed in this project is available in our GitHub repository.

## 4.2. Testing

We start by examining the most simple case we can consider, corresponding to a chain of  $n = 3$  spin- $\frac{1}{2}$  particles. It is interesting to start to obtain results with the smallest systems we can think of because we can consider them as parts of a larger spin system that we eventually may want to tune. Also, for a three-spin chain, it is still easy to obtain results analytically, which help us to make sure that our general code works properly. The Hilbert space of this type of triple spin systems is of dimension  $2^3 = 8$  and it can be split into two doublet subspaces and a quadruplet. The shape of the Hamiltonian matrices in the product and total spin basis can be seen in Figure 4.1.

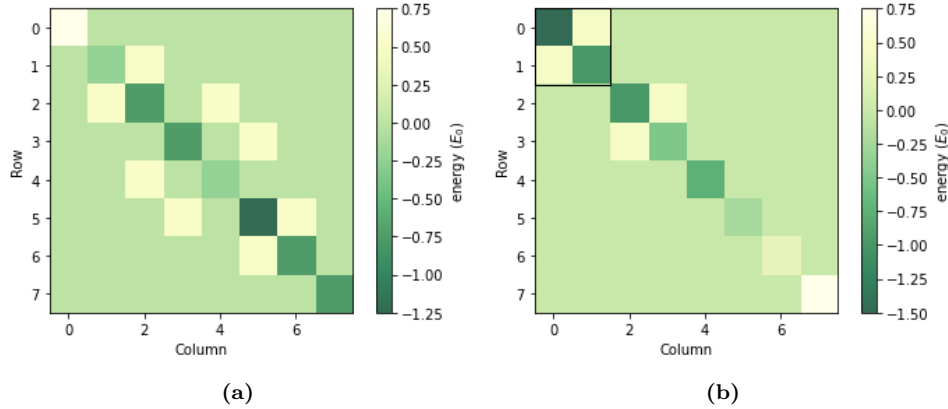


**Figure 4.1:** Representation of the Hamiltonian matrix for the triple spin chain in the homogeneous regime ( $J_{ij} = 1$  for every possible nearest neighbors  $i$  and  $j$  of the system) and for  $\tilde{B} = 0.5$ . (a) The Hamiltonian is represented in the product basis. (b) The Hamiltonian is represented in the total spin basis. The first doublet (black square) is the subspace with  $S_T = \frac{1}{2}$  and  $m_T = -\frac{1}{2}$ .

Given that now the Heisenberg Hamiltonian of this system only has two parameters, the most straightforward way to obtain the homogeneous exchange condition is to use a single step process where we sweep the two exchanges  $J_{12}$  and  $J_{23}$  antisymmetrically. Since the energy splitting among the states in the quadruplet is only due to the Zeeman term, in order to see how the energies of the eigenstates of a specific subspace depend on the values  $J_{ij}$  we necessarily need to examine a doublet subspace. The first doublet, with  $S_T = \frac{1}{2}$  and  $m_T = -\frac{1}{2}$  is the one we will use to examine the homogeneous condition for being lower in energy. The energy of its eigenstates as a function of  $J_{12} - J_{23}$  can be seen in Figure 4.2.

We can observe that, similarly as we observed in chapter 3, there is a clear signature of homogeneous exchange. At the exchange crossing point we observe that, within the considered subspace, the energy of the first eigenstate maximizes and the energy of the second eigenstate minimizes. Therefore, the energy gap between these two eigenstates becomes minimum at the homogeneous point, which will correspond

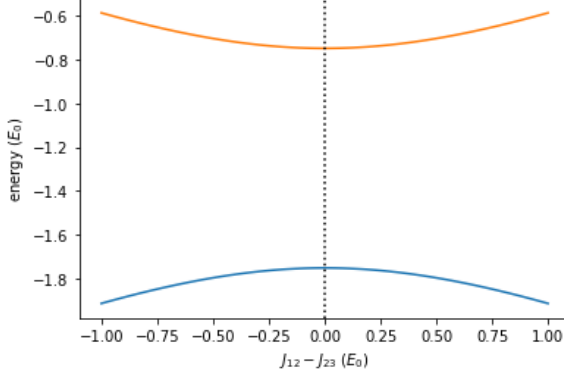


**Figure 4.2:** Eigenenergies of the  $S_T = \frac{1}{2}$  and  $m_T = -\frac{1}{2}$  doublet subspace ordered from lower ( $E1$ ) to higher ( $E2$ ) energy as a function of the difference of exchange couplings  $J_{12} - J_{23}$  for a triple spin chain. The dotted line indicates the point where  $J_{12} = J_{23}$ .

to a minimum of oscillation frequency if we input a superposition of these two states as initial state. If we now plot the coherent oscillations of an input state  $|S \downarrow\rangle$ , we observe the results displayed in Figure 4.3.

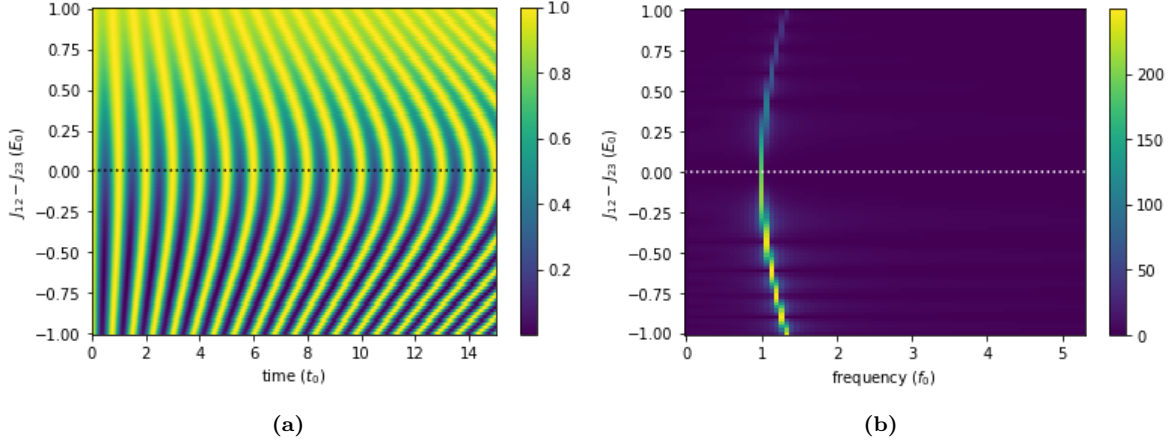


**Figure 4.3:** Time evolution of an initial state of the triple spin chain. (a) Oscillations of the probability of measuring state  $|S \downarrow\rangle$  as a function of time and  $J_{12} - J_{23}$ . The colorbar indicates the value of the probability of finding the state in  $|S \downarrow\rangle$ . (b) Fourier transform of (a). The colorbar indicating a range of the values of the dominating frequency amplitudes. The dotted line indicates the point where both exchanges become equal.

As we already mentioned, for these small systems, it is reasonable to perform analytical calculations of the Hamiltonian subspace we are considering. This is especially useful if we want to extract the value of  $J_{12} = J_{34} = J$  that our system has, in the homogeneous exchange case, only from the experimental results we would get if this process was carried out in the lab, which would be essentially Figure 4.3. In other words, we are interested in obtaining the analytical formula that tells us how the energy difference of the eigenstates of the considered subspace as a function of the  $J_{ij}$  values.

Using  $|J_{12} = 0, J_T = \frac{1}{2}, m_T = -\frac{1}{2}\rangle = \frac{1}{\sqrt{2}}(|3\rangle - |5\rangle) = |S \downarrow\rangle$  and  $|J_{12} = 1, J_T = \frac{1}{2}, m_T = -\frac{1}{2}\rangle = \frac{1}{\sqrt{6}}(|3\rangle + |5\rangle - 2|6\rangle) = \frac{1}{\sqrt{3}}(|S\rangle_{13}|\downarrow\rangle_2 + |\downarrow S\rangle)$  as the first doublet basis vectors in the total spin basis, we can compute the matrix elements of this subspace analytically, resulting in a doublet subspace Hamiltonian given by

$$H_{(\frac{1}{2}, -\frac{1}{2})} = \begin{pmatrix} -J_{12} - \frac{1}{4}J_{23} - \frac{\tilde{B}}{2} & \frac{3}{4\sqrt{3}}J_{23} \\ \frac{3}{4\sqrt{3}}J_{23} & -\frac{3}{4}J_{23} - \frac{\tilde{B}}{2} \end{pmatrix} \quad (4.15)$$

Diagonalizing the doublet subspace matrix (Equation (6.4)), we can obtain the energy gap between the two eigenstates, which is given by

$$\Delta E_{1,2} = \sqrt{J_{12}^2 + J_{23}^2 - J_{12}J_{23}} \quad (4.16)$$

In order to check our analytical derivation of Equation (4.16), the energy landscape of the eigenstates has also been computed for the same range of values we use to obtain Figure 4.2. We indeed find complete correspondence both for the energy values of the eigenstates and also for the energy gap between them. In the homogeneous exchange case, Equation (4.16) reduces to  $\Delta E_{1,2} = J$ . Therefore, the  $J$  value of the triple spin system is given by  $J = f_{min}$ , where  $f_{min}$  is the oscillation frequency we can extract from the right panel of Figure 4.3.

Some final tests have been made for systems related to the three-spin chain. On the one hand, we thought it could be useful to examine the three-spins plaquette. We have found that this geometry is intrinsically bond to magnetic frustration, in particular its exchange-homogeneous regime. Some of the results we obtained can be found in Appendix A. In addition we also tested the single-step three-spin chain protocol in a six-spin ladder and we tried to tune this latter system into the homogeneous regime assuming that we could start from tuning two triple spin chains within the big six-spin system. Some of the results we obtained are shown in Appendix B.

## 4.3. Partial readout

So far, all of our results rely on being able to measure the probability of our system to be in a certain state. As we have seen, these measurements are repeated for different evolution times and sets of exchange values to obtain plots similar to the ones shown in Figure 4.3. For an increasing number of spins, it becomes hard to reliably read out the state of our complete system. For example, as we previously introduced, a correct readout of the system using PSB readout on the  $2 \times 4$  spin ladder would require to measure the state of four pairs of spins correctly. Thus, it is worth to see if we can still obtain enough information about the exchange crossing features only reading out the state of a reduced number of the spins. In this section we will investigate the process and consequences of a partial readout for the four-spin chain.

### 4.3.1. Theory and implementation

In order to model the fact of experimentally performing readout to a subsystem of our collection of spins in our computer simulations, we will make use of the reduced density operator theory. The reduced density operator is a mathematical tool that allows us to describe the state of a subsystem of a larger quantum system. In general, if we consider a composite quantum system consisting of two subsystems, labeled  $A$  and  $B$ , the reduced density operator for system  $A$  is given by

$$\rho^A = \text{tr}_B(\rho^{AB}) \quad (4.17)$$

where  $\text{tr}_B$  means the partial trace over the subsystem  $B$ . A short justification why this operation should correctly describe subsystem  $A$  is that it provides the correct measurement statistics for measurements made on this subsystem [12]. Then, if we apply this operation to the density matrix of the system after the time evolution, it gives us the density matrix of a subsystem. This density matrix gives us the correct statistics describing what would happen if we only experimentally performed readout of the state of the spins belonging to that subsystem.

Despite all of this, there is no obvious reason why only reading out a subsystem should give us enough information about the whole system in order to be able to extract the probability measurements that show a feature at certain exchange crossing points, as we have been doing according to the method proposed by Ref. [6]. However, the fact that the reduced density operator provides a way to quantify entanglement between subsystems gives us some hints towards that this is indeed the case.

The way this was implemented in the code that we use for our simulations is the following. The first steps remain the same, these include settling up the Hamiltonian and the initial state in the computational basis, applying the base transformation and letting the initial state evolve under its

corresponding subspace in the transformed Hamiltonian. However, differently as we have been doing so far, the expectation value of a certain state cannot be taken yet. Instead, the final state is retrieved from the time-evolution solver. Given that using the DM solver presented some technical difficulties for this step, all the time-evolution simulations in which we aim to take a partial readout of the system are done using exclusively QuTiP functionalities. After that, the retrieved final state is transformed back to the computational basis where we can easily trace out the information of the desired number of spins.

### 4.3.2. Results and experimental verification

In order to test the results of our simulations, we go back to the four-spin chain protocol presented in section 3.3. Specifically, we test the simulation with partial readout with the first step of the protocol reading out only the information of a single pair of spins and a single spin. However, given the presented method of spin-state readout, we are not able to perform single spin measurements<sup>1</sup>. Despite of this, we still find interesting to show the findings for this case as well. The results that we obtain attempting to readout state  $|S\rangle_{34}$  and  $|\uparrow\rangle_1$  are presented in Figure 4.4.

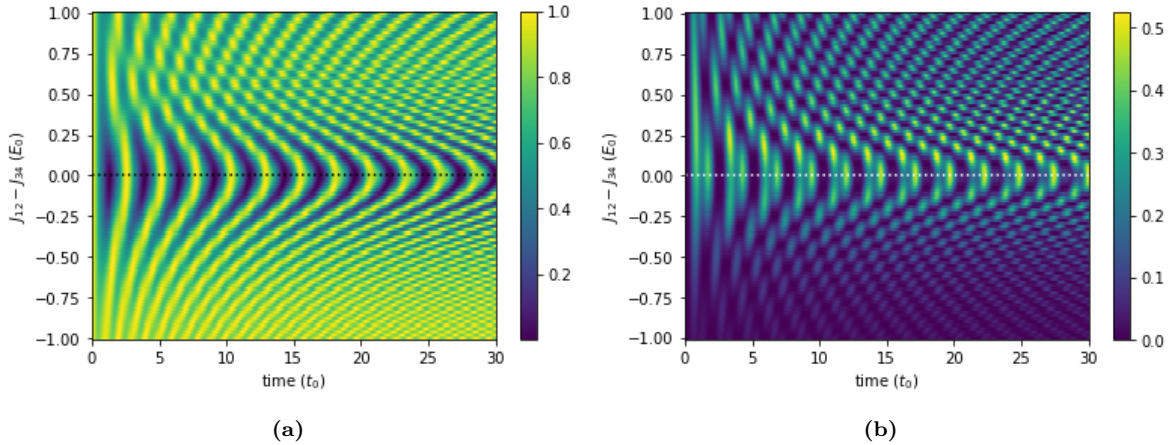


**Figure 4.4:** Time evolution of an initial state of the quadruple spin chain. (a) Oscillations of the probability of measuring state  $|S\rangle_{34}$  (on spins 3 and 4) as a function of time and the difference of exchange couplings  $J_{12} - J_{34}$ . (b) Oscillations of the probability of measuring state  $|\uparrow\rangle_1$  (on spin 1) as a function of time and the difference of exchange couplings  $J_{12} - J_{34}$ . Middle exchange coupling is set to  $J_{23} = 0.6$  for both cases. The colorbar indicates the value of the probability of finding the measured state for both plots respectively initializing  $|T-S\rangle$ .

We can see that both cases reliably show the exchange crossing feature in terms of a frequency minimum in one of the frequency signals. In fact, in the case of measuring  $|S\rangle_{34}$  we find the same pattern that we found in Figure 3.3. An explanation about why this is the case is given further in the text. In the case of measuring  $|\uparrow\rangle_1$ , we can see that the output has more contribution of energy gaps that are not  $E_2 - E_1$ , allowing us to conclude that this measurement would be less clear for our purposes. Nonetheless, we can see that the visibility of the oscillations is reduced (note the scale of the colorbar in Figure 4.4b). In any case, these results are interesting because they show that the information obtained with a few spins or even a single spin readout could, in principle, give us information to tune a distant exchange coupling.

The partial readout has also been tested with measuring  $|S\rangle_{14}$ ,  $|S\rangle_{24}$  and  $|S\rangle_{23}$ . The plots can be found in the Appendix C, Figure C.1, and some interesting results are worth to be commented. For example, we may note that in some cases, the visibility of the oscillations is lower with respect to Figure 3.3, contrarily as observed when measuring  $|S\rangle_{34}$ . Additionally, for the three cases but most noticeably when measuring this state  $|S\rangle_{23}$ , we find an average higher probability of measuring this state for  $J_{12} - J_{34} < 0$ . In this sense, could use these probability results to get more information about the value of the exchanges beyond just the crossing point of the exchanges we are sweeping.

<sup>1</sup>In principle, single spin readout in quantum dots can be implemented using Elzerman-style readout [3], given that the spin is next to a reservoir and that the spin splitting is large enough compared to the reservoir broadening.

The plot with the measurements of  $|S\rangle_{14}$  also manifests that the most visible frequency is in this case the one associated with the energy gap  $E_3 - E_1$  instead of  $E_2 - E_1$ , as we find in section 3.3. This is also an interesting result because even though it is already known that the initial state affects the visibility of the different frequency signals of the subspace [6], the state we use for measurement appears to make an impact on this as well. This indicates us that the state we use for readout actually helps in enhancing or suppressing the frequency signals we are interested in. PSB-based readout does not allow us to obtain results for the measurement of  $|S\rangle_{13}$  and  $|S\rangle_{14}$  experimentally, but it does allow us to obtain them when measuring  $|S\rangle_{23}$ . Moreover, correlations of measurements could be used to extract probability measurements indirectly.

Lastly we compare our findings with the raw data of Ref. [6]. Unfortunately, once again, because of the readout technique based on PSB, we can only do the testing for the case in which we readout state  $|S\rangle_{34}$ . For this first step, four rounds of measurements are done in Ref. [6] after letting initial state  $|ST_+\rangle^2$  evolve over time. These four cases include the measurements of states  $|SS\rangle$ ,  $|ST\rangle$ ,  $|TS\rangle$  and  $|TT\rangle$ . Given that we are interested in obtaining a plot where the probability of measuring  $|S\rangle_{34}$  is displayed, we are only interested in the first and third sets of data out of the four. We can write

$$P_{|S\rangle_{34}} = P_{|TS\rangle} + P_{|SS\rangle} \quad (4.18)$$

Since our Hamiltonian conserves the total spin and total spin projection of the states (and assuming that there is no leakage outside the subspace  $S_T = 1$ ,  $m_T = -1$ ), we can substitute  $P_{|TS\rangle} = P_{|T_+S\rangle}$  and set  $P_{|SS\rangle} = 0$ . This tells us that the probability of measuring the initial state is exactly equal to the probability of measuring singlet in spins 3 and 4. This result would be supported by the fact that Figure 3.3a and 4.4a give the same output. This is also supported by the experimental data, shown in Figure 4.5.

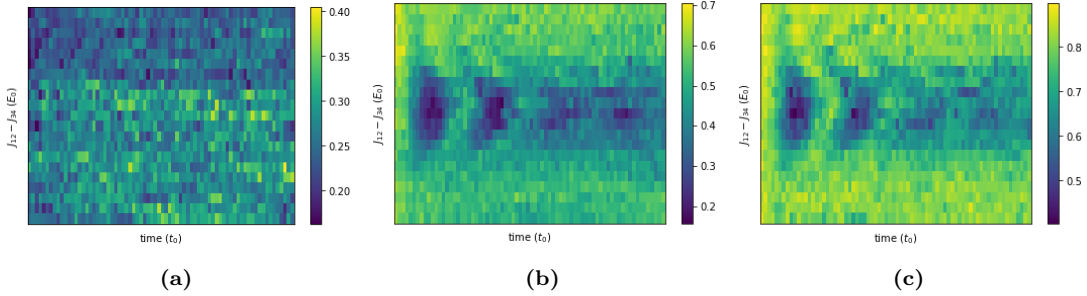


**Figure 4.5:** (a) Experimental data showing the probability of measuring states  $|SS\rangle$ . (a) Experimental data showing the probability of measuring states  $|TS\rangle$  (b). Both plots representing the probability oscillations of the first step of the protocol presented in section 3.3. Raw data extracted from the repository of Ref. [6]. (c) Sum of (a) and (b), which would be equivalent to the probability of measuring  $|S\rangle_{34}$  according to Equation (4.18).

We can see that the measurements of  $|SS\rangle$  (Figure 4.5a) are close to zero everywhere in the plot, therefore the only contribution to the reduced probability plot is coming from the measurements of  $|TS\rangle$ . Therefore, the plot showing the sum of these two collections of probabilities (Figure 4.5c) accordingly gives the pattern found in the simulations. This partial readout technique could be applied to larger spin systems and verify to what extent it is feasible to use it in these type of tuning protocols. In this work we will examine this with the  $2 \times 4$  spin ladder.

These results give us insight about a very useful consequence of restricting us to the single-singlet subspace. If in general we attempt to measure a state where the singlet is in a specific pair of the system, it is enough to only measure these two spins being in a singlet state. The contributions by the rest of the states should be zero either for total spin conservation (states with more than singlet do

<sup>2</sup>We remind the reader that the time evolution of this initial state in this case is analogous to the time evolution of  $|ST_-\rangle$  (or  $|ST_0\rangle$ ). The only difference between the value of the eigenenergies in each of the triplets is a global energy shift of  $\tilde{B}$ . The reason why we use  $|ST_+\rangle$  is that in Ref. [6] a  $g < 0$  is considered, making the time evolution in a different triplet.

not contribute) or total spin projection conservation (states with different triplets do not contribute). Using the definition of partial trace [12], it can be shown that

$$P_{|\uparrow\rangle\otimes\cdots\otimes|S\rangle_{ij}\otimes\cdots\otimes|\uparrow\rangle} = P_{|S\rangle_{ij}} \quad (4.19)$$

for a measurement in the highest spin projection single-singlet subspace of a Hamiltonian obeying total spin and total spin projection symmetry. In fact, comparing the results obtained in section 5.1 with Figure C.2 in the Appendix C we can see that Equation (4.19) verifies.

## 4.4. Symmetries

In the process of attempting to set the  $2 \times 4$  spin ladder into homogeneous-exchange regime we realized that symmetry is a key requirement for the proper functioning of a tuning protocol that is based on a sequential equalization of pairs of exchanges. In fact, the approaches presented in Ref. [6] and Ref. [7] already hint towards this direction. However, a main difference separates these two four-spin cases and the eight-spin ladder, and this can be understood with the help of the diagrams presented in Figure 4.6.

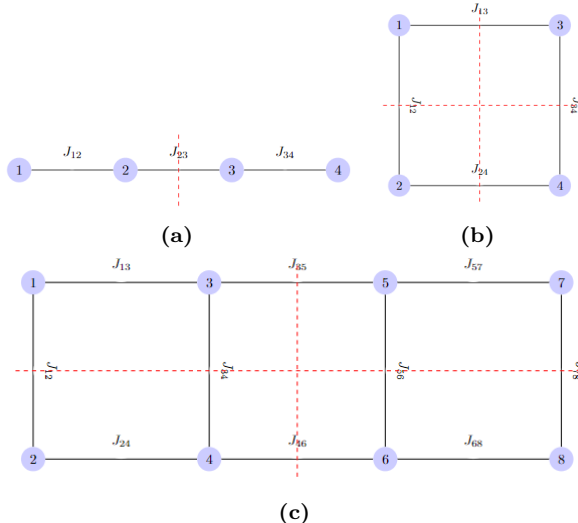


**Figure 4.6:** Representation of some symmetry axis for spin system geometries, represented in a red dashed line.

As we can see, at each side of the symmetry axes for the four-spins configurations there is only one exchange value. This is convenient because it allows us to directly equalize it with a single step with the exchange it has in front. Symmetry arguments based on the observations obtained via the computer simulations give support to the fact of finding a feature at this point. On the contrary, for the spin ladder geometry, there are either three or four exchanges at each side of the symmetric axis, depending on which one we choose. This forces us to have some previous exchange-homogenization work done before being able to exploit any of the two shown symmetry axis to set the exchange values of one side equal to the ones in the other side via a feature in the energy spectrum of a subspace.

This serves as a motivation for the approach we have decided to follow, which consists on a piece-wise tuning approach. The idea relies on being able to partially tune our system by tuning subsystems of the array independently. Then, we can use this previous work to facilitate the final goal of obtaining a complete exchange-homogeneous system by using the symmetries of the array. This way of proceeding is also convenient because, as we can see in sections 3.3 and 3.4, we already know the way to do it with some of the subsystems that we can find in the  $2 \times 4$  ladder geometry.

Despite not being a formal proof, we present some intuition about the reason why it is convenient to take symmetry into account when sequentially tuning an array. Consider the following change of

variables

$$\begin{aligned} J_p &= J_{ij} + J_{kl} \\ \delta_p &= J_{ij} - J_{kl} \end{aligned} \quad (4.20)$$

for a selected pair of exchanges of an arbitrary system we aim to tune. As usual, we are interested in fixing the dependency of the Hamiltonian with all the exchange values except for the pair  $J_{ij}$  and  $J_{kl}$  because we attempt to find an exchange-crossing feature when using the usual method. It has been observed that there are at least two general characteristics that play a key role in the fact of observing or not an exchange-crossing feature in the energy landscape of specific subspaces of the system. (1) Which exchanges we choose to sweep (selected pair  $J_{ij}$  and  $J_{kl}$ ) and (2) what are the values of the rest of the exchanges in the system. A favorable observation of exchange-crossing features is linked to the fact that these two characteristics obey certain symmetries. It is suspected that this has relation with the Hamiltonian turning into a symmetric function<sup>3</sup>. This would make  $H(\delta_p)|_{J_p=const.}$  an even function and therefore show features at the point  $J_{ij} = J_{kl}$  for all the eigenenergies of a subspace (unless all of them turn out to be zero-slope straight lines). The constraint of  $J_p = const.$  is not always necessary to see these features.

The discussion in the paragraph above perhaps could be relaxed by not forcing the whole Hamiltonian to be symmetric under the swap of certain exchanges but only certain subspaces, eigenenergy function expressions or even the difference between certain eigenenergy function expressions. However, we are interested in general symmetries of the full Hamiltonian because these are the ones that have been observed to relate the previously discussed mathematical functional symmetries with the geometrical shape of the quantum dot array.

We may illustrate this with the four-spin plaquette. If we consider the Heisenberg Hamiltonian of this particular geometry, Figure 3.7, it will in general be a matrix which is function of variables  $J_{12}$ ,  $J_{34}$ ,  $J_{13}$  and  $J_{24}$ . Similarly as the authors present in Ref. [7], a legit change of variables that can always be done is

$$\begin{aligned} J_h &= J_{13} + J_{24} \\ \delta_h &= J_{13} - J_{24} \end{aligned} \quad (4.21)$$

Indeed, we observe that an antisymmetric sweep of exchanges  $J_{13}$  and  $J_{24}$  gives an exchange-crossing feature no matter the value of the rest of the exchanges. However, if we do the same with  $J_{12}$  and  $J_{13}$ , a feature is not observed (unless  $J_{12} = J_{13}$ ). For the  $2 \times 4$  spin ladder however, even if we choose symmetric exchanges like  $J_{35}$  and  $J_{46}$  (see Figure 2.2) if  $J_{13} = J_{24}$  and  $J_{57} = J_{68}$  is not satisfied, an the crossing of  $J_{35}$  and  $J_{46}$  cannot be detected. A feature can be observed if the equalities in the previous sentence are satisfied.

## 4.5. Visibility

When we look at the Fourier transform of our probability measurement results, two of the problems that examining larger spin systems may exhibit are that, on the one hand, we may not see the frequency signal we are interested into, and on the other hand, we may see too many frequency signals that we are not interested into. For example, in Figure 3.5b, it could have been the case that we did not get the signal for the energy gap  $E2 - E1$ , making us fail when it comes to resolving the homogeneity feature. Likewise, in Figure 3.3b, we see that the three frequency components of the oscillations are visible while we would only like to see one of them. This second problem might not seem to be very important, but in fact it has been observed to be more usual than the first one. This is especially inconvenient when the size of the considered subspace grows, because then the number of energy gaps grows even faster than the size of the subspace and the resolution of the feature of interest becomes harder.

---

<sup>3</sup>In general, a symmetric function of  $k$  variables is a function that remains unchanged when its variable inputs are permuted. In this case, the drop of the dependence in all the variables except for  $J_{ij}$  and  $J_{kl}$  would give us  $H(J_{ij}, J_{kl})$ .

Both of these problems can be minimized by choosing an appropriate initial state for the measurements. The fact that makes certain frequency components more visible than others is given by the rule of thumb for which the more the initial state overlaps with a certain pair of eigenstates, the clearer are the oscillations related to their energy gap [6]. Back to the example of Figure 3.3, if we were interested in extracting the oscillation frequency associated to the energy gap between the  $E_3 - E_1$ , the initial state that is used would possibly not be the best one to choose.

This problem is relatively easy to solve efficiently if we have complete freedom of initial states. If we do not have this complete freedom, which is the case, it is useful to make a selection. If the subspace is small enough, this can be guided by computing the overlap of our set of initial states with the eigenvalues of the subspace of interest at the exchange crossing condition for which we intend to observe a feature. For example, if we take the four spins chain and a set of experimentally initializable states given by

$$I_4 = \{|ST-\rangle, |T-\rangle_{14} |S\rangle_{23}, |T-S\rangle\} = \{|i_1\rangle, |i_2\rangle, |i_3\rangle\} \quad (4.22)$$

we can compute the overlaps of these states with the eigenstates of the system when  $J_{12} = J_{34}$  and  $J_{23}$  free.

	$ i_1\rangle$	$ i_2\rangle$	$ i_3\rangle$
$ e_1\rangle$	0.68	0.87	0.68
$ e_2\rangle$	0.71	0.	0.71
$ e_3\rangle$	0.19	0.49	0.19

**Table 4.1:** Modulus of the overlap of our set of possible initializable states with the eigenvectors of the low energy triplet of the four-spin chain Hamiltonian with exchange values  $J_{12} = J_{34} = 1$  and  $J_{23} = 0.6$ . The displayed values are rounded to the second decimal value. Eigenstates ordered by energy (low to high) and are labelled  $|e_m\rangle$  with  $m = 1, 2, 3$ .

In Table 4.1 we can see the overlaps of the initializable states in Equation (4.22) and the eigenvectors of the triplet subspace. We can clearly see that  $|i_1\rangle$  overlaps mostly with the first and the second eigenstates, which is supported by the results obtained in Figure 3.3. Moreover, it has been checked that initializing state  $|i_2\rangle$  exclusively gives signal for the frequency  $E_3 - E_1$  around  $J_{12} = J_{34}$ . For different values of  $J_{23}$ , it can also be checked that overlap  $\langle e_1|i_2\rangle = 0$  and overlaps  $\langle e_3|i_1\rangle$  and  $\langle e_3|i_2\rangle$  are always kept low. While this approach is not perfectly accurate in terms of which frequency signals we see the most in our Fourier plots, it gives us an idea of the first candidates to use in our simulations.

The reader should note that since the set of eigenvectors is a valid orthonormal basis, we can rewrite the initial states in terms of the eigenstates. This forces that summing the square of the entries presented in Table 4.1 in a same column necessarily has to give 1 because of the normalization constraint. These results allow us to conclude that indeed all initial states could be used for the first step of the protocol in section 3.3 but  $|i_2\rangle$  would fail for the second step because it would not give signal for the energy gaps that involve the second eigenstate. In general, we do not only seek that the initial states overlap maximally with the pair (or pairs) of eigenstates that constitute the energy gap (or gaps) we are interested in but that they also have minimum overlap with the rest.

# 5

## Tuning a $2 \times 4$ ladder

In this chapter we present the detailed process of tuning a  $2 \times 4$  spin ladder into the homogeneous exchange condition using the code developed in chapter 4. This system of eight interacting spins is challenging to tune for its size and geometry, resulting in a considerable number of exchanges to play with. A nine-step protocol is used in order to accomplish this task and two different paths are presented. For both protocols we need to tune smaller subsystems of the array in order to be able to complete the final steps of the protocol using symmetry in our favor. Several tests of the first subsystem-tuning steps have been done in the ladder simulation, for example, tuning the four-spins plaquette in one of the sides of the  $2 \times 4$  ladder, and proper crossing feature results have been obtained with low enough exchanges separating the subsystems. It has also been tested whether a partial readout would still give us signal for the crossing feature detection, which is also the case.

### 5.1. Protocol A

The first protocol relies on tuning to the homogeneous regime the two separate four-spin plaquettes in the system, composed by spins 1 – 4 and spins 5 – 8 respectively (see Figure 2.2). In order to do that, we follow the protocol described in section 3.4, based on Ref. [7]. This must be done in both of the plaquettes separately, as if they were independent, which is achieved by setting the mid exchanges  $J_{35} = J_{46} = 0$ . However, it is not experimentally realistic to think that exchanges can be set to zero.

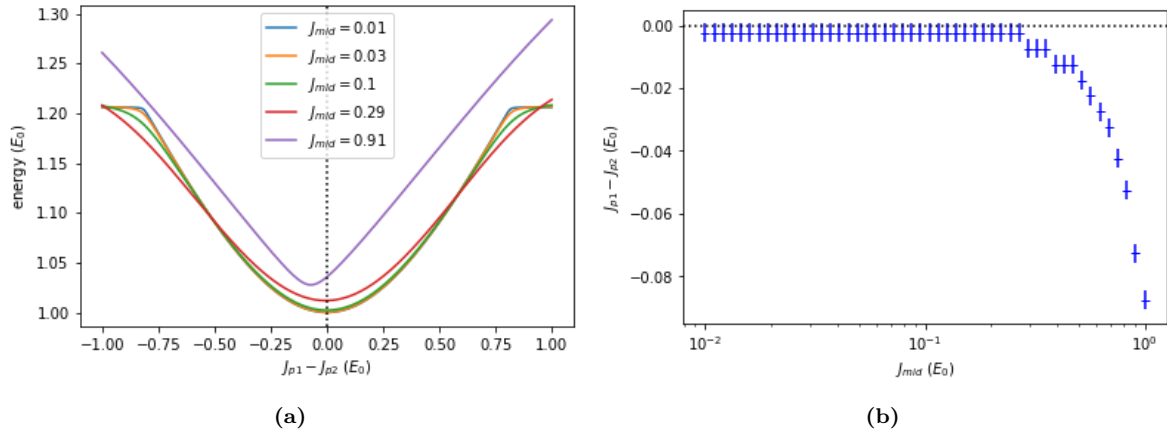


**Figure 5.1:** Study of the position of the exchange crossing feature of step one of the protocol described in section 3.4 for the plaquette composed by spins 1 – 4 as a function of the value of the mid exchanges  $J_{mid}$ . Exchanges of the plaquette composed by spins 5 – 8 are set to random values around 1. (a) Energy gap  $E_6 - E_2$  for different values of  $J_{mid}$  as a function of  $J_{p1} - J_{p2}$ . (b) Position of the minimum of the energy gap  $E_6 - E_2$  as a function of  $J_{mid}$ . Vertical error bars accounting the discretization error, points represented with an horizontal line. Dotted lines point out the crossing point for the swept exchanges. These results are tests of the first step of the four-spin plaquette protocol (see section 3.4) applied to the left plaquette of the  $2 \times 4$  ladder.

An overview about the accuracy of how steps one to three would work if these mid exchanges are set to a low value is presented in the following. The cases for which this is evaluated span a range of orders of magnitude below the typical order of magnitude used for the rest of the exchanges. As Figure 5.1 indicates, the lower the value of the mid exchanges the more centered at zero is the feature we seek.

A value approximately one order of magnitude below the working point for the mid exchanges  $J_{35}$  and  $J_{46}$  would be required for a nearly-perfect performance of the independent tuning of the plaquettes. It is also worth to mention that setting both exchanges to a large value gives approximately the same results as only doing it for one of them, and it is not relevant which of the two is chosen to be the large one. That is the reason behind using  $J_{35} = J_{46} = J_{mid}$  as the independent variable. Lastly, the values of the exchanges in the other plaquette do not seem to affect the deviation of the feature away from the point where the swept exchanges cross if these are kept on the order of magnitude of 1 or lower. A sweeping of exchanges for the six first steps of the protocol (three steps for each plaquette) has been tested and satisfactory results are found using  $J_{mid} = 0.1$ . Once the first six steps are already completed, we are left with two homogeneous independent plaquettes, with exchanges  $J_{p1}$  and  $J_{p2}$  in general.

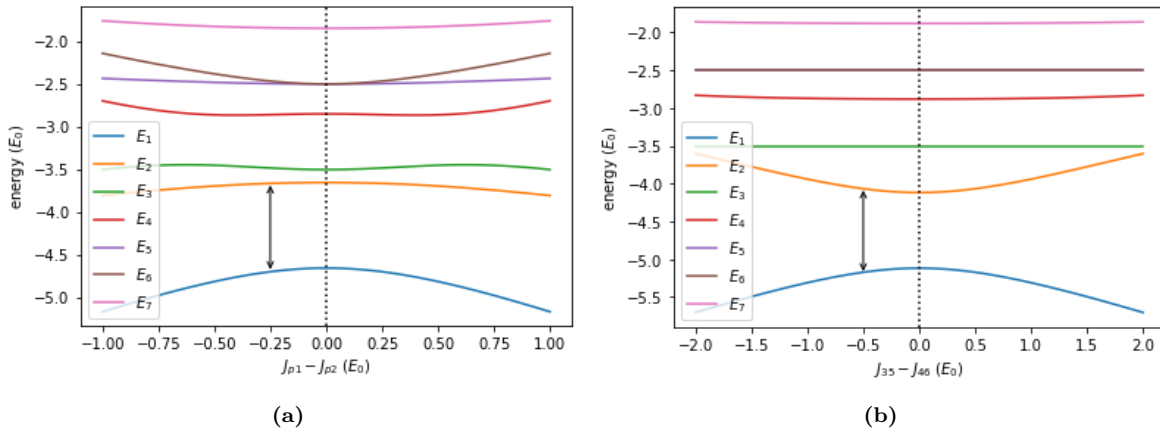


**Figure 5.2:** Dependence of the eigenenergies of the septuplet subspace as a function of (a)  $J_{p1} - J_{p2}$  and (b)  $J_{35} - J_{46}$  for steps seven and eight of protocol A respectively. For step seven, exchanges are set to  $J_{35} = J_{46} = 1.5$ . For step eight,  $J_{p1} = J_{p2} = 1$  and  $J_{35} = J_{46} = 2$  at the crossing point. The black arrow indicates the energy gap most visible when state  $|i_2\rangle = |s(3,5)\rangle$  is initialized and measured. Dotted lines point out the crossing point for the swept exchanges.

The next step consists of setting  $J_{p1} = J_{p2}$ . Sweeping antisymmetrically the exchanges of both plaquettes gives us a crossing condition in the septuplet subspace. In this case, at least one of the middle exchanges  $J_{35}$  and  $J_{46}$  needs to be set to a non-zero value. The energies of the eigenstates in this case can be found in Figure 5.2a, and we observe that this step of the protocol is robust to unknown values of  $J_{35}$  and  $J_{46}$ . We can clearly see that all the eigenenergies in this septuplet subspace are even functions of the variable  $J_{p1} - J_{p2}$ , so we can use the gap between any possible pair of eigenenergies to detect a crossing feature using the probability oscillations method we rely on experimentally. After this step, we are left with two homogeneously tuned plaquettes at  $J_{p1} = J_{p2} = J_p$  and unknown value of middle exchanges. In general, steps seven to nine would require global virtual exchange gates that allow us to modify the exchange value of the whole plaquette without losing the plaquette's internal homogeneity. This would be one of the main experimental challenges that this approach would face.

The two last steps of the protocol focus on tuning the middle exchanges  $J_{35}$  and  $J_{46}$  to the value of the rest. The best way we have found in order to carry this out is first setting  $J_{35} = J_{46}$  by finding a condition for exchange crossing and then finally setting these two middle exchanges equal to the rest with a last tuning. Given that  $J_{13} = J_{24}$  and  $J_{57} = J_{68}$  is already satisfied, we expect to find features at the exchange crossing when sweeping  $J_{35}$  and  $J_{46}$  antisymmetrically. Indeed, the energy spectrum of the septuplet subspace as a function of  $J_{35} - J_{46}$  is displayed in Figure 5.2b and this time we see that all the eigenenergies are even functions of the variable  $J_{35} - J_{46}$ .

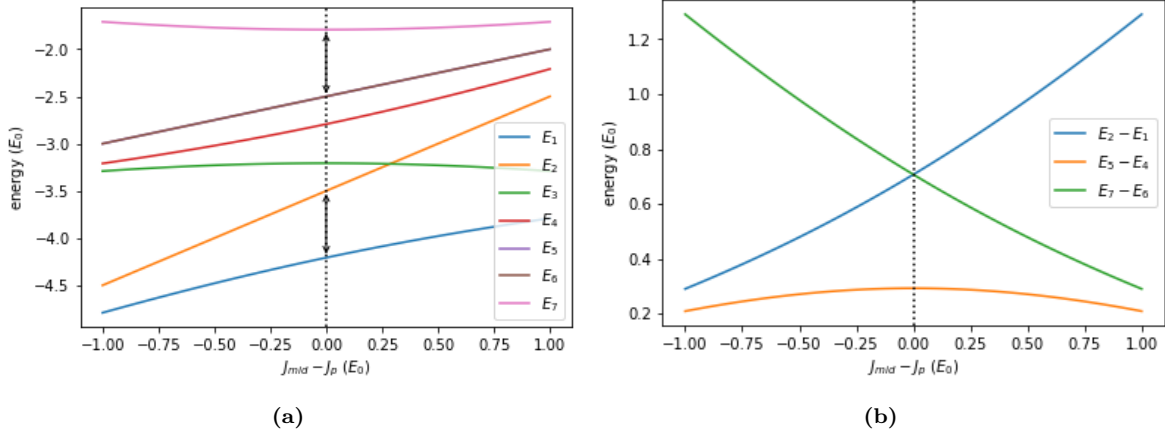


**Figure 5.3:** (a) Dependence of the eigenenergies of the septuplet subspace and (b) energy differences between a selected pairs of eigenstates as a function of  $J_{mid} - J_p$  for step nine of protocol A. The black arrows indicate the energy gaps that become equal at the exchange crossing. In (b) we show the energy gaps that are capable and are observed to give a crossing feature for initial state  $|i_8\rangle = |s(2,4)\rangle$ . Dotted lines point out the crossing point for the swept exchanges.

The last step consists on sweeping the middle exchanges  $J_{35} = J_{46} = J_{mid}$  altogether versus the rest of the exchanges of the system  $J_p$ , finding a crossing feature to set them equal. Plotting again the energy landscape of the septuplet subspace in Figure 5.3a, we can detect some energy gaps that allow us to get the desired particularity at the homogeneous condition. We may refer to Figure 5.3b to see more clearly the specific energy gaps that we use to detect that target point.

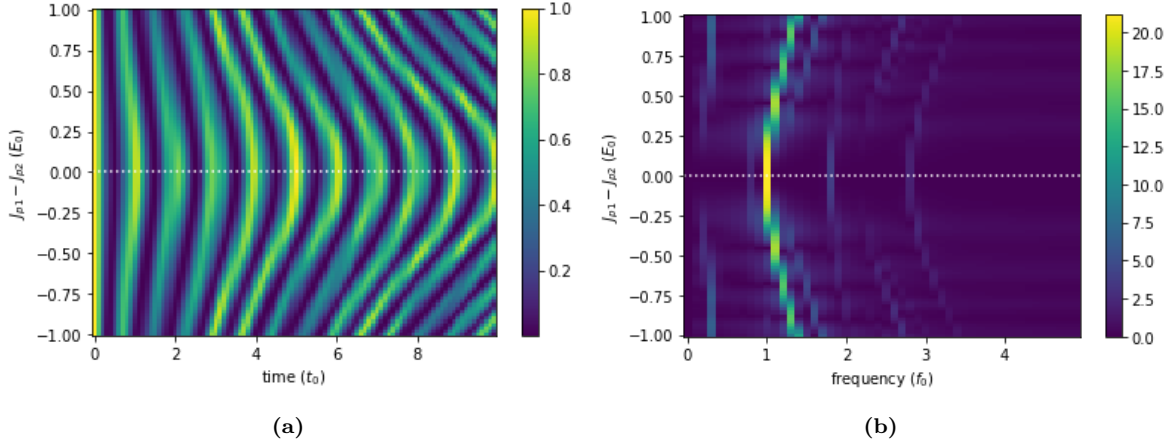


**Figure 5.4:** (a) Probability of initializing-measuring  $|i_2\rangle$  as a function of time and exchange values  $J_{p1} - J_{p2}$  and  $J_{35} = J_{46} = 1.5$  for step seven of protocol A. The colorbar indicates the probability of measurement. (b) Fourier transform of the oscillating pattern of (a). The dotted lines indicate  $J_{p1} = J_{p2}$ . The colorbar indicating the amplitude of oscillation of the signal and dotted line the exchange-crossing point.

The evolution of a particular state will give us oscillations signaling one or several of the energy gaps of the plots we have shown in Figures 5.2 and 5.3. In order to choose a suitable initial state we will use the insight obtained in section 4.5. To label the set of possible initializable states in the eight-spin ladder we will use

$$|s(i,j)\rangle = |\downarrow\rangle \otimes \dots |S\rangle_{ij} \otimes \dots |\downarrow\rangle \quad (5.1)$$

which will be labelled  $|i_m\rangle$  for  $m = 1, \dots, 10$  according to the position of the exchanges from top to bottom and from left to right (similarly as we do it for  $p_m$  values in Figure 6.3). For example,

$|i_1\rangle = |s(1, 3)\rangle, |i_2\rangle = |s(3, 5)\rangle$ , etc. These are all the states composed by a singlet pair on spins  $i$  and  $j$ ,  $|S\rangle_{ij}$  being nearest neighbors, and the rest down states (corresponding to a tensor product of three  $|T\rangle$  states in the remaining positions). There are ten possible pairs to put a singlet on, which correspond to the ten exchanges of the ladder. For clarity we will explicitly write them down in

$ i_1\rangle$	$ i_2\rangle$	$ i_3\rangle$	$ i_4\rangle$	$ i_5\rangle$	$ i_6\rangle$	$ i_7\rangle$	$ i_8\rangle$	$ i_9\rangle$	$ i_{10}\rangle$
$ s(1, 3)\rangle$	$ s(3, 5)\rangle$	$ s(5, 7)\rangle$	$ s(1, 2)\rangle$	$ s(3, 4)\rangle$	$ s(5, 6)\rangle$	$ s(7, 8)\rangle$	$ s(2, 4)\rangle$	$ s(4, 6)\rangle$	$ s(6, 8)\rangle$

**Table 5.1:** Short notation for the set of initializable states for the eight-spin ladder.

In order to choose the suitable initial state, we will compute the overlap of our set of experimentally possible initializable states with the eigenvectors corresponding to the configuration of exchanges we look for in that particular step. This can be seen in Table 5.2 for step seven. We can clearly see that  $|i_2\rangle$  and  $|i_9\rangle$  are the best choices if we are interested in a strong signal for the  $E_2 - E_1$  energy gap exclusively around the crossing point. Therefore, the initial state that we will use for the simulation in this case will be  $|i_2\rangle$ .

	$ i_1\rangle$	$ i_2\rangle$	$ i_3\rangle$	$ i_4\rangle$	$ i_5\rangle$	$ i_6\rangle$	$ i_7\rangle$	$ i_8\rangle$	$ i_9\rangle$	$ i_{10}\rangle$
$ e_1\rangle$	0.44	0.68	0.44	0.2	0.68	0.68	0.2	0.44	0.68	0.44
$ e_2\rangle$	0.44	0.68	0.44	0.	0.	0.	0.	0.44	0.68	0.44
$ e_3\rangle$	0.5	0.	0.5	0.5	0.5	0.5	0.5	0.5	0.	0.5
$ e_4\rangle$	0.24	0.2	0.24	0.68	0.2	0.2	0.68	0.24	0.2	0.24
$ e_5\rangle$	0.16	0.	0.16	0.47	0.47	0.47	0.47	0.16	0.	0.16
$ e_6\rangle$	0.47	0.	0.47	0.16	0.16	0.16	0.16	0.47	0.	0.47
$ e_7\rangle$	0.24	0.2	0.24	0.	0.	0.	0.24	0.2	0.24	

**Table 5.2:** Modulus of the overlap of our set of possible initializable states with the eigenvectors of the low energy septuplet of the spin ladder Hamiltonian with exchange values  $J_p = 1$  and  $J_{35} = J_{46} = 1.5$ . The displayed values are rounded to the second decimal value. Eigenstates ordered by energy (low to high) and are labelled  $|e_m\rangle$  for  $m = 1, \dots, 7$ .

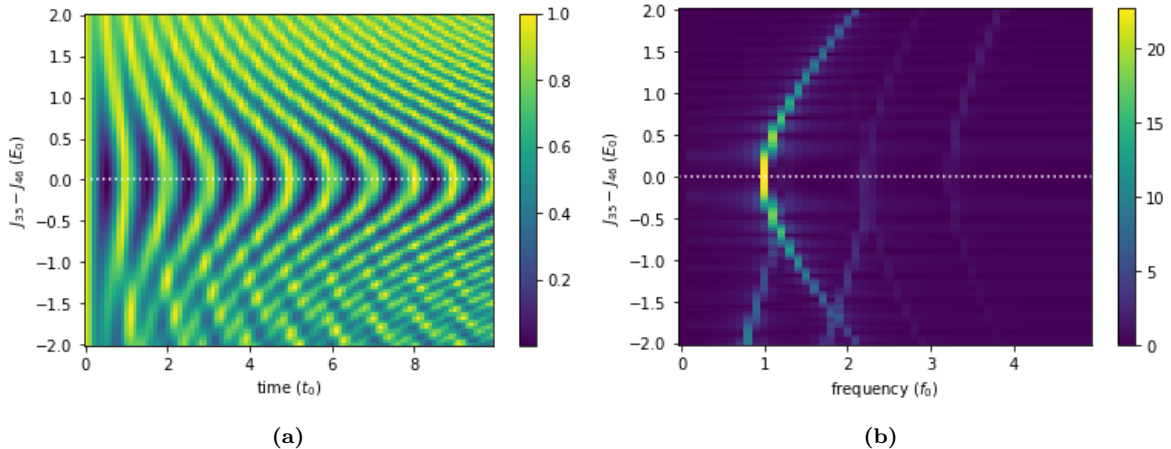


**Figure 5.5:** (a) Probability of measuring  $|i_2\rangle$  as a function of time and exchange values  $J_{35} - J_{46}$  with the rest of exchanges  $J_p = 1$  for step eight of protocol A. Initial state  $|i_2\rangle$  and colorbar indicating the probability values. At the crossing point  $J_{35} = J_{46} = 2$ . (b) Fourier transform of (a). Colorbar indicating the amplitude of oscillation and the crossing point  $J_{35} = J_{46}$  indicated with a dotted line.

In Figure 5.4 we can see how this energy gap gives a crossing feature at the corresponding value of  $J_{p1} = J_{p2}$ . Given that the width of the gap can be reduced lowering the values of the exchanges  $J_{35}$  and  $J_{46}$ , it is interesting to note that in this case we are not interested in keeping the mid exchanges

low because if so this energy gap becomes very small and therefore a substantial amount of evolution time is needed to get a proper signal. In a similar way and using the same state for initialization and measurement we can obtain Figure 5.5.

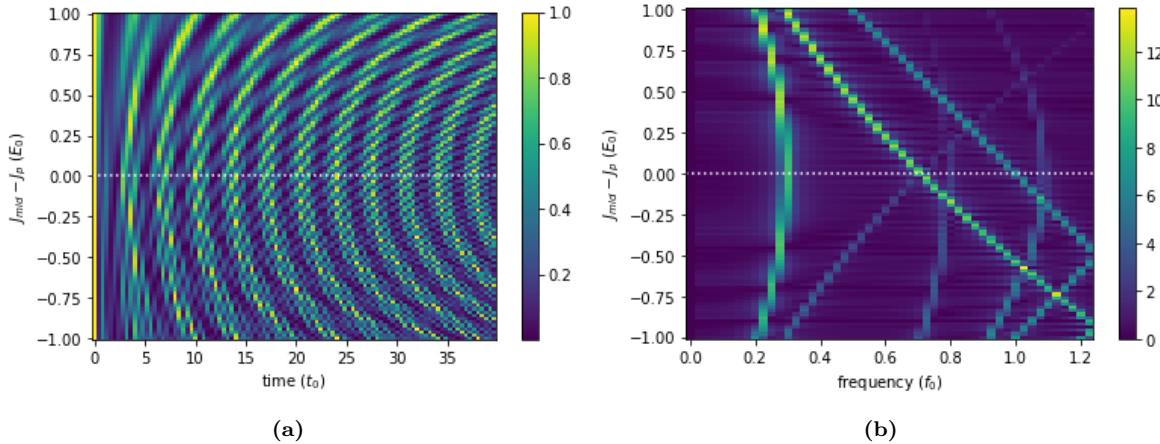


**Figure 5.6:** (a) Probability of measuring  $|i_7\rangle$  as a function of time and exchange values  $J_{mid} - J_p$  for step nine of protocol A. Colorbar indicating the probability values. (b) Fourier transform of (a). Colorbar indicating the amplitude of oscillation and the crossing point  $J_{mid} = J_p$  indicated with a dotted line.

To get a feature for the crossing of exchanges for the last step both states is is not useful to use  $|i_2\rangle$  for the initialization and measurement. For the probability measurement plots,  $|i_4\rangle$  and  $|i_7\rangle$  give fairly good results, overall with the energy gap  $E_5 - E_4$ , which can be seen in Figure 5.6. In this case we need to observe a low frequency signal, so a longer measurement time is needed but the fast-frequency part of the Fourier analysis can be disregarded. Another reason why restricting us to low frequency signals may be desirable is that we can make use of the measurement device resolution to “blend out” the fast oscillating frequencies to filter them out and see the oscillation of interest in a clearer way. This could be contemplated in a step like this last one.

As previously mentioned, partial readout tests have been done for this protocol A. Steps seven to nine are shown in Figure C.2 in Appendix C, for which the initial states are the same as we presented above but the probability we measure for the readout consists only on measuring singlet state in the pair of spins where we initialized the singlet state. As we previously remarked, complete correspondence between the plots shown in section 5.1 and Figure C.2 is found.

## 5.2. Protocol B

The second protocol we present has the same objective as the first one but the procedure followed is slightly different. The reason why this alternative procedure is also interesting is because it may be useful if we are interested in separating the exchange values of the system into two groups (horizontal and vertical exchanges) that have different exchange values but they share the same within the group. With this protocol this can be done with less steps, although using protocol A and detuning horizontal exchanges against vertical ones as an extra step would also work. This separation of horizontal and vertical exchanges is particularly of interest in theoretical studies of magnetic properties of ladders, specifically, spin dimer to liquid transitions [13]. In this case, instead of initially tuning two independent plaquettes, we set  $J_{12} = J_{34} = J_{56} = J_{78} = J_v = 0$  and we apply the four-spin chain protocol in both top and bottom chains, as shown in section 3.3 and Ref. [6]. We should finish this step with two chains tuned to different exchange values  $J_{c1}$  and  $J_{c2}$  in general. A similar study about determining the strength of the vertical exchanges needed for a proper operation of the protocol can be done the same way as presented in section 5.1 for protocol A. The testing has also been successful using  $J_v = 0.1$  taking into account the conditions that would apply if the process was tested experimentally.

This four steps are followed by a fifth one which sets the top chain and bottom chain exchanges

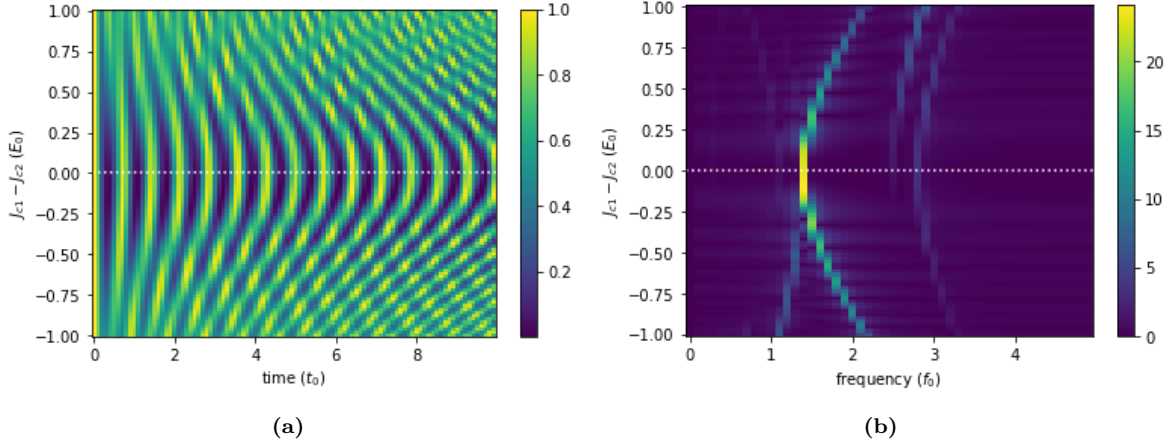


**Figure 5.7:** (a) Probability of measuring  $|i_2\rangle$  as a function of time and exchange values  $J_{c1} - J_{c2}$  for step five of protocol B. The rest of the exchanges are set to  $J_{12} = J_{78} = 0.2$  and  $J_{34} = J_{56} = 1.5$  and the initialized state is  $|i_2\rangle$ . Colorbar indicating the probability values. (b) Fourier transform of the oscillating pattern in (a). The colorbar indicates the amplitude of oscillation and the dotted line the exchange crossing point. The dotted line indicates the position where the feature should be observed.

to the same value by sweeping them antisymmetrically. The probability measurements associated to initialized-measured state  $|i_2\rangle$  for this step are shown in Figure 5.7. For this protocol, the suitable initial states for each step are chosen the same way as presented in section 5.1. Step five can be done by setting at least one of the vertical exchanges to a non-zero value, keeping  $J_{12}$  and  $J_{78}$  low while  $J_{34}$  and  $J_{56}$  are high. This allows us to get a less flat energy gap between eigenenergies  $E_1$  and  $E_3$ , which is the one that gives substantially decent signal for this initial state. This step is robust to the actual values of the vertical exchanges, that means that we will obtain a feature at the exchange crossing regardless the strength of the vertical exchanges. This results in two homogeneously tuned chains with exchange value  $J_h$

The three next steps of the protocol aim to tune the vertical exchanges to the same value. The best way to proceed with the tuning is to sweep symmetric vertical exchanges pair-wise ( $J_{12}$  with  $J_{78}$  and  $J_{34}$  with  $J_{56}$ ) and then equalize the four exchange values. However, we have observed that step six works properly if the system is symmetrical under swap of these exchanges forming the pair. That means that a first step consisting of sweeping  $J_{34}$  versus  $J_{56}$  with arbitrary  $J_{12}$  and  $J_{78}$  does not give a feature exactly at the crossing point in general. It is interesting to note this in Figure 5.8.

In order to characterize the effect of the detuning  $\Delta J = J_{78} - J_{12} > 0$  over the position of the feature used to detect the crossing  $J_{34} = J_{56}$ , we are going to study the position of the minimum of the energy gap  $E_2 - E_1$  as a function of the detuning  $\Delta J$ . Figure 5.9 shows that raising the value of both exchanges at the same time by  $J_{out}$  does not affect the position of the crossing feature of  $J_{34}$  and  $J_{56}$  (Figures 5.9a and 5.9b) while detuning the two outer-vertical exchanges by  $\Delta J$  actually does (Figures 5.9c and 5.9d). This result is also observed to be applicable if  $\Delta J < 0$  and if the outer and inner pairs of vertical exchanges change their role. We can also note that in order to be successful with step six,  $\Delta J$  needs to be kept at least one order of magnitude lower than the typical order of magnitude of the remaining exchanges.

A way to achieve this minimum difference between arbitrary exchanges would be setting their value to zero for both. This way, we are able to perform the first antisymmetric sweep of exchanges  $J_{34}$  and  $J_{56}$  as the sixth step of the protocol, setting  $J_{34} = J_{56} = J_{in}$ . Since symmetry is already satisfied for step seven, we are able to sweep exchanges  $J_{12}$  and  $J_{78}$  normally and achieve  $J_{12} = J_{78} = J_{out}$ . The order of step six and seven can be reversed but the symmetry requirement should be kept.

Step eight focuses on setting all the vertical exchanges equal, which is done by getting a feature for the crossing of the exchanges forming the two respective pairs introduced in the paragraph above. This

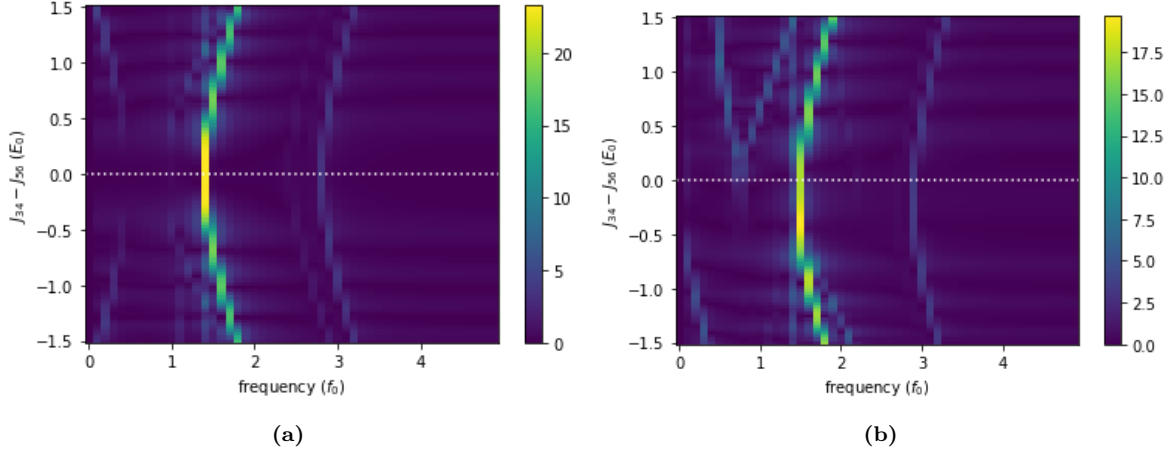


**Figure 5.8:** Fourier transform for the probability oscillations of step six of protocol B, seeking for a crossing feature when sweeping exchanges  $J_{34} - J_{56}$ . Initialized and measured state  $|i_2\rangle$ . Pairs of remaining vertical exchanges **(a)**  $(J_{12}, J_{78}) = (0.1, 0.3)$  and **(b)**  $(J_{12}, J_{78}) = (0.1, 1.8)$ . Horizontal exchanges set to  $J_h = 1$  and value of the exchanges  $J_{34} = J_{56} = 1.5$  at the crossing point.

step will give us the final state where all the horizontal exchanges are set to a certain value  $J_h$  and all the vertical exchanges will take  $J_v$ . The energy landscapes associated to steps five to eight can be found in Figure C.6 in Appendix C. The last step then consists on sweeping all the exchanges with value  $J_h$  against the vertical ones with value  $J_v$ . Despite the difficulty to find homogeneous feature for this last step, a signal for the crossing between  $E_5$  and  $E_6$  can be observe using two different initial states. The complete set of results for protocol B can be found in Figure C.6.

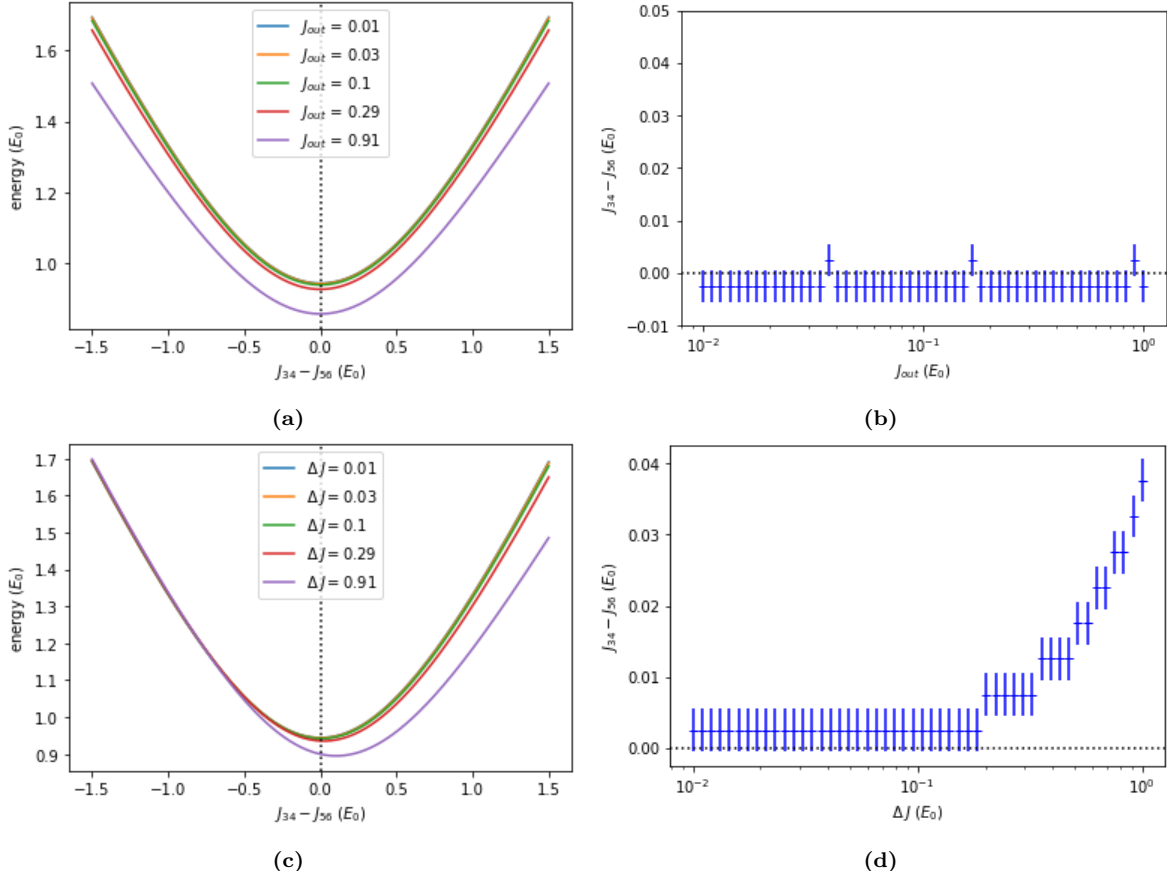


**Figure 5.9:** Study of the position of the exchange crossing feature of step six of protocol B as a function of the value of the outer vertical exchanges  $J_{out}$  and the detuning between the outer vertical exchanges  $\Delta J$ . (a), (c) Energy gap  $E_2 - E_1$  for different values of  $J_{out}$  and  $\Delta J$  as a function of  $J_{34} - J_{56}$  respectively. (b), (d) Position of the minimum of the energy gap  $E_2 - E_1$  as a function of  $J_{out}$  and  $\Delta J$  respectively. Vertical error bars accounting the discretization error, points represented with an horizontal line. Entries of  $\Delta J$  in the legends rounded to the second decimal value. Dotted line indicates the point of exchange-crossing.

# 6

## Alternative approaches

For the last part of the project, we take a step back and attempt to investigate if a more scalable approach to tune a quantum dot array could be used. As we already mentioned, we will eventually need to get rid of classical calculations to tune quantum simulators in the future if we want them to be useful. In this chapter we introduce an alternative approach that could also help or be used to solve our problem of tuning a half-filled quantum dot array to the homogeneous-exchange regime. This approach is based on examining in more detail the lowest total spin subspace. For the spin systems considered in this work, it has been observed that this subspace is the one where the ground state lives if the magnetic field  $\tilde{B}$  is low enough. So far, for the considered systems, we have restricted ourselves to the fully polarized  $(\frac{n}{2} - 1)$ -total spin subspace when examining possible features of homogeneity of exchanges. We want to delve into the physics within the singlet and doublet subspaces because this might give us some insight about how to tune the device more reliably. In particular, we want to focus on the ground state of the systems and how the time evolution within the lowest total spin subspace is described in terms of the resonating valence bond (RVB) theory.

### 6.1. Resonating valence bond theory

As we have already seen, our system of interest is a collection of spins that are coupled via an antiferromagnetic interaction,  $J_{ij} > 0$  for a given set of pairs of spins  $i$  and  $j$ . Classically, the ground state is typically described by a state that antialigns spin orientations of every interacting pair in the system [14]. Nevertheless, its corresponding quantum mechanical state, known as the Néel state, does not correspond to the ground state of finite-sized antiferromagnetically-interacting systems [15]. In fact, for these type of systems described by the Heisenberg Hamiltonian, its ground state tends to form singlet pairs between the interacting spins.

An RVB state is a superposition of valence bond states, which are singlet states of two  $S = \frac{1}{2}$  spins at sites  $i$  and  $j$  [13]. Its general form is described by

$$|\Psi_{RVB}\rangle = \sum_{i_1, j_1, \dots, i_k, j_k} a_{(i_1, j_1, \dots, i_k, j_k)} |S\rangle_{i_1 j_1} \dots |S\rangle_{i_k j_k} \quad (6.1)$$

where the  $k$  valence bond pairs cover the entire lattice and the sum is over all the possible ways to arrange singlet pairs in the system [13]. In the cases considered in our work, if the magnetic field is low enough, for an even number of spins the ground state lives in the singlet subspace of total spin  $S_T = 0$  and therefore it can be described as an RVB. Investigating these singlet subspaces from the perspective of the RVB states is interesting because it may give us hints to tune the considered system into the homogeneous-exchange regime in a different way with respect to how we have done it so far.

In order to investigate the  $S_T = 0$  subspace one may find useful to use a more suitable basis to describe its states. For a system with an even number of spins  $n = 2m$ , with  $m \in \mathbb{N}$ , its number of possible valence bond tilings is given by

$$T(m) = \frac{(2m)!}{2^m m!} \quad (6.2)$$

As the number of spins  $n = 2m$  grows, all these possible combinations of valence bonds states, candidates of being part of the new valence bond basis, increase faster in number with respect to the dimension of the singlet subspace of a system composed of  $2m$  spins, which is given by

$$C_{S=0}(m) = \frac{(2m)!}{m!(m+1)!} \quad (6.3)$$

That means that a valence bond basis based on creating a product state of singlets between every possible pair of spins in our system would give us an over-complete basis of states. Despite all of this, one can find some ways to reduce the dimension of this collection of states so it properly matches with the dimensions of the singlet subspaces [16][17].

Lastly, it is worth to remark that the RVB theory can also be applied to systems with an odd number of spins. The key is that the state that describes the system can be expressed in terms of valence bonds, which are expected to persist in the system rearranging the pairings of spins that form them due to the effect of quantum fluctuations [14]. For the systems we have considered in this work with  $n = 2m + 1$  spins, the non-fully polarized ground state lives in the  $S_T = \frac{1}{2}$  subspace and it can be checked that it forms a coherent superposition of valence bond states, giving it the benefit to lower its energy with respect to a Néel state or a state with a single valence bond.

## 6.2. Motivation

We start investigating the behavior of RVB states with the four-spin plaquette. In fact, the motivation to tackle this topic with the objective of tuning the exchanges of our quantum system comes from several results and observations presented in Ref. [7]. The Hamiltonian of the four-spin plaquette for the singlet subspace can be written exclusively in terms of  $J_h = J_{13} + J_{24}$  and  $J_v = J_{12} + J_{34}$ . This means that the energies governing this subspace are insensitive to antisymmetric variations of symmetric exchanges. In principle this is something that is not of our interest when we aim to tune a device but it is still worth to keep with the inspection. The matrix form of this Hamiltonian subspace is given by

$$H_{(0)} = \begin{pmatrix} -J_h - \frac{J_v}{4} & \frac{\sqrt{3}}{4} J_v \\ \frac{\sqrt{3}}{4} J_v & -\frac{3}{4} J_v \end{pmatrix} \quad (6.4)$$

in the basis  $\{|S\rangle_{13}|S\rangle_{24}, \frac{1}{\sqrt{3}}(|T_+\rangle_{13}|T_-\rangle_{24} + |T_-\rangle_{13}|T_+\rangle_{24} - |T_0\rangle_{13}|T_0\rangle_{24})\}$ . The more different the values of  $J_h$  and  $J_v$  take, the more the system resembles two uncoupled pairs of spins and therefore, in the limit  $J_h \gg J_v$  and  $J_h \ll J_v$ , the ground state is given by  $|S_h\rangle = |S\rangle_{13}|S\rangle_{24}$  and  $|S_v\rangle = |S\rangle_{12}|S\rangle_{34} = |SS\rangle$  respectively. However, when  $J_h = J_v$  is satisfied, the eigenstates of the system are given by

$$|s\rangle = \frac{1}{\sqrt{3}}(|S_h\rangle - |S_v\rangle) \quad \text{and} \quad |d\rangle = |S_h\rangle + |S_v\rangle \quad (6.5)$$

which completely lose the dependence on  $J_h$  and  $J_v$  on their coefficients [7]. This is precisely due to the fact that in general, the eigenvectors of Equation (6.4) depend on  $\frac{J_h}{J_v}$  because the coefficients of the eigenvectors can be taken real and one of them is already fixed by normalization. Therefore, this loss of dependence of the eigenstates with respect to  $J_h$  and  $J_v$  is due to setting  $J_h = J_v$ . Another thing to note is that for a range of values of magnetic field, including  $\tilde{B} = 0$ ,  $|s\rangle$  is the ground state of the system.

Attending to the definitions of the concepts introduced in section 6.1, the set  $\{|S_h\rangle, |S_v\rangle\}$  is a valid RVB basis. The observation of interest is that, as the authors introduce in Ref. [7], if the (ground) state  $|s\rangle$  is accessible experimentally (with good fidelity), the condition of  $J_h = J_v$  could be detected by measuring the coefficients that express the state in terms of the RVB basis. This is especially useful given that the measurement technique we use is capable of measuring the states that form this basis.

Therefore, the third step of the protocol presented in section 3.4 could be done the same way replacing the measurements over time with measuring the probability of finding states  $|S_h\rangle$  and  $|S_v\rangle$ .

The moment when these probabilities are equal, if the system is perfectly behaved, we have reached the condition of homogeneity. Measuring individual pairs of singlets can also be used for the same purpose. Figure 6.1 left panel shows the expected probabilities of measurement of individual singlets in each of the exchanges of the plaquette. It is interesting to note the counter-intuitive correlation within the groups of horizontal and vertical singlet measurements. Even if we do not keep  $J_{13} = J_{24}$  and  $J_{12} = J_{34}$ , the correlation of measuring singlets in one direction (horizontal or vertical) is still perfect. It might be helpful to look at how this ground state is written in terms of the RVB basis (Equation 6.5) in order to understand this behavior.

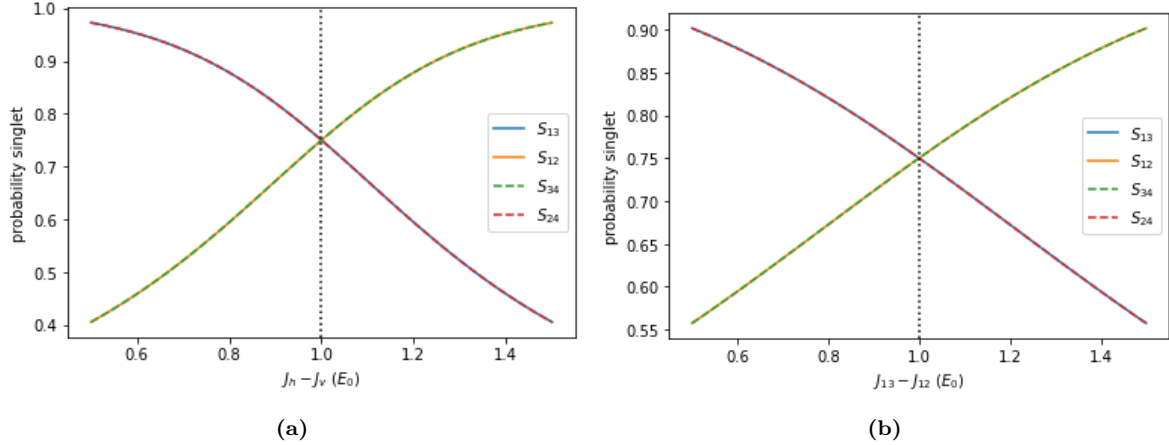


**Figure 6.1:** Probability of measuring singlet on spins  $i, j$  (labelled  $S_{ij}$ ) as a function of  $J_h - J_v$  keeping  $J_{13} = J_{24}$  and  $J_{12} = J_{34}$  (left panel) and as a function of  $J_{13} - J_{12}$  keeping  $J_{24} = J_{34} = 1$  (right panel).

Another of the consequences of Equation (6.4) is that, as we have seen for the rest of the subspaces, initializing a state which is not an eigenstate gives an oscillating pattern when measuring the probability of the final state to be in a certain other state. However, for this specific case, an exchange-crossing feature at the  $J_h = J_v$  point will not happen when looking at the frequencies of the oscillations. The eigenstates' energy gap is given by

$$E_g = \sqrt{J_h^2 - J_h J_v + J_v^2} \quad (6.6)$$

which minimizes at  $J_h = \frac{J_v}{2}$  for  $J_h, J_v > 0$ . Nevertheless, there is another observable which is given by these same measurements and it also depends on these exchange values, the visibility of the oscillations. In general, this observable is defined by

$$\mathcal{V}_{|i\rangle,|k\rangle} = P_{|i\rangle,|k\rangle}^{\max} - P_{|i\rangle,|k\rangle}^{\min} \quad (6.7)$$

where  $|i\rangle$  represents the state that is initialized,  $|k\rangle$  is the state that we measure and the superindices maximize/minimize the value of the probability with respect to time  $t$ . As shown in Ref. [7], initializing the state  $|S_h\rangle$  and measuring  $|S_v\rangle$ , which we will label as “1”, the probability of measurement is given by

$$P_1(t) = \frac{1}{4} (1 + 2\mathcal{V}_1(J_h, J_v) (1 - \cos E_g t)) \quad (6.8)$$

with

$$\mathcal{V}_1(J_h, J_v) = \frac{3J_h J_v}{4(J_h^2 - J_h J_v + J_v^2)} \quad (6.9)$$

so the visibility for this set of initialize-measure states is precisely  $\mathcal{V}_1(J_h, J_v)$ . It is interesting to note that  $\mathcal{V}_1$  maximizes at  $J_h = J_v$  therefore it shows a feature that can be detected experimentally as a crossing of these two values of exchanges. Moreover, if state  $|S_h\rangle$  is measured, the visibility then becomes

$$\mathcal{V}_2(J_h, J_v) = \frac{3J_v^2}{4(J_h^2 - J_h J_v + J_v^2)} \quad (6.10)$$

which takes the same value as  $\mathcal{V}_1$  only when  $J_h = J_v$ . By symmetry arguments, we can reason that the same happens if we swap  $|S_h\rangle \leftrightarrow |S_v\rangle$  for both of the results above. Once again using the third step of section 3.4 as an example, in Figure 6.2 we can see that the visibility indeed goes maximum for measuring  $|S\rangle_{13}|S\rangle_{24}$  and it is equal to the one obtained for measuring  $|S\rangle_{12}|S\rangle_{34}$  but the minimum of frequency is localized at  $J_v = \frac{1}{2}J_h$ .

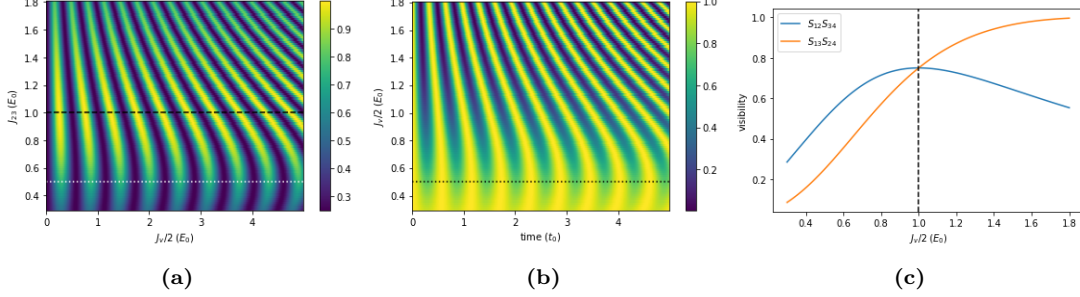


**Figure 6.2:** State evolution within the singlet subspace for the four-spin chain. Left and mid panel, oscillations of the probability of measuring states  $|S\rangle_{12}|S\rangle_{34}$  and  $|S\rangle_{13}|S\rangle_{24}$  respectively, with initial state  $|S\rangle_{13}|S\rangle_{24}$  as a function of  $J_v$  keeping  $J_{13} = J_{24} = 1$  and  $J_{12} = J_{34}$ . Dashed line on the left panel indicating the maximum visibility and dotted line on the left and mid panel indicating the point  $J_v = \frac{1}{2}J_h$ .

Both of these procedures rely on having excellent fidelity of probability measurement of the states. This is a strong drawback when compared to relying on measuring frequency as it has been done in the previous chapters. The accuracy of these probability measurements is affected by errors in the preparation, initialization and readout of the states and leakage outside the subspace amongst other possible problems. Meanwhile, these results could also be used as a check for certain steps of the protocols presented.

Lastly, it is worth to remark that very similar results are observed when testing the low-energy three-spin chain doublet subspace, with  $|s\rangle = \frac{1}{\sqrt{6}}(|S\downarrow\rangle - |\downarrow S\rangle)$  as the ground state for low  $\tilde{B}$  and  $\{|S\downarrow\rangle, |\downarrow S\rangle\}$  as the set of RVB basis vectors [14]. Therefore, despite the enlargement of the singlet subspace, a similar study could be done for the eight-spin ladder. Some initial results have been obtained for this central geometry of this work. The first one is that it has been checked that the ground state, for low values of  $\tilde{B}$ , indeed belongs to the singlet subspace, which is 14-dimensional.

The last result obtained for the  $2 \times 4$  spin ladder is similar to the first test presented for the four-spin ladder in this chapter. We computed the single-singlet probabilities for every possible nearest-neighbor pair for the exchange-homogeneous case. Figure 6.3 shows the values extracted. It can be noted that the probabilities of measuring singlet are symmetrical with respect to the horizontal and vertical axis that cross the ladder as depicted in Figure 4.6c.

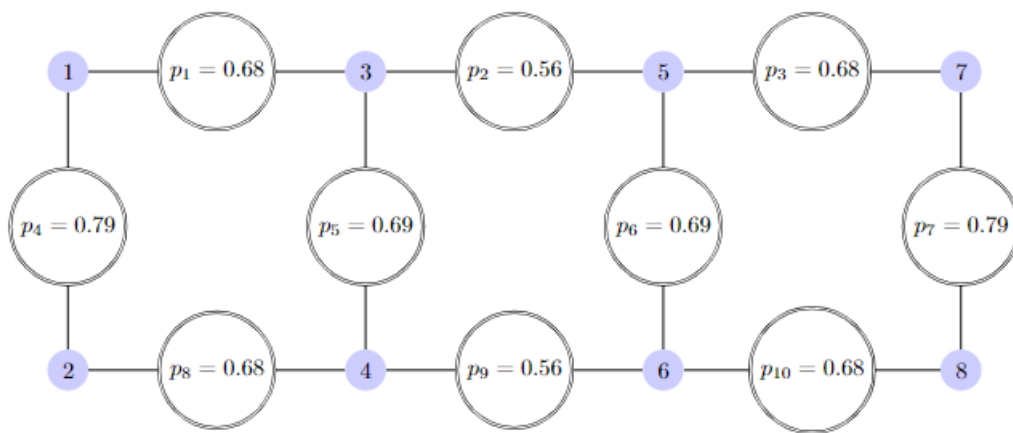


**Figure 6.3:** Extracted value of the probability of measuring a singlet in all the nearest-neighbor pairs of the eight-spin ladder in the exchange-homogeneous condition.

# 7

## Conclusions and outlook

We have been able to propose a method to tune an eight-spin ladder system into the homogeneous regime using sequential homogenization of exchange coupling pairs in the system. This has been achieved by means of classical numerical simulations of a simplified model of the real system, localized spins in quantum dots. The simulations have been used both to create and verify the correct operation of the method. Symmetry has been observed to be a key requirement for the success of the proposed steps of the method.

Although the totality of our results is theoretical, a point of view focused on being able to use the presented methods experimentally has been considered throughout the whole project. Other factors to improve the experimental feasibility of the method have also been investigated, improving the readout requirements of the method or the quality of the results obtained in each step. In particular, partial readout of the system has been observed to be a useful tool, at least if the dynamics remain in the most energetically favorable  $(\frac{n}{2} - 1)$ -total spin subspace.

However, to this day, the experimental requirements that our approach demands for tuning the exchanges of the  $2 \times 4$  spin ladder are notably challenging. A part from the fact of not being able to maintain quantum coherence in the system for enough time, other problems could appear in terms of the control we can achieve of the device. A solid plunger and barrier gate virtualization would be needed and being able to maintain the subsystem's homogeneity during the remaining steps of the protocol would also be a key to succeed. The readout of the state of the system should also be good enough to be able to resolve all of the oscillation patterns.

Finally, an alternative approach to tune spin systems into the homogeneous regime is investigated. Results that could be used in some steps of a homogenization protocol for a four-spin plaquette system are obtained. However, the fact that the proposed steps require exceptionally good state probability measurements for their well operation makes these less experimentally feasible. The inspection of this approach for the eight-spin ladder system remains as an outlook for this project.

Following with the alternative approach, the first interesting result that would be useful to have is rewriting the ground state of the singlet subspace in a suitable RVB basis. This would perhaps give us some more insight about correlations between pairs of singlets or how the dynamics in the lowest-spin subspace. General rules with respect to this applicable to arbitrary-sized systems would likely be useful for attempting to tune classically intractable systems.

A part from the already discussed problem of the classical intractability, the scaling of this method consisting on sequentially equalizing pairs of exchanges of the system is not ideal. It should be noted that if this method is followed, for a system with  $k$  exchanges,  $k - 1$  steps consisting on obtaining a probability map as a function of the value of some exchanges  $\{J_{ij}\}$  and time  $t$  is needed. This could perhaps be improved.

Another way of expanding this work would be to inspect the tuning of larger spin systems based on triangular lattices, in particular triangular spin ladders, given the fact that the developed code is already capable to do it. It would be interesting to see to what extent the insight in this project can be useful to generate a possible new tuning protocol. One could also introduce next-next-nearest neighbors terms to the Heisenberg Hamiltonian to be able to simulate a system with more spin-spin coupling terms.

Finally, it is remarkable that the underlying theory over which our simulations are based is fairly general but also highly simplified. Another direction towards which this work could be expanded would be adding corrections to the current theory we are using, relaxing some assumptions or using a theory that describe a system in a more specific way, such as the behaviour of spins in quantum dots based on Ge/SiGe.

# Acknowledgements

I am genuinely grateful to the people who have accompanied me throughout the development of this project. These last words recognize the enormous impact they have had on me. Without them, this would not have been possible. To all those who have been a part of this journey, I want to extend my sincerest appreciation and gratitude.

In the first place, I would like to express my gratitude to professor L. M. K. Vandersypen, for providing me with the opportunity to work in his group. I am also thankful for his guidance and support throughout my master's thesis as my direct supervisor. His expertise has been a source of inspiration and motivation, I am honored to have been a part of his team.

Equally, I would like to thank my daily supervisor P. Cova Fariña, whose guidance, patience, and encouragement have been indispensable throughout this project. I have learnt a lot from him and he has been an outstanding mentor. This work is also his.

I am also thankful to the members of Vandersypen's group for their valuable feedback and assistance during my research. Special thanks to T.-K. Hsiao, D. Jirovec, S. Philips and M. Rimbach-Russ for their insightful discussions and suggestions that have contributed to the success of this work. I also acknowledge the other members of other groups in QuTech who have crossed my path for their positive impact. I am also grateful to QuTech management staff, especially M. Plas, and Qutech communications team for their help. I would also like to acknowledge the external committee members M. Blaauboer and M. Veldhorst for their review and assessment.

To finish with, I would like to show my gratitude to my friends, who have been a constant source of support and encouragement throughout my master's thesis and my master's programme in general. Special thanks to K. Capannelli and A. Teruel for their input. Finally, I would like to thank my family for their unwavering support and encouragement throughout my academic journey. I am incredibly fortunate to have them in my life.

# References

- [1] H. Tasaki. *Physics and Mathematics of Quantum Many-Body Systems*. Graduate Texts in Physics. Springer International Publishing, 2020. ISBN: 9783030412654.
- [2] B. Abolfazl, S. Bose, and H. Johannesson. *Entanglement in Spin Chains: From Theory to Quantum Technology Applications*. Springer International Publishing, 2022. ISBN: 9783031039980. URL: <https://doi.org/10.1007/978-3-031-03998-0>.
- [3] R. Hanson et al. “Spins in few-electron quantum dots”. In: *Rev. Mod. Phys.* 79 (4 Oct. 2007), pp. 1217–1265. DOI: 10.1103/RevModPhys.79.1217. URL: <https://link.aps.org/doi/10.1103/RevModPhys.79.1217>.
- [4] Y. P. Kandel, H. Qiao, and J. M. Nichol. “Perspective on exchange-coupled quantum-dot spin chains”. In: *Applied Physics Letters* 119.3 (2021), p. 030501.
- [5] P. Barthelemy and L. M. K. Vandersypen. “Quantum dot systems: a versatile platform for quantum simulations”. In: *Annalen der Physik* 525.10-11 (2013), pp. 808–826.
- [6] C. J. van Diepen et al. “Quantum Simulation of Antiferromagnetic Heisenberg Chain with Gate-Defined Quantum Dots”. In: *Physical Review X* 11.4 (Nov. 2021). DOI: 10.1103/physrevx.11.041025. URL: <https://doi.org/10.1103%2Fphysrevx.11.041025>.
- [7] C. A. Wang et al. “Probing resonating valence bonds on a programmable germanium quantum simulator”. In: (2022). DOI: 10.48550/ARXIV.2208.11505. URL: <https://arxiv.org/abs/2208.11505>.
- [8] T. Hengsens et al. “Quantum simulation of a Fermi-Hubbard model using a semiconductor quantum dot array”. In: *Nature: international weekly journal of science* 548.7665 (2017), pp. 70–73. ISSN: 0028-0836. DOI: 10.1038/nature23022.
- [9] D. J. Griffiths and D. F. Schroeter. *Introduction to quantum mechanics*. Cambridge university press, 2018.
- [10] V. Devanathan. *Angular Momentum Techniques in Quantum Mechanics*. United States of America: Kluwer Academic Publishers, 1999.
- [11] J. L. Basdevant and J. Dalibard. *Quantum Mechanics*. École Polytechnique. Springer Berlin Heidelberg, 2005. ISBN: 9783540277064.
- [12] M. A. Nielsen and I. L. Chuang. *Quantum Computation and Quantum Information: 10th Anniversary Edition*. Cambridge University Press, 2010. DOI: 10.1017/CBO9780511976667.
- [13] Y. Zhou, K. Kanoda, and T.-K. Ng. “Quantum spin liquid states”. In: *Reviews of Modern Physics* 89.2 (2017), p. 025003.
- [14] K.-Y. Yang et al. “Probing resonating valence bond states in artificial quantum magnets”. In: *Nature communications* 12.1 (2021), p. 993.
- [15] J. B. Parkinson and D. J. J. Farnell. *An introduction to quantum spin systems*. Vol. 816. Springer, 2010.
- [16] K. S. D. Beach and A. W. Sandvik. “Some formal results for the valence bond basis”. In: *Nuclear Physics B* 750.3 (Aug. 2006), pp. 142–178. DOI: 10.1016/j.nuclphysb.2006.05.032. URL: <https://doi.org/10.1016%2Fj.nuclphysb.2006.05.032>.
- [17] J. Gerratt et al. “Modern valence bond theory”. In: *Chemical Society Reviews* 26.2 (1997), pp. 87–100.
- [18] H. Diep. *Frustrated Spin Systems*. World Scientific Publishing Company, 2005. ISBN: 9789814481458.

# A

## Three-spins plaquette

For completeness, we also wanted to analyze our test system of spins (the triple spins chain) with periodic boundary conditions. This system can be seen as three spins settled up in a triangular geometry. Figure A.1 shows a sketch of it. This extension of the three-spins chain tuning is interesting to consider because it allows us to examine the exchange-crossing features of closed-loop systems.

However, this system is also interesting for its physical behavior. Magnetic frustration happens in a nearest-neighbor spin lattice when it is not possible to find a state that satisfies all the favoured paired states that the Hamiltonian dictates. One of the causes of magnetic frustration is the geometry of the lattice in which the spins are located [18]. This cause is reasonably intuitive, as we can see with the triangular geometry. If we consider three spins in a triangular geometry (see Figure A.1) with antiferromagnetic interaction, we can see that once one pair satisfies a favorable antiferromagnetic state, there is no way that both other pairs are able to form this favorable bond at the same time. This makes that the ground state energy of the system does not correspond to the energy given by the minimum of the interaction of every spin pair.

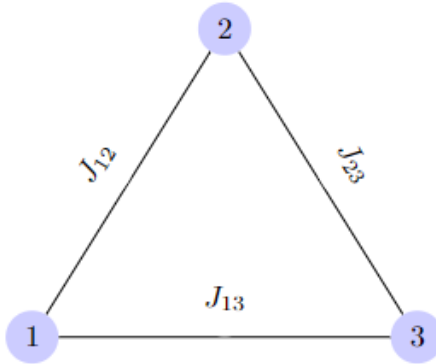


**Figure A.1:** Geometrical representation and labelling of the spins and exchanges in a triangular shape.

Given that we now have three exchange couplings in our system instead of two, we believe it is sensible to try to reach the homogeneous exchange condition the same way we did it for the quadruple spin chain. Therefore, we initialize a state  $|S \downarrow\rangle$  and we let it evolve in time within the doublet subspace with lowest energy. We obtain the probabilities of this state being  $|S \downarrow\rangle$  as a function of time and  $J_{12} - J_{23}$  keeping the remaining  $J_{13} = 0.6$ . We obtain the results shown in Figures A.2 and A.3.

Our results for the periodic bounded trio of spins substantially resemble the ones for the three-spin chain. Again, we see that at the value where  $J_{12} = J_{23}$  cross we observe the minimum frequency of oscillation (see Figure A.3). As a final step, sitting where  $J_{12} = J_{23} = 1$  and sweeping the value of  $J_{13}$

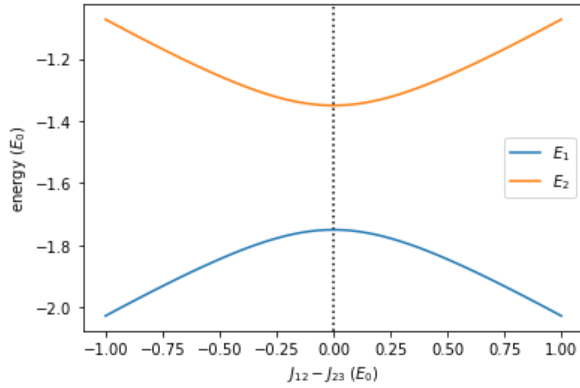


**Figure A.2:** Energies of the eigenstates of the  $S_T = \frac{1}{2}$  and  $m_T = -\frac{1}{2}$  doublet subspace ordered from lower ( $E_1$ ) to higher ( $E_2$ ) energy as a function of  $J_{12} - J_{23}$  for a triple spin chain with periodic boundary conditions. Exchange  $J_{13} = 0.6$  fixed and dotted line indicates the exchange crossing point.

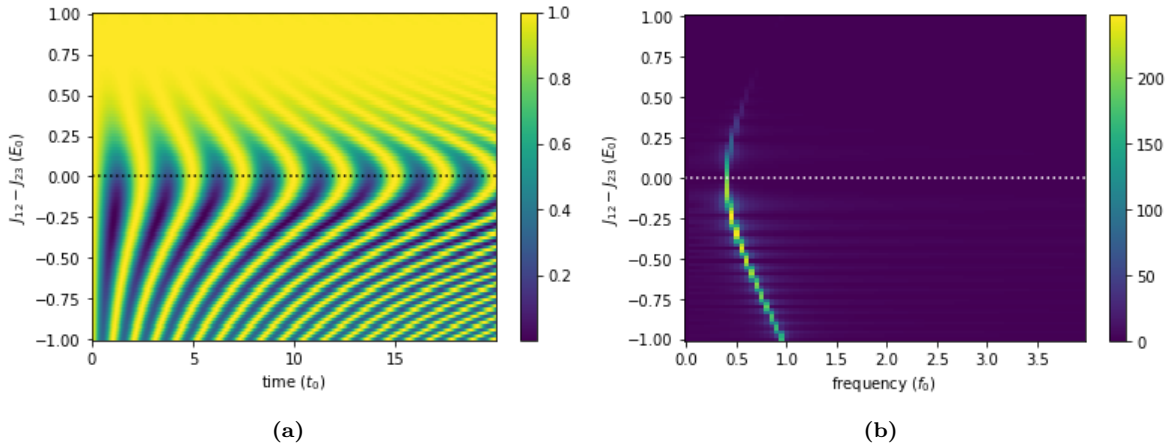


**Figure A.3:** Time evolution of an initial state of the triple spin chain with periodic boundary conditions. (a) Oscillations of the probability of measuring state  $|S \downarrow\rangle$  as a function of time and the difference of exchange couplings  $J_{12} - J_{23}$ . Exchange  $J_{13} = 0.6$  fixed. The colorbar indicates the value of the probability of finding the state in  $|\Psi_0\rangle$ . (b) Fourier transform of (a). The colorbar gives a range of the values of the dominating frequency amplitudes. The dotted lines indicate the point  $J_{12} = J_{23}$

gives us the results we display in Figures A.4 and A.5.

From these last results, we can once more see a signature of the homogeneous exchange case, given now by a crossing of the eigenenergies. This means that in the situation where  $J_{12} = J_{23} = J_{13} = J$ , all energies in this subspace are degenerate and there is no evolution of any initial state built exclusively from any of the  $|J_T = \frac{1}{2}, m_T = -\frac{1}{2}\rangle$  basis states. This is reveals a connection between magnetic frustration caused by geometry and the condition of exchange homogeneity in the system [13][18]. In fact, the low-energy doublet matrix in the same basis as we presented Equation 6.4 now reads as

$$H_{(\frac{1}{2}, -\frac{1}{2})}^p = \begin{pmatrix} -J_{12} - \frac{1}{4}(J_{23} + J_{13}) - \frac{\tilde{B}}{2} & \frac{3}{4\sqrt{3}}(J_{23} - J_{13}) \\ \frac{3}{4\sqrt{3}}(J_{23} - J_{13}) & -\frac{3}{4}(J_{23} + J_{13}) - \frac{\tilde{B}}{2} \end{pmatrix} \quad (\text{A.1})$$

which after diagonalizing it, we are able to extract the energy gap between the two eigenstates, which is given by

$$\Delta E_{1,2}^p = \sqrt{J_{12}^2 + J_{23}^2 + J_{13}^2 - J_{12}J_{23} - J_{12}J_{13} - J_{23}J_{13}} \quad (\text{A.2})$$

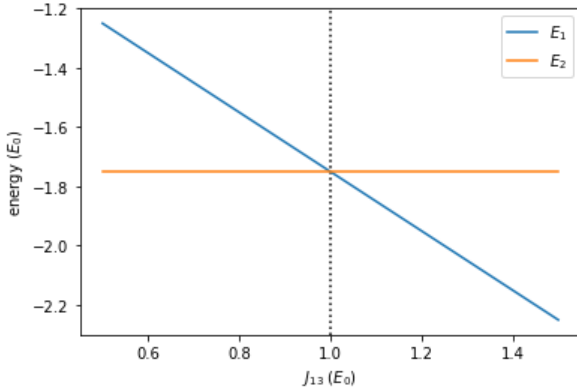


**Figure A.4:** Energies of the eigenstates of the  $S_T = \frac{1}{2}$  and  $m_T = -\frac{1}{2}$  doublet subspace as a function of the exchange coupling  $J_{13}$  for a triple spin chain with periodic boundary conditions. Exchanges  $J_{12} = J_{23} = 1$  fixed. The dotted line indicates the homogeneous point of the system.

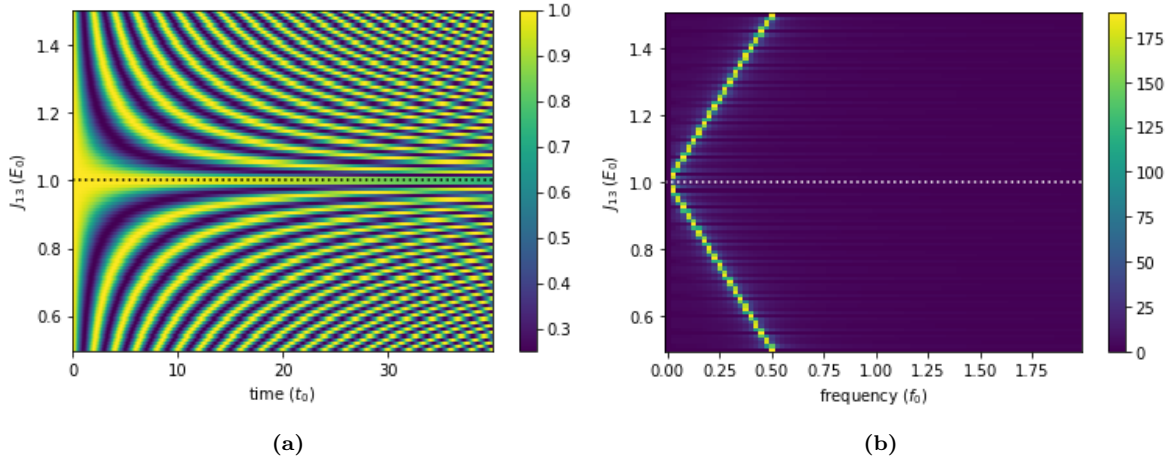


**Figure A.5:** Time evolution of an initial state of the triple spin chain with periodic boundary conditions. (a) Oscillations of the probability of measuring state  $|S \downarrow\rangle$  as a function of time and  $J_{13}$ . Exchanges  $J_{12} = J_{23} = 1$  fixed. The colorbar indicates the value of the probability of finding the state in  $|S \downarrow\rangle$ . (b) Fourier transform of (a). The colorbar gives a range of the values of the dominating frequency amplitudes. The dotted line indicates the homogeneous point of the system.

It is immediate to see that if  $J_{12} = J_{23} = J_{13}$ , then  $\Delta E_{1,2}^p = 0$  as we find in Figures A.4 and A.5. It is also insightful to note that the Expression (A.2) is a symmetric function (see footnote 3) under permutation of any of the exchanges acting as independent variables. This is translated to the complete geometrical exchange-swap symmetry of this system.

A last remark should be commented regarding the experimental point of view in these two steps presented above: even though the initialized-readout state is not a combination of singlet and triplet pairs, because we only have three spins, it may still be possible to observe the results of the probability oscillations experimentally, for example, using a partial readout technique.

# B

## Six-spins chain

The extension of the three-spin chain as a subsystem to tune a larger array is briefly commented in the following. We consider a six-spin chain, as shown in Figure B.1, composed of two three spin chain connected by their ends. We present some results to verify to what extent can reach a complete homogeneous regime starting from the base of having two homogeneous three-spin chains with a different value of exchanges  $J_{l1}$  and  $J_{l2}$ .

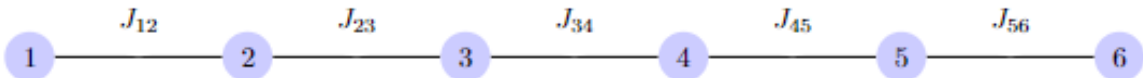


**Figure B.1:** Geometrical representation and labelling of the spins and exchanges in a six-spin chain.

Restricting ourselves into the fully polarized  $(\frac{n}{2} - 1)$ -total spin subspace, we examine the low-energy quintuplet of the block-diagonal Hamiltonian. Step one would require obtaining a condition in the energy spectrum of the quintuplet subspace as a function of  $J_{l1} - J_{l2}$ . The results for this step are shown in Figure B.2. We can clearly see that many frequencies allow us to detect the exchange crossing using the initial state  $|ST-T-\rangle$ , in particular the one of the lowest ones at that point ( $E_3 - E_2$ ).

Once it is satisfied that  $J_{l1} = J_{l2} = J_l$ , we attempt to control  $J_{34}$  to find a feature at the crossing of exchanges. The results obtained are shown in Figure B.3. In this case, conditions between different energy gaps have to be leveraged to be able to distinguish the homogeneous regime of the chain using this method. Specifically, we see that energy gaps  $E_2 - E_1 = E_5 - E_4$  and  $E_3 - E_2 = E_4 - E_3$  at  $J_l = J_{34}$  (Figures B.3a and B.3b). For this case, we need a longer evolution time to be able to distinguish the frequencies clearly. We can see that again using the initial state  $|ST-T-\rangle$ , we can detect one of these two gap equalities:  $E_3 - E_2 = E_4 - E_3$ .

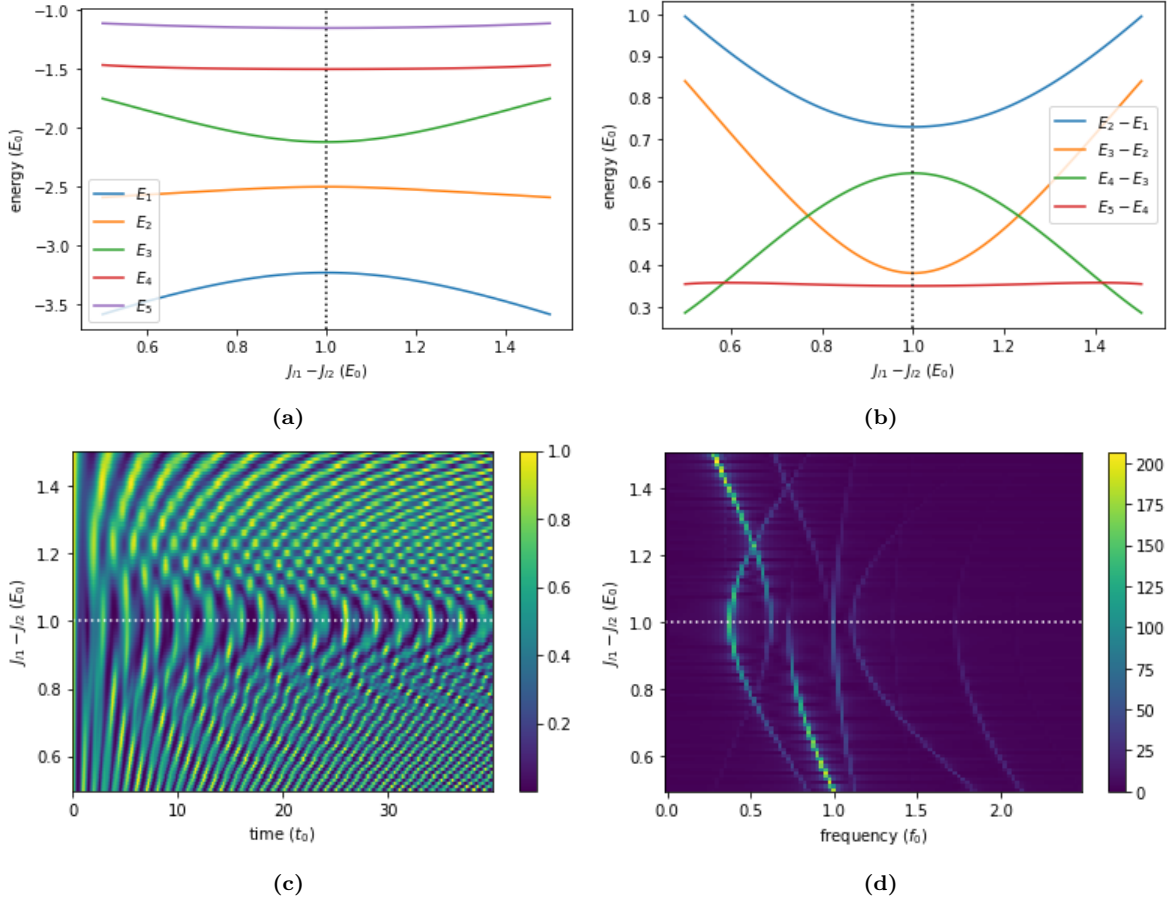


**Figure B.2:** Equalization of two spin-three chains connected by one side. **(a)** Eigenenergies of the lowest-energy quintuplet for the six-spin chain as a function of  $J_{11} - J_{12}$ . **(b)** Energy differences of the adjacent eigenenergies plotted in (a). **(c)** Oscillations of the probability of measuring state  $|ST-T-\rangle$ . The colorbar indicates the probability values. **(d)** Fourier transformation of the data in (c). The colorbar indicates the strength of the amplitude of oscillation. Initial state is  $|ST-T-\rangle$ . The dotted lines indicate the value where the exchange coupling of both sub-chains is the same. The exchange  $J_{34} = 1.5$  fixed.

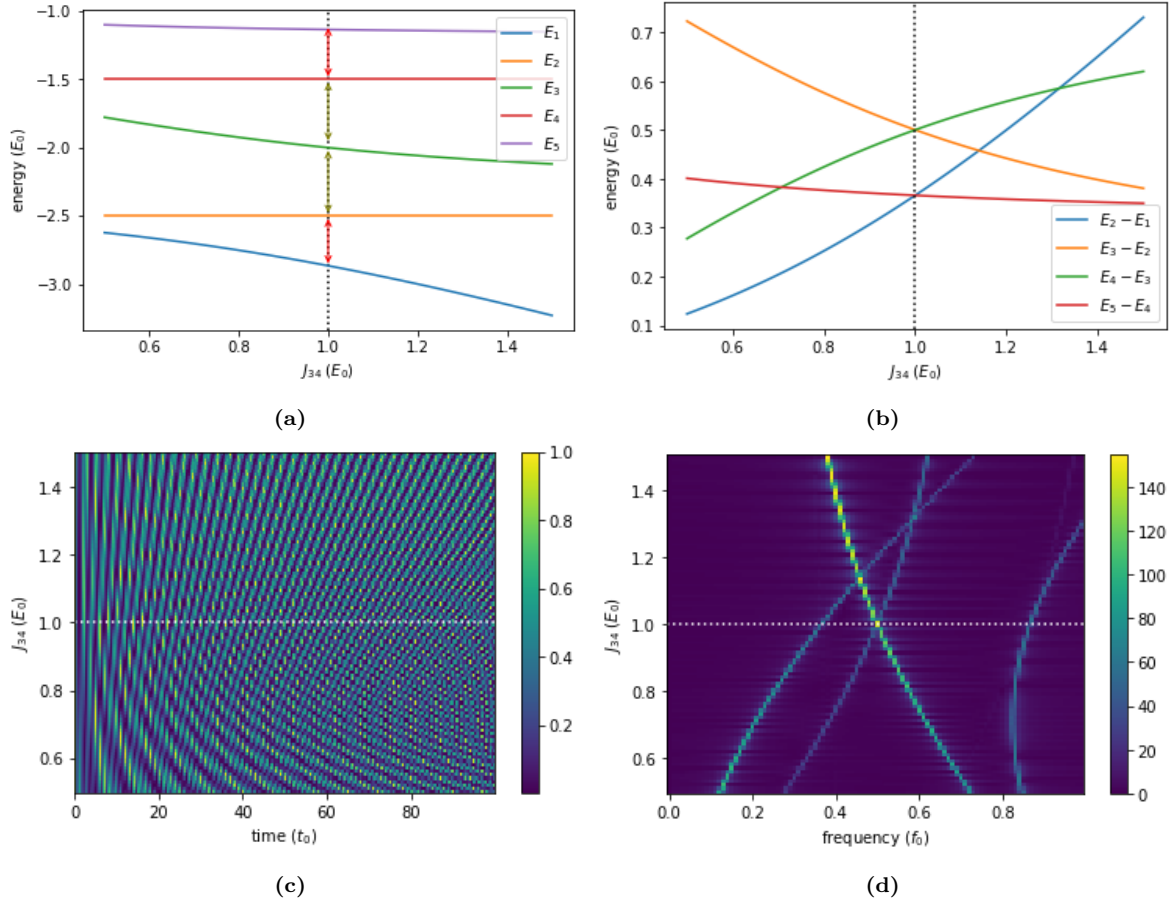


**Figure B.3:** Homogenization of the exchanges of a six-spin chain. (a) Eigenenergies of the lowest-energy quintuplet for the six-spin chain as a function of  $J_{34}$ . The red arrows indicate same-sized energy gap  $E_r$  as well as the olive arrows, which indicate energy gap  $E_o$ . (b) Energy differences of the adjacent eigenenergies plotted in (a). (c) Oscillations of the probability of measuring state  $|ST-T-\rangle$ . The colorbar indicates the probability values. (d) Fourier transformation of the data in (c). The colorbar indicates the strength of the amplitude of oscillation. Initial state is  $|ST-T-\rangle$ . The dotted lines indicate the homogeneous point. At this point, the two frequencies with value  $E_o$  act as features for the detection of the homogeneous regime.

# C

Supplementary figures

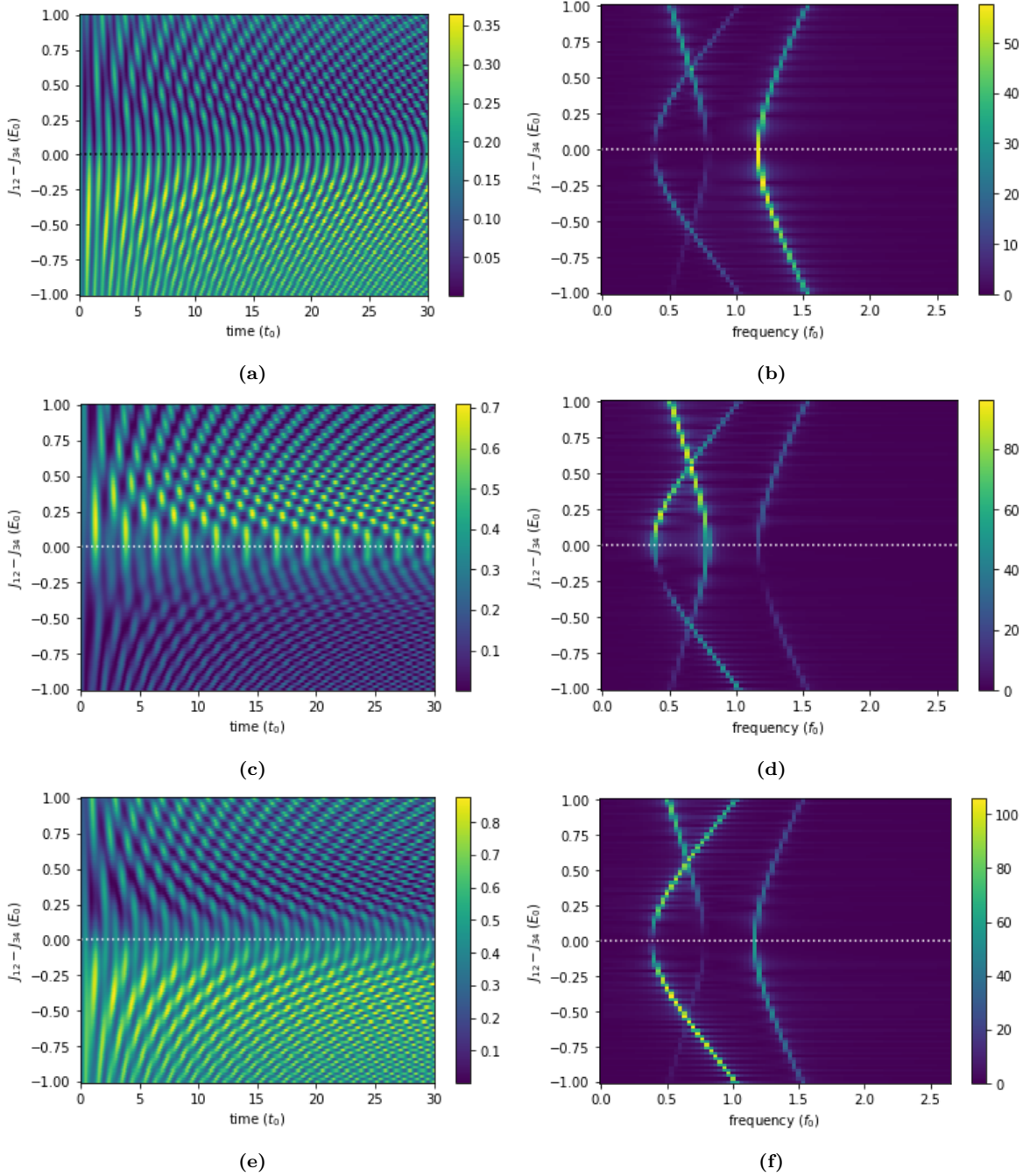


**Figure C.1:** Time evolution of an initial state of the quadruple spin chain. Step one of the tuning protocol presented in section 3.3. Oscillations of the probability of measuring state (a)  $|S\rangle_{14}$ , (c)  $|S\rangle_{24}$  and (e)  $|S\rangle_{23}$  as a function of time and the difference of exchange couplings  $J_{12} - J_{34}$ . The colorbar indicates the value of the probability of finding the measured state for both plots respectively initializing  $|T-S\rangle$ . (b), (d), (f) Fourier transform of the oscillating pattern of the measurement probabilities of (a), (c) and (e) respectively. Middle exchange coupling is set to  $J_{23} = 0.6$  for all cases. The colorbar indicating a range of the values of the dominating frequency amplitudes. The dotted line points out the exchange-crossing point.

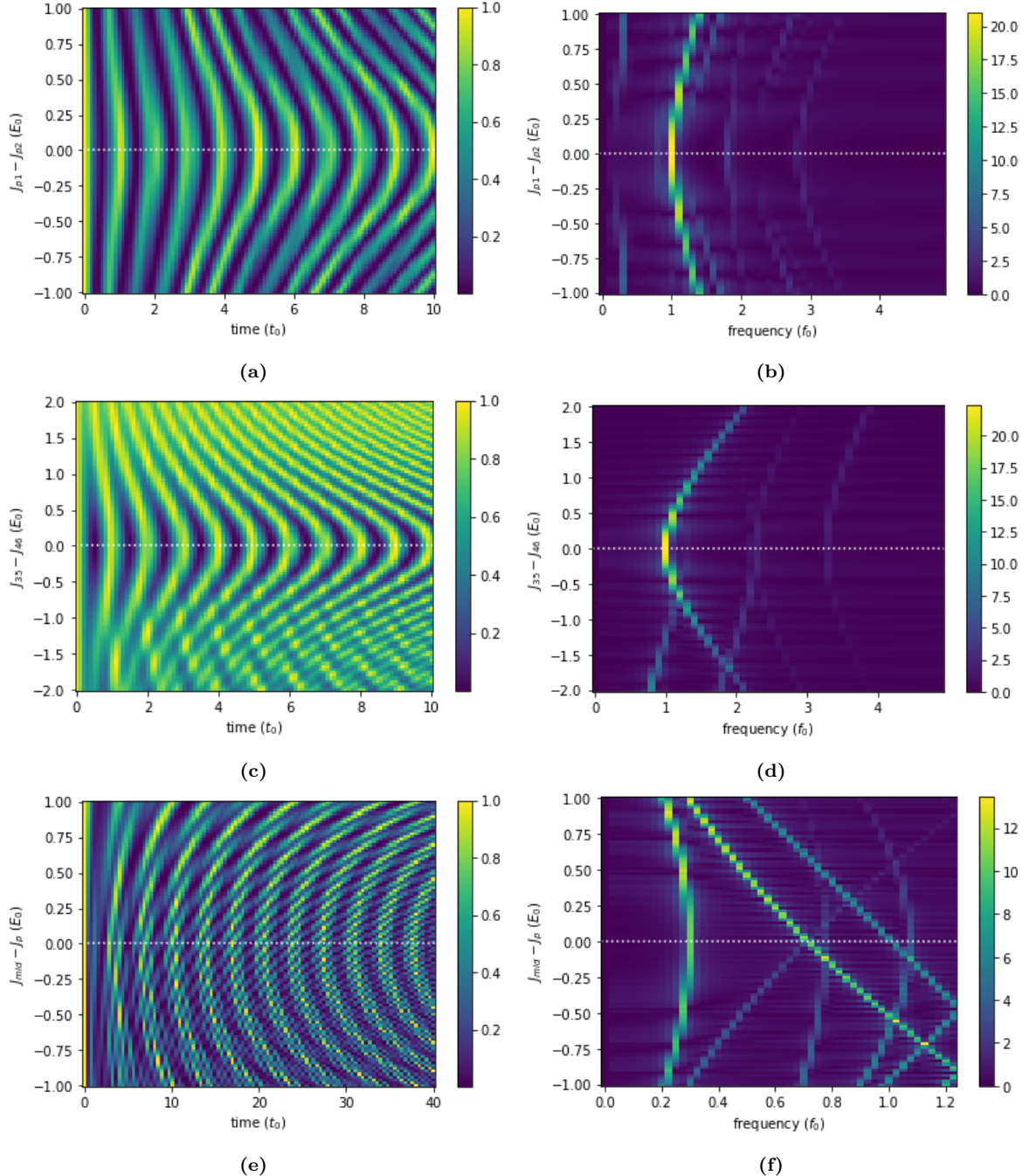


**Figure C.2:** Time evolution of an initial state of the eight-spin ladder. Steps seven to nine of the tuning protocol A presented in section 5.1 using partial readout. (a), (b) Step seven of the protocol. State  $|i_1\rangle$  is initialized, (a) the probability of state being singlet is readout for spins 3 and 5 and (b) the Fourier transform of this signal is shown. Similarly for (c), (d) with step eight of the protocol. (e), (f) Same representation as the other two pairs but in this case the initial state is  $|i_7\rangle$  and the pair of measured spins in a singlet state is (7,8). See Figures 5.4, 5.5 and 5.6 for more details.

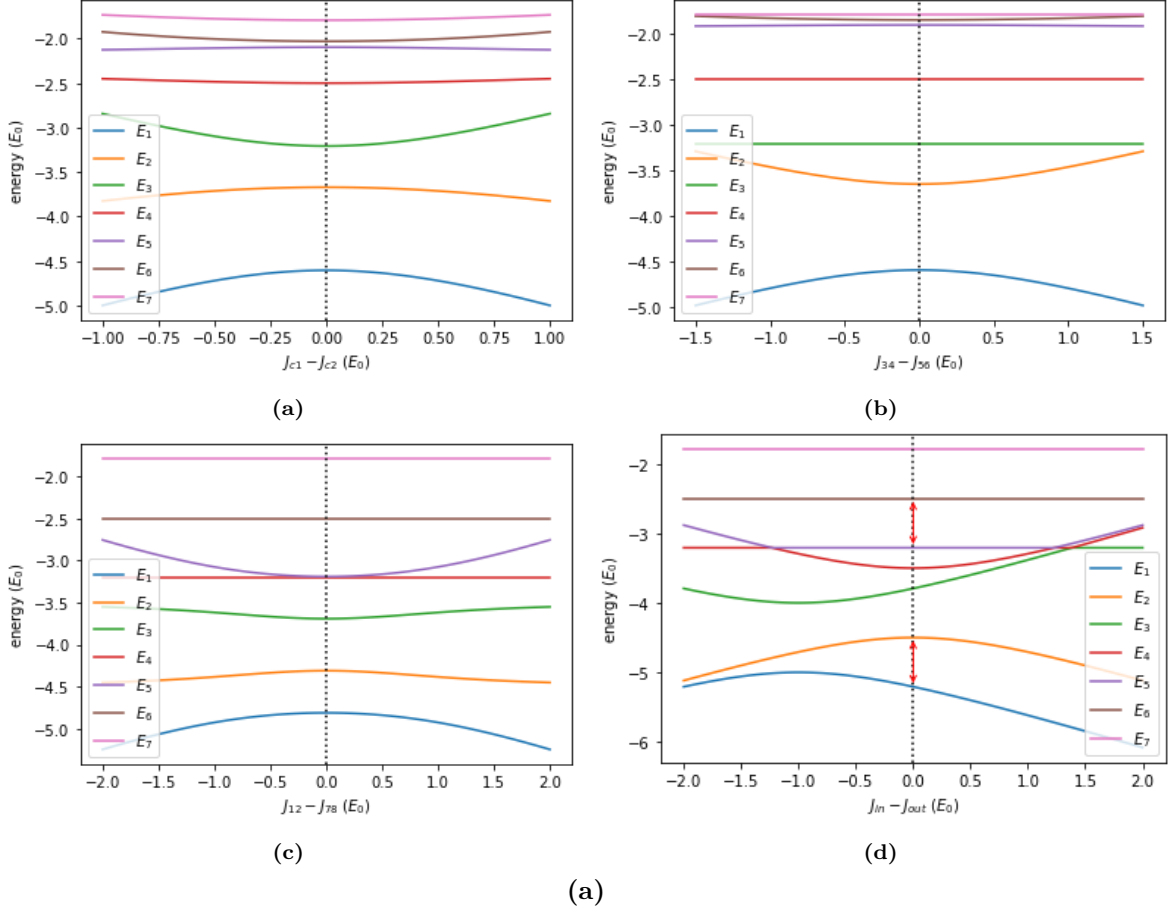


**Figure C.3:** Energy landscape of the low energy septuplet of the eight spin ladder. Steps five to eight of protocol B presented in section 5.2. **(a)** Step five, energies as a function of  $J_{c1} - J_{c2}$  with  $J_{12} = J_{78} = 0.2$  and  $J_{34} = J_{56} = 1.5$ . **(b)** Step six, consisting on sweeping exchanges  $J_{34} - J_{56}$  with the horizontal ones fixed at 1 and  $J_{12} = J_{78} = 0$ . At the crossing point  $J_{34} = J_{56} = 1.5$ . **(c)** Step seven, maintaining  $J_{34} = J_{56} = 1.5$  and  $J_h = 1$ , we sweep  $J_{12} - J_{78}$  with  $J_{12} = J_{78} = 2$  at the crossing. **(d)** Step eight, eigenenergies as a function of  $J_{in} - J_{out}$  crossing at value 2 keeping the other horizontal exchanges constant at 1. Red arrows indicate The dotted lines indicate the zero-difference point between swept exchanges.

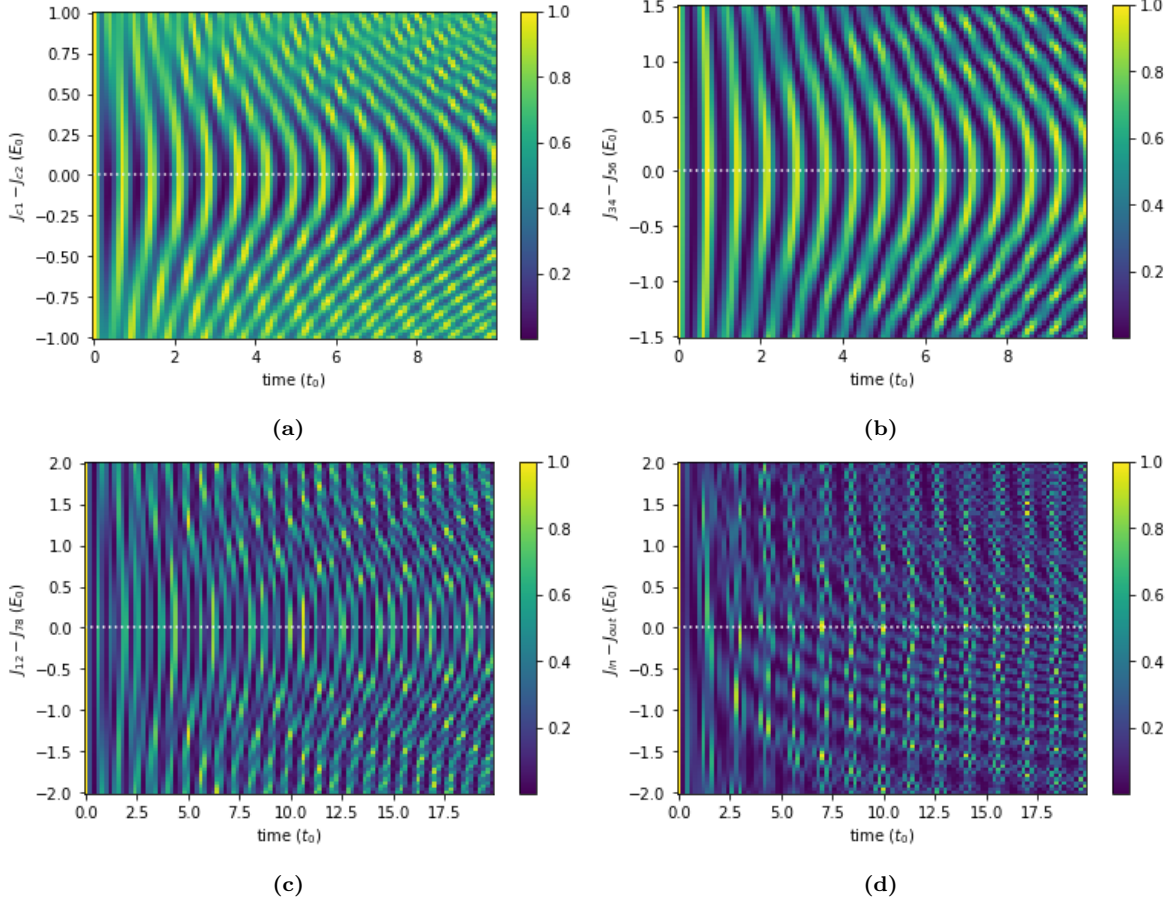


**Figure C.4:** Probability oscillations of states in the low energy septuplet of the eight spin ladder. Steps five to eight of protocol B presented in section 5.2. **(a), (b), (c)** Step five, six and seven respectively, initial state  $|i_2\rangle$  evolving in time. **(d)** Step eight, initial state  $|i_3\rangle$ . All the probabilities are computed for the measured state being the initial state. The colorbar indicates the values of these probabilities and the dotted line indicates the crossing point of the swept exchanges. For more information see Figure C.3.

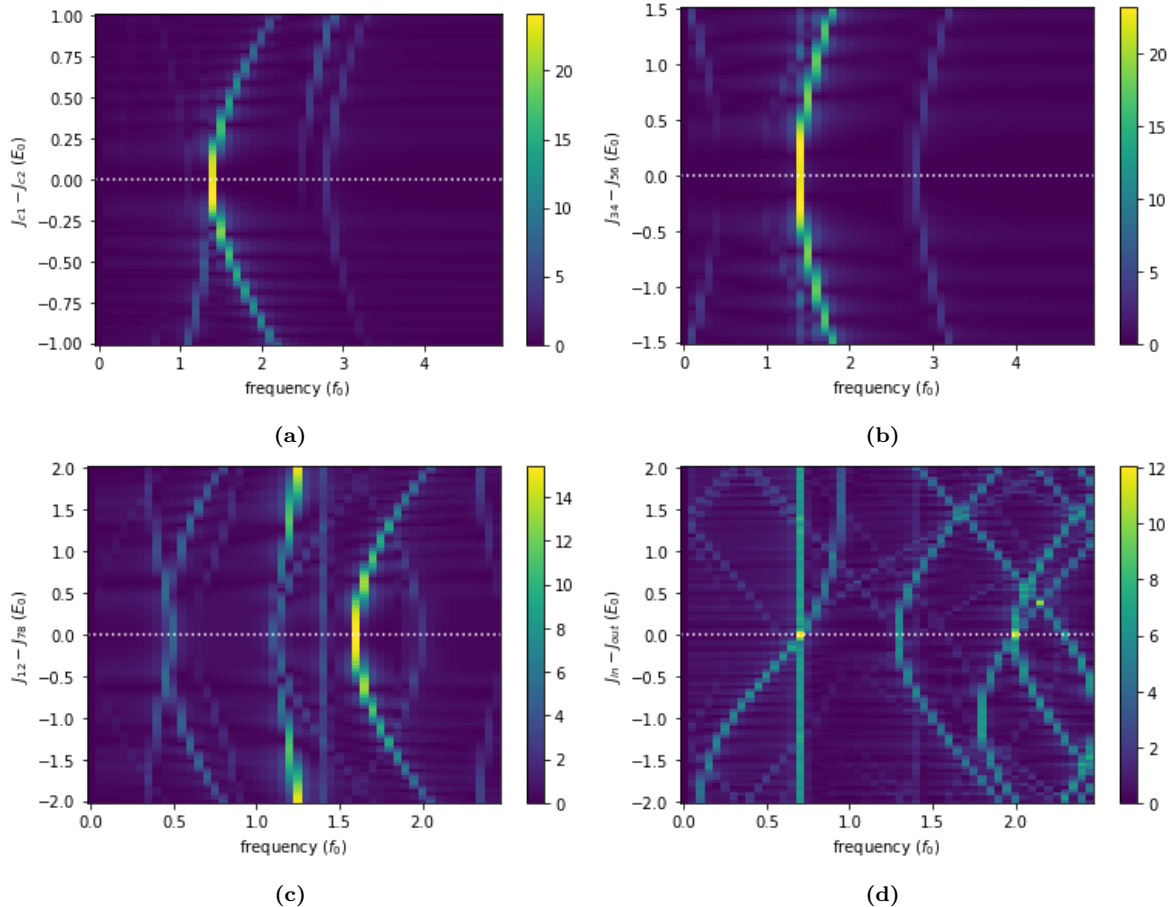


**Figure C.5:** Fourier transform of the oscillating probability plots shown in Figure C.5. (a), (b), (c), (d) Steps five, six, seven and eight of protocol B presented in 5.2 respectively. The colorbar indicates the amplitude of oscillation and the dotted line the point of exchange crossing.

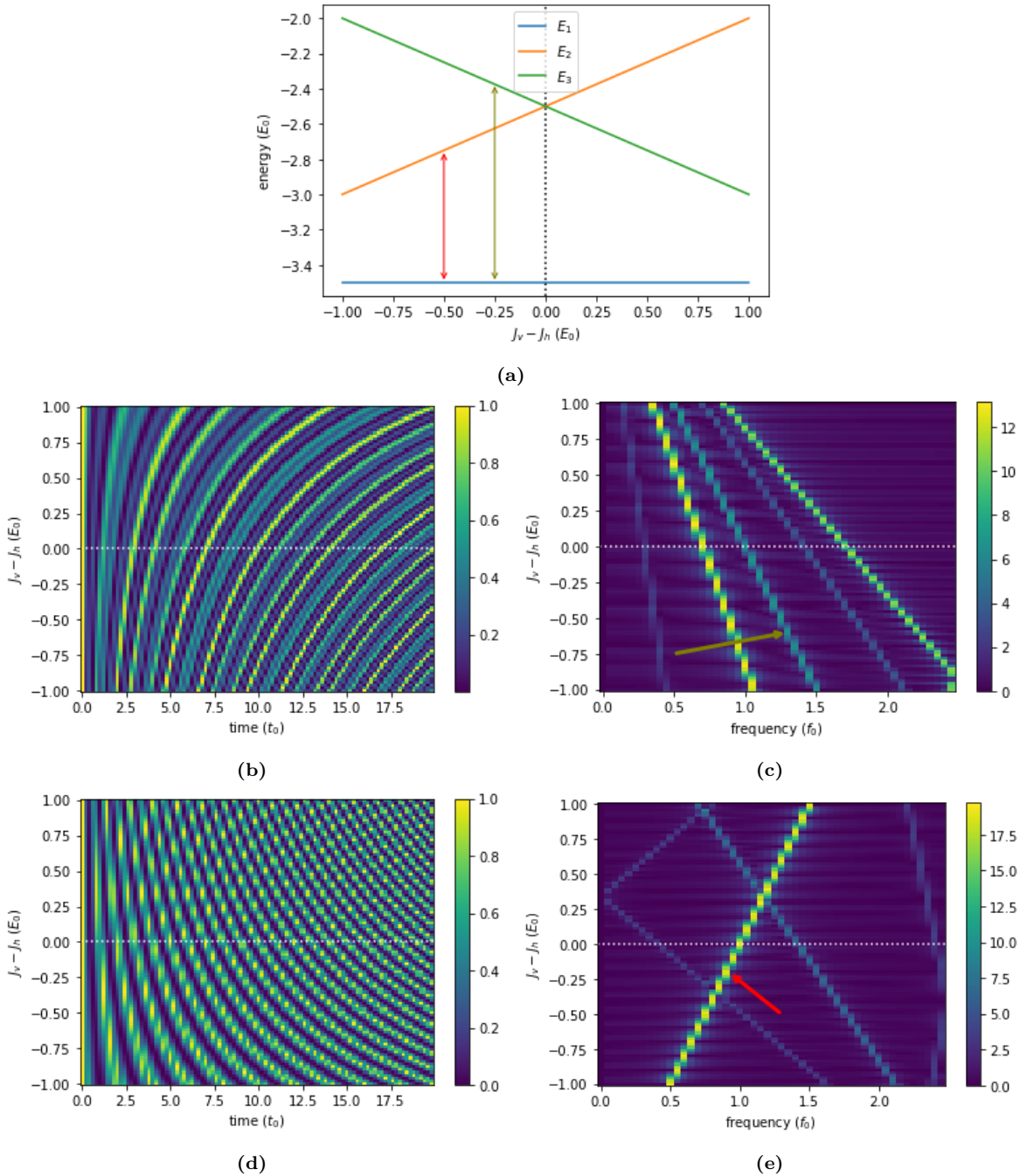


**Figure C.6:** Homogenization of the exchanges of the eight-spin ladder. Homogenization of the exchanges of the eight-spin ladder. (a) Eigenenergies of the lowest-energy septuplet for as a function of  $J_v - J_h$ . The red arrows indicate the energy gap for which initial state  $|i_6\rangle$  gives signal and the olive arrows indicate the energy gap for which initial state  $|i_9\rangle$  gives signal. (b), (d) Oscillations of initial state  $|i_6\rangle$  and  $|i_9\rangle$  respectively. The colorbar indicates the probability of measuring the initial state. (c), (e) Fourier transformation of the signals in (b) and (d) respectively. The colorbar indicates the amplitude of oscillation. The red and olive arrows in (c), (e) indicate the frequency contributions of interest, associated to the energy gaps in (a) indicated with the same color. The dotted lines indicate the point when exchanges  $J_v$  and  $J_h$  are equal. At this point the red and olive marked frequency signals cross.